# Numerical Renormalization Group Study of the Two-Channel Kondo Model

Ph.D. Dissertation

Anna Tóth

Advisor: Prof. Gergely Zaránd

Theoretical Physics Department
Budapest University of Technology and Economics

Toronto, 2009

We generalize the spectral sum rule preserving density matrix numerical renormalization group method (DM-NRG) in such a way, that it can make use of an arbitrary number of local, compact Lie group symmetries of a quantum impurity model. As one of its applications, we study the Green's functions of the highest-weight fields in the spin-half two-channel Kondo (2CK) model. We use a conformal field theory based scaling approach to predict the analytic properties of the various Green's functions in the vicinity of the 2CK fixed point and confirm these predictions by DM-NRG calculations. We also calculate the zero temperature, frequency-dependent linear conductance of the double quantum dot device that has recently been built to justify the existence of the 2CK states.

# Acknowledgments

I thank my colleagues from Budapest and Karlsruhe for several interesting discussions, and my coauthors for fruitful collaboration.

I thank Prof. Gergely Zaránd for the excellent topic. I am grateful to Prof. Gerd Schön for his generous support and for the provision of appropriate work conditions. I would like to thank Ilona Cseppkövi for solving my language related problems. I am grateful to Bertalan Horváth for his help in getting hold of high quality lecture notes every time I asked for them. I thank Dr. Catalin Pascu Moca for the mutual work (actually Fig. 3.1 was prepared by him), Dr. Valentina Brosco for explaining me about single electron devices. I thank Béla Tóth for managing the printing. I thank Prof. János Kertész for his support and Dr. Daniel Hermann for his expert help with computer related matters. I am grateful to Dr. Eszter Szegő for her good ideas. I appreciate George Mátrai's good advice.

This work has also been supported by Hungarian grants OTKA nos. NF061726, K73361, NK63066 and by the Landesstiftung Baden-Württemberg via the Kompetenznetz Funktionelle Nanostrukturen.

# Contents

# 1 Introduction

We study strongly correlated electron systems due to their central importance in condensed matter physics. These systems involve a large number of degrees of freedom that interact in complicated ways. It is extremely challenging to resolve their properties since descriptions based on single-particle pictures and non-interacting models are usually inadequate. Prominent examples of strongly correlated electron systems are high-temperature superconductors [1, 2], heavy fermion materials [3, 4] and electrons in fractional quantum Hall states [5].

Even under such complicated circumstances sometimes it is possible to identify the relevant parameters that describe the physics at a certain length scale and relate them through so-called scaling laws. These laws cover e.g. the power-law dependence of thermodynamic quantities on the distance from a critical point, and help understand robust, universal features of experimental data observed under varying circumstances. Markedly different models may also display similar universal features that are insensitive to the microscopic details of the interactions and depend only on the number of dimensions, on the model symmetries, etc.

Scaling laws can be derived using Renormalization Group (RG) methods. RG methods are techniques to calculate averages over configurations of many degrees of freedom in cases when characteristic length scales are not important in the problem. Such situations arise e.g. at continuous phase transitions or in certain field theories [6]. A common feature of all RG methods is that they transform the model parameters, while keeping the physical properties fixed at a certain length scale. Successive transformations define a trajectory in the parameter space. The existence of fixed points of the RG transformations and the near fixed point behavior is used to explain the universality observed under differing conditions.

At continuous phase transitions, fluctuations appear on every length scale, i.e. the maximal wavelength of fluctuations, the so-called correlation length becomes infinite. Such phase transition occurs e.g. at the liquid-vapor critical point.[1] Here, critical opalescence can be inspected as an accompanying phenomenon. It is due to the fact that at the critical point fluctuations can be found in the state of the system between the two phases on every length scale, and so on the wavelength of light as well. These fluctuations and a difference between the refraction indices of the two phases lead to the scattering of light. Long or short wavelength fluctuations do not play special role at these transitions, rather fluctuations at all wavelengths contribute to the critical phenomena.

The lack of characteristic energy scale is also encountered in quantum field theories at the evaluation of Feynman diagrams when integrating over intermediate states. In many cases, integrals of the $\int \frac{dE}{E}$ kind appear, where all orders of magnitude range of energies contribute the same, finite amount to the integral.

In 1949 Dyson showed that quantum electrodynamics (QED) is renormalizable, i.e. UV divergences can be eliminated from the diagrammatic expansion of almost every, so called physical

[1] Further examples are the Curie point of a ferromagnet, or the superfluid transition in $^4$He.

quantities[2] in all orders of perturbation theory [8]. This has been accomplished by the introduction of the concepts of bare and renormalized electron charge and mass, and electron and photon field strengths in addition to using a regularization scheme to render divergent loop integrals finite. A field theory is called renormalizable if there are only a finite number of physical quantities that diverge when removing the regularization. The bare parameters of a theory are the couplings of the original Lagrangian. Renormalized parameters are observable quantities, like the electron mass measured at a chosen length or energy scale. The predictions of the theory need to be independent of the choice of this length scale called the normalization point or the renormalization condition. In other words, bare Green's functions must remain the same functions of the bare couplings and the cutoff for any choice. As the bare and the renormalized Green's functions are the same up to some renormalized field strength factors, certain relations, called the Callan–Symanzik equations [9, 10], can be derived for the renormalized Green's functions. These equations have many implications. One of them is that interactions can generate scales and cause the fields to acquire new dimensions even though a bare Lagrangian could have been scale invariant (i.e. containing only dimensionless couplings) [11].

Special invariance properties of certain field theories were recognized already in 1953 by Stueckelberg and Petermann [12]. One of the early forms of perturbative RG methods has been applied to QED [13]. It relies on its renormalizability and corresponds to summing up the leading logarithmic terms, $\propto \log^n (E\,/\,\mu)$ that appear in all orders, $n$ of the renormalized perturbation theory, (with $E$ the energy characteristic of the process and $\mu$ the normalization point where the values of the renormalized couplings are known). This method leads to renormalization group equations which determine the change in the renormalized coupling constant due to a small change in the chosen normalization point, $\mu$.

This perturbative form of RG applies only to models which can be treated by means of diagrammatic expansion, where only a few diagrams are important, like in QED. In this formulation, suited for weak coupling, the contribution of fluctuations coming from all length scales and their coupling cannot be fully appreciated.

In the sixties Kadanoff worked out the scaling theory of critical phenomena [15] (see also Refs. [16, 17, 18]). He realized that grouping together degrees of freedom at the critical point induces transformations on the Hamiltonian and on the statistical ensemble, but it does not change the overall physical picture on larger length scales. Successive applications of the transformation eventually probe the large distance/low energy properties of the system. Kadanoff derived scaling equations for correlation functions through the application of block spin transformations. His method works for lattice models defined in real-space in contrast to momentum space approaches that are used in general in the field theoretical formulation of RG.

It is difficult to carry out exact RG transformations, as e.g. block spin transformations in two dimensions, nevertheless there are a few approximation schemes like the $\epsilon$-expansion [17]. It is also a perturbative form of RG for critical phenomena and can be solved in dimension $d = 4 - \epsilon$ with $\epsilon$ small.

In low-dimensions, the study of strongly correlated systems is aided by other powerful approaches like integrability or conformal field theory [19, 20] besides RG methods.

In this dissertation RG methods are used to deal with special types of low-dimensional systems showing strong correlations, called quantum impurity models. Such models describe interactions between local degrees of freedom – like a spin – and a continuum of extended states – as e.g.

[2] For a discussion see e.g. Ref. [7].

a conduction electron band. Their prototypes are the Anderson and the Kondo models. These models account for several experimental findings like the resistance minimum and power law-like behavior observed in non-magnetic metals in the presence of magnetic impurities. More recent experiments exploring Kondo physics take place in mesoscopic systems with reduced dimensionality such as thin films and wires of dilute magnetic alloys, metallic point contacts, nanoscopic electronic devices like quantum dots, etc.

We mainly focus on the spin-half two-channel Kondo (2CK) model which is the simplest variant of overscreened multi-channel Kondo models that exhibit non-Fermi liquid properties. These properties cannot be described in terms of weakly interacting quasiparticles. Non-Fermi liquid phenomena have been observed in a number of strongly correlated systems, e.g. in heavy fermion materials [21, 22, 3, 4]. Examples for concentrated heavy fermion compounds are $UBe_{13}$ and $CeCu_2Si_2$. In these systems magnetic impurities, such as $f$-shell local moments of rare-earth or actinide ions are immersed in a conducting host. Non-Fermi liquid quantum impurity models are expected to be relevant in their description. Another type of systems where NFL physics can been observed are single electron devices. Recently a double dot system has been designed and built to justify the feasibility of the two-channel Kondo state [23].[3]

Further motivation for the investigation of quantum impurity models is that it is the starting point to understand more complex, strongly correlated systems in the framework of Dynamical Mean Field Theory (DMFT) [24]. DMFT is a tool for the investigation of lattice models like the Hubbard or the Kondo lattice models. It is able to handle strong electron correlations as it was demonstrated e.g. through various three-dimensional materials displaying Mott-transition.

The solution of quantum impurity models for low-energies was a major issue in theoretical condensed matter research and led to the development of various non-perturbative techniques. One of them is the Numerical Renormalization Group (NRG) method developed by Wilson around 1975. NRG not only solves the strong coupling limit of these models but it also accounts for the weak coupling and the crossover regions. It is still possibly the most reliable and versatile method for studying quantum impurity models, and its influence over the development of other methods is significant.

In this dissertation we present some results of our research carried out in the past four years. It is accompanied by an extensive introduction to NRG in Chapter 2, and a brief overview of the low-temperature transport properties of single electron devices in Chapter 4.

Our first research project, discussed in Chapter 3, was motivated mainly by the ever increasing interest in understanding the characteristics of nanoscopic electronic devices that can be described by quantum impurity models. As a natural extension contributed to recent efforts improving the accuracy of the NRG calculations, we have generalized the spectral sum rule preserving density matrix numerical renormalization group (DM-NRG) method in such a way that it can make use of an arbitrary number of local compact Lie group symmetries that a quantum impurity system may possess.

Based on the above, we have developed a flexible DM-NRG code [25, 26] that can easily be adapted to the problem of interest and could make use of an arbitrary number of compact Lie group symmetries. We demonstrated that the use of non-Abelian symmetries is advantageous for reliability and performance reasons.

As one of the applications of our code, in Chapter 4, we study the Green's functions of the

[3] For further details on non-Fermi liquid physics and single electron devices see Section 4.1 and Section 4.2, respectively.

highest-weight fields in the electron-hole symmetrical spin-half two-channel Kondo (2CK) model. Even though this model became paradigm for describing non-Fermi liquid physics, so far little has been published about its dynamical properties. Up to this date, these properties can be reliably computed for the whole frequency range only with NRG. Nevertheless, in the vicinity of the 2CK fixed point a conformal field theory based scaling approach can be used to predict the analytic properties of the various Green's functions. We confirmed all of our predictions by DM-NRG calculations.

This dissertation is organized as follows:

Chapter 2 is an introductory chapter that does not contain any new results. In this chapter we introduce the Kondo and Anderson models and talk about the Kondo problem. After a brief discussion on scaling, we give a detailed analysis of the numerical renormalization group. It means that this part involves all the formulas that are necessary to understand NRG and to write an NRG code. We have added this summary for clarifying the values of all the constants appearing in the calculations and to be able to use it as source of reference.

In Chapter 3 it is shown how symmetries appear in the NRG calculations and also present the density matrix numerical renormalization group method from the point of view of symmetries. This part contains the following new results: the generalization of the recursive steps in NRG for an arbitrary number of local compact Lie group symmetries of a quantum impurity system, and the generalization of the density matrix numerical renormalization group method for the case of non-Abelian symmetries. The importance of symmetries is demonstrated through calculations for the two-channel Kondo model.

Chapter 4 is devoted mainly to the study of the two-channel Kondo (2CK) model. First we analyze its importance in the description of non-Fermi liquid phenomena. Then we make a short detour to discuss the low energy transport properties of single electron devices, and in particular the observation of the one- and two-channel Kondo effects in quantum dot systems. Afterwards we present a detailed analysis about the dynamical properties of the 2CK model. This part contains the following new results: Using conformal field theoretical methods we have classified the boundary highest-weight fields of the electron-hole symmetrical 2CK model at the 2CK fixed point, just as the relevant and leading irrelevant perturbations to the fixed point Hamiltonian according to the symmetry group $\mathrm{SU}_{C1}(2) \times \mathrm{SU}_{C2}(2) \times \mathrm{SU}_S(2)$. Here $C1$, $C2$ are referring to the charge (or flavor) symmetries in the two channels, whereas $\mathrm{SU}_S(2)$ denotes the spin SU(2) symmetry of the system. Such classification has already been carried out but with using a different symmetry group [27]. As it is demonstrated in Chapter 3, the choice of the symmetry group is crucial in the DM-NRG calculations.

Based on simple scaling arguments and conformal field theoretical considerations the highest-weight field can be expanded in terms of the operators of the free theory. Moreover the analytic properties of the universal scaling curves can be determined in the asymptotic regions. In all cases, our DM-NRG calculations reinforced our analytic expectations for the universal scaling curves. We have computed the universal scaling curves connecting the 2CK scaling regimes and the channel anisotropy or magnetic field induced Fermi liquid scaling regimes. We have found that the boundaries of the various 2CK scaling regimes depend not only on the type of the perturbation but also on the operator investigated. In small magnetic field, a universal resonance has been observed in the local fermion's spectral function. The dominant superconducting instability was found in the composite superconducting channel, just as it was anticipated in Ref. [28]. This latter observation could be relevant for multi-impurity heavy fermion systems.

In this chapter we also study the zero temperature, finite frequency transport properties of the double quantum dot device that has recently been built to justify the feasibility of the 2CK states.

In Chapter 5 the dissertation is concluded by presenting the thesis points.

Four appendices are attached to this thesis:

Appendix A contains the definition of the retarded Green's function and related notions.

In Appendix B we discuss how to deal with energy-dependent density of states in the NRG calculations.

In Appendix C we show how to initialize the one-channel Kondo model for the NRG calculations using the group $\mathrm{SU}_S(2) \times \mathrm{SU}_C(2)$, with $S$ and $C$ referring to spin and charge, respectively.

In Appendix D using group theoretical tools, we prove that the reduced density matrix is diagonal in the representation indices in case when the local symmetries of the quantum impurity model are direct products of SU(2) groups.

The new results of my research are presented in Sections 3.1.3, 3.2.2, 3.2.3, 3.3, 4.3.1–4.3.7 and in Appendix D.

# 2 Scaling & numerical renormalization group for quantum impurity models

In this chapter we give an introduction to two notions which are closely linked and most frequently referred to in this the thesis. The two main concepts are ($a$) scaling and ($b$) Numerical Renormalization Group (NRG). This chapter does not contain any new results. It is organized as follows. In Section 2.1 we describe the 1-Channel Kondo (1CK) problem[1] which motivated the development of NRG [30], and introduce 1CK Hamiltonian. In Section 2.2 we do the same for the Anderson model and discuss some link between these two models. Section 2.3 offers a brief introduction into the poor man's scaling approach as applied to the Kondo model. In Sec. 2.4 succeeds a detailed description of NRG. We show how the Anderson and the 1CK Hamiltonians are mapped onto the so-called Wilson chain to make them amenable to an NRG analysis.

## 2.1 The one-channel Kondo problem

Originally the one-channel Kondo problem was concerned with the influence of magnetic impurities in a non-magnetic metal, and in particular with the low-temperature behavior of such systems. These questions are interesting since, as was found experimentally, even small impurity concentrations can have substantial impact on the low-energy system properties. Such impacts include a minimum followed by an anomalous increase in the resistance with decreasing temperature. This phenomenon was revealed already in 1934 in measurements on Au samples [31] but its origin had remained obscure for 30 years. It could not have been attributed either to the scattering of electrons on each other, or on phonons, or even to their potential scattering on structureless impurities. Such possibilities have been ruled out as these processes imply a resistance that increases monotonously with the temperature. Among others, susceptibility measurements made the localized moments suspicious as the cause, and the first explanation came from Kondo [32]. He calculated the scattering probability of the conduction electrons up to second order in perturbation theory using the $s$-$d$ interaction, also called the one-channel Kondo model, assuming a weak, antiferromagnetic exchange coupling, $J > 0$ between an impurity spin, $\vec{S}$ localized at $\vec{r} = 0$ and the conduction electron spin density at the place of the impurity

$$\mathcal{H}_{1CK} \;=\; J\vec{S}\Psi^{\dagger}_{\mu}(0)\vec{\sigma}_{\mu\nu}\Psi_{\nu}(0)\,, \tag{2.1}$$

with $\mu, \nu$ the spin indices and $\vec{\sigma}$ denoting the Pauli matrices. The $\Psi_{\mu}(\vec{r})$'s are electron fields obeying anticommutation relations

$$\left\{\Psi^{\dagger}_{\mu}(\vec{r}), \Psi_{\nu}(\vec{r}')\right\}_{+} \;=\; \delta(\vec{r}-\vec{r}')\;\delta_{\mu,\nu}\,. \tag{2.2}$$

[1] See e.g. Hewson's book [29] for a review.

Kondo's calculations agreed with the experimental findings on the logarithmic temperature dependence of the resistivity and on the impurity concentration dependence of the resistance minimum. To extract one-channel Kondo behavior small impurity concentration is needed (around or less than 0.01% of impurity atoms). Examples for experimentally well-studied bulk dilute magnetic alloys are Cr/Mn/Fe in Cu, Vn in Au, Ce in $LaAl_2$ or in $LaB_6$ .

Lately the focus of studies has shifted towards mesoscopic systems of reduced dimensionality, as the following examples show. The emergence of Kondo physics has been investigated in the context of thin films and wires of dilute magnetic alloys [33, 34, 35, 36, 37, 38, 39, 40, 41]. It has also been used to explain the scanning tunneling microscope spectra of single impurities absorbed onto different metallic surfaces (see e.g. [42, 43, 44, 45, 46]), just as the zero-bias anomaly in metallic point contacts [47, 48, 49], and the behavior of the dephasing time of electrons at low-temperatures (for references see e.g. [50]). Kondo physics has also been observed in quantum dots, which are nanoscopic devices that permit the controlled study of various strongly correlated phenomena via transport measurement. This latter topic is discussed in more detail in Chapter 4.

Beyond the above, in the Kondo model an excellent breeding ground has been found for many concepts of physics. In this thesis we mainly concentrate on scaling and renormalization.

At low-temperatures there are strong effects because of the presence of a spinful impurity. Due to them some decades ago it used to be a great theoretical challenge to predict the system properties. Although the coupling $J$ is weak, yet perturbation theory cannot be pursued at low temperatures since in each order $n$ of the perturbation theory terms of the form $\propto \log^n(D_F/k_BT)$ (with $D_F$ the conduction electron bandwidth) appear in the diagrammatic expansion. The value of the effective coupling, which characterizes the given energy (or temperature) scale, can be obtained by summing up the leading logarithmic terms in all orders of perturbation theory. This effective, energy dependent coupling is called the running coupling constant.

## 2.2 The Anderson model

The Anderson model was introduced in 1961 [51, 52] to investigate the conditions needed for the appearance of localized magnetic moments in metals, but lately its relevance has also been recognized in the description of transport through quantum dots (see Chapter 4) and in the context of dynamical mean field theory [53].

We start with the following form of the three-dimensional, single-impurity Anderson Hamiltonian

$$\mathcal{H}_A \;=\; \mathcal{H}_A^{kin} + \mathcal{H}_A^{d} + \mathcal{H}_A^{t}\,, \tag{2.3}$$

with

$$\mathcal{H}_A^{kin} \;=\; \sum_{\vec{k}} \epsilon(\vec{k})\; c_\mu^\dagger(\vec{k})\; c_\mu(\vec{k})\;, \tag{2.4}$$

$$\mathcal{H}_A^{d} \;=\; \epsilon_d\; d_\mu^\dagger d_\mu \;+\; U\; d_\uparrow^\dagger d_\uparrow d_\downarrow^\dagger d_\downarrow\;, \tag{2.5}$$

$$\mathcal{H}_A^{t} \;=\; \sum_{\vec{k}} \Big( t(\vec{k})\; c_\mu^\dagger(\vec{k})\; d_\mu \;+\; h.c. \Big)\;, \tag{2.6}$$

where $\mathcal{H}_A^{kin}$ is the conduction electron kinetic energy with the dispersion $\epsilon(\vec{k}) \equiv E(\vec{k}) - \epsilon_F$ measured from the Fermi level $\epsilon_F$, and $c_\mu^\dagger(\vec{k})$ creates a spin-$\mu$ conduction electron with a wavefunction $\propto \exp(i\,\vec{k}\,\vec{r})$. Eq. (2.5) is the impurity part with $\epsilon_d$ the energy of the localized level also measured from $\epsilon_F$, $\epsilon_d \equiv E_d - \epsilon_F$. The localized level can be occupied by localized electrons with two kinds of spin orientation created by $d_\mu^\dagger$, whereas the second term describes the Coulomb repulsion between $d$-level electrons. The $d$-level and the free electrons are coupled through a hopping term with the amplitude $t(\vec{k})$, as it is expressed by the tunneling part $\mathcal{H}_A^t$. Repeated spin indices $(\mu)$ are to be summed over $\{\uparrow, \downarrow\}$. The conduction electron operators are normalized to anticommute in such a way that

$$\left\{c_\mu^\dagger(\vec{k}), c_\nu(\vec{k}')\right\}_+ \;=\; \delta_{\mu,\nu}\,\delta_{\vec{k}\,,\vec{k}'}\,, \tag{2.7}$$

whereas

$$\left\{d^\dagger, d\right\}_+ \;=\; 1\,, \tag{2.8}$$

and the localized and conduction electron states are assumed to be orthogonal to each other.

Based on the average $d$-level occupancy, $\langle\, n_d \,\rangle \equiv \left\langle d_\mu^\dagger\, d_\mu \right\rangle$, we can distinguish four different types of parameter regimes [29]. The local moment regime, also called the Kondo regime, is characterized by $\langle\, n_d \,\rangle = 1$ and by the relations

$$E_d \ll \epsilon_F \ll E_d + U\,, \qquad\qquad \Delta \ll |\epsilon_d|\,,\, |\epsilon_d + U|\,, \tag{2.9}$$

where $\Delta(\epsilon) \equiv \pi \sum_{\vec{k}} |\,t(\vec{k})\,|^2\,\delta(\epsilon - \epsilon(\vec{k}))$ is the hybridization parameter, that describes the $d$-level broadening due to the tunneling between the $d$-level and the conduction electrons. This regime can be described by an effective Kondo model and additional potential scattering [54, 55].

Another magnetic regime is called intermediate valence regime. It occurs when $E_d$ or $E_d + U$ get within a distance of $\approx \Delta$ from the Fermi level, $\epsilon_F$. Then the charge fluctuations within the $d$-level become important, and $\langle\, n_d \,\rangle$ is no longer 1 but neither 0 nor 2.

Thus the above conditions imply the occurrence of a localized magnetic moment, that Anderson was looking for using the Hartree–Fock approximation [51].

There are two non-magnetic regimes as well, the doubly occupied and the empty orbital regimes with $\langle\, n_d \,\rangle = 2$ and $0$, respectively, occuring when $E_d + U$ is far below the Fermi level or $E_d$ is far above it.

The different regimes have first been looked into in detail in Ref. [56] using the numerical renormalization group (see Sec. 2.4).

## 2.3 Poor man's scaling approach

The poor man's scaling approach was introduced in 1970 by Anderson [57, 29] to derive the low-energy properties of the Kondo model. The idea of this method is that these properties are not affected if we reduce the conduction electron bandwidth, $D_F \;\rightarrow\; D \equiv D_F - \Delta D$ in small steps, $\Delta D$, and the effect of scattering into the high-energy excited states, that is into states near the band edges in the ranges $[\epsilon_F + D\,,\, \epsilon_F + D_F]$ and $[\epsilon_F - D\,,\, \epsilon_F - D_F]$, is taken into

account in the renormalization of the exchange coupling, $J$. Considering only second order scattering processes, this redefinition of the exchange coupling leads to the scaling equation

$$\frac{d\,J(D)}{d\,\log(D)} \;=\; -\,2\,\rho\,J^2(D)\,, \tag{2.10}$$

with $\rho$ the conduction electron density of states assumed to be constant (see Eq. (2.30)). This equation can be integrated to yield

$$J(D) \;=\; \frac{J\,(D_F)}{1\,+\,2\,\rho\,J\,(D_F)\,\log\,(D/D_F)}\,. \tag{2.11}$$

The form of $J(D)$ suggests that below a certain energy scale this perturbative description looses its validity as $J(D)$ becomes infinitely strong. The point, where the divergence sets in, is called the Kondo temperature, $T_K$. Up to second order in $J$, it is approximated by

$$k_B\,T_K \;=\; D_F\,\exp\{-\,1/\,[2\,\rho\,J(D_F)]\}\;. \tag{2.12}$$

The relevant energy scale is the temperature, $k_B\,T$ and the perturbative scaling approach works down to energies $D \;\approx\; \max(k_B\,T\,,\,k_B\,T_K)$. Eq. (2.10) describes trajectories on the $(D, J)$ plane. For $\rho\,J \;\ll\; 1$ each trajectory is characterized by a single parameter, $T_K$ which is thus scaling invariant. Points of the trajectories correspond to different systems that have a universal low-energy behavior in common.

The same approach has also been applied to the Anderson model [58], which is a more complicated problem in that it involves the renormalization of more model parameters.

As it is based on a weak coupling expansion, the poor man's scaling approach is successful only in energy domains higher than $k_B\,T_K$, but not suited for treating the strong coupling limit. Its significance lies in that the same scaling ideas combined with a non-perturbative approach led to solution of the Anderson and Kondo models in the strong coupling limit, as we will shortly see it in Section 2.4.

## 2.4 Numerical renormalization group

The numerical renormalization group is a non-perturbative RG technique, applicable to quantum impurity models and carried out numerically. It was devised by Wilson in the seventies [30] to overcome the shortcomings of analytic scaling approaches [59, 60, 57] that brake down once the amplitude of a relevant interaction becomes so large that it can no longer be treated perturbatively. These approaches are not good enough to solve the Kondo model in all the strong-, weak-coupling and crossover regimes simultaneously. Wilson's NRG was not only the first to describe all these regions, but up to this date it remained possibly the most reliable and versatile quantum impurity solver. There are many alternatives to NRG, like the Bethe ansatz [61, 62, 63, 64], boundary conformal field theory [27, 65], Abelian bosonization [28], the Yuval–Anderson [66, 67, 68] and the poor man's scaling approach [57], perturbative calculations [69, 59, 60], the Fermi liquid theory [70], the non-crossing approximation [71, 72] or other large-$N$ expansions [73], to name some of the most prominent ones. Apart from being very useful as these methods approach the problem from an analytic angle and contribute considerably to the understanding of quantum impurity physics, yet every method other than NRG has a narrower

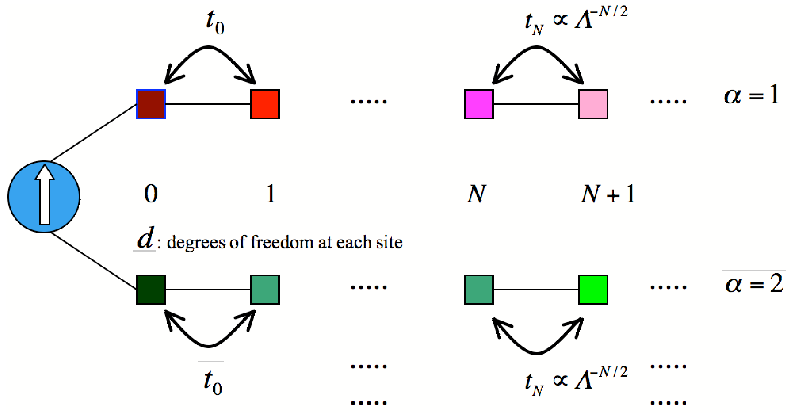


Figure 2.1: The Wilson chain. The impurity, represented by the circle on the left, couples only to the zeroth sites of the chains, $t_N$ stands for the hopping amplitudes between adjacent sites that decrease exponentially with the distance from the impurity. The number of independent degrees of freedom is $d$ at each site. Different chains, distinguished by the index $\alpha$, correspond to different types of electrons.

domain of applicability, i.e. can be applied only to a subrange of models, or to restricted regions in parameter space, or it is appropriate only for the calculation of certain properties.

Next we outline how NRG works so that it is possible to appreciate better the achievements listed afterwards. A detailed analysis of NRG is presented in the next subsections: 2.4.1–2.4.5.

To make a model amenable to NRG, first it is mapped into one dimension (1D) in energy space. Then, by choosing a discretization parameter $\Lambda > 1$, comes the logarithmic division of the conduction band into slimmer and slimmer intervals around the Fermi level: $\pm D_F \left[\Lambda^{-(n+1)}, \Lambda^{-n}\right]$ (with $D_F$ the conduction bandwidth and $n \in \mathbb{Z}^+$). To replace the continuum of electron states by a discrete set with countably infinitely many states, in each interval a new electron operator basis is introduced by means of a Fourier series expansion. This expansion is the reason for calling this part of the procedure "(logarithmic) discretization". Those electron states, that do not couple directly to the impurity, are neglected. These are the states, which are far from the impurity in position space and from the Fermi surface in momentum space. A unitary transformation takes the remaining degrees of freedom into a basis where the conduction electron kinetic energy assumes a hopping form with exponentially decreasing hopping amplitudes between adjacent sites along a 1D chain, the so-called Wilson chain. This situation is depicted in Fig. 2.1, where the possibility of having more chains, each corresponding to different types of electrons, is also included. The chains couple only through the impurity, and are distinguished by the index $\alpha$.—Recently there have been attempts to study impurities in a bosonic bath by applying NRG to Hamiltonians which are not of hopping form, that is omitting the last step of the transformations. This goes under the name of star-NRG [74, 75].—On the Wilson chain the impurity interacts only with the zeroth electron state sitting at only the zeroth site of the chain. This state is the possible most localized state at the impurity while still being in the conduction band. The subsequent states, corresponding to subsequent spherical layers surrounding the impurity, increase in width and consequently their momentum spread decreases.

The first step of the NRG procedure is solving the part of the hopping Hamiltonian which contains only the impurity and its coupling to the zeroth site. Each consecutive step consists in taking into account the coupling to electrons one site further away from the impurity. Due to

the exponentially decaying hopping amplitudes, by diagonalizing the subsequent Hamiltonians we can resolve the system properties at ever decreasing energy scales as new sites are considered. The knowledge of the energy spectrum and the eigenstates makes it possible to calculate thermodynamic properties [30], and, as it has become clear only later than the first applications of NRG, it can also be used to compute dynamical quantities [76, 77, 53, 78, 79, 80]. Such a quantity is e.g. the Laplace transform of the retarded Green's function, defined by

$$G^R_{A,B}(z) \equiv \int_{-\infty}^{\infty} G^R_{A,B}(t) e^{izt} dt \equiv -\frac{i}{\hbar}\int_0^{\infty} \mathrm{Tr}\left\{\hat{\varrho}\left[\hat{A}(t), \hat{B}(0)\right]_\xi\right\} e^{izt} dt \,, \tag{2.13}$$

where $\left[\hat{A}, \hat{B}\right]_\xi = \hat{A}\hat{B} - \xi\hat{B}\hat{A}$ with $\xi = \pm 1$ for bosonic/fermionic operators and $\hat{\varrho}$ the equilibrium density matrix. (Further explanation about the spectral and Green's functions is inserted in Appendix A.) In NRG $G^R_{A,B}(z)$ can be computed for local operators. Local means that they act only at the impurity or nearby sites. A detailed discussion of how to calculate $G^R_{A,B}(z)$, i.e what the natural basis is for the evaluation of the trace and what approximations are involved, is presented in Chapter 3 and in particular in Subsection 3.2.3.

The Hilbert space grows exponentially with the inclusion of extra sites by a factor of $d$ at each step (with $d$ the dimension of the local Hilbert space at the added site). This growth poses a problem in the numerical calculations. Due to this at each step, a part of the high-energy states are discarded. This truncation, just as the omission of certain states and thus certain terms from the Hamiltonian introduce systematic errors into the calculations. Remarkable improvements dated from the nineties to enhance the precision of NRG calculations, are the interleaving or $z$-averaging, which is an improved discretization scheme [81, 82]; and the self-energy trick for the calculation of Green's functions [83]. An alternative discretization with the use of an overcomplete basis has been proposed recently [84]. Its application can be advantageous for models with more than one impurity. Another very recent proposal to achieve better resolution at high-energies is described in [85].

Recent important conceptual advances in the field of calculating dynamical quantities are the Density Matrix-NRG (DM-NRG) algorithm [86] and the use of a complete basis on the Wilson chain [87]. This latter concept was originally introduced to study time-dependence, and it was found out only recently that by using it in combination with the reduced density matrix, very precise, spectral sum rule preserving spectral functions can be computed [88, 89, 102]. Further innovations were the incorporation of non-Abelian symmetries into DM-NRG [90, 91], which is the subject of Chapter 3; and the scattering state NRG formalism for the study of finite-bias steady-state situations [100].

The scope of NRG includes an exceptionally wide range of models. Originally it has been applied to the 1-Channel spin-half Kondo (1CK) model [30], but soon it was extended to deal with the one-channel spin-half Anderson model [56]. Furthermore it was used to study the superposition of potential scattering and the 1CK model [92, 93, 91], the spin-one and spin-3/2 Kondo models [94, 95] e.g. for finding the right spin model for Fe impurities in Au and Ag. Applications include the 2-Channel spin-half Kondo (2CK) model [96, 110, 65, 91] as well as the two-impurity Kondo [106, 107, 126] and the two-impurity Anderson models [125, 127], that are basic patterns for describing non-Fermi liquid (NFL) physics (see Chapter 4). Even clusters of three-impurities have been considered [128, 129]. The domain of NRG now also covers impurities coupled to a local phonon mode, such as the Anderson–Holstein model [130, 131, 132, 133], impurities in bosonic baths [74, 75], such as the spin-boson model, and the Bose–Fermi Kondo

model with coupling both to a fermionic conduction band and to a dissipative bosonic bath [134, 135].

In the past ten years NRG became increasingly popular for with the development of nanotechnology it has got feasible to create tunable mesoscopic devices which made a way to the thorough examination of strongly correlated phenomena. Such devices are quantum dots in various setups coupled to normal, superconducting, spin-polarized, etc. leads which can be described by quantum impurity models. Several NRG calculations of transport through quantum dots have appeared [136, 137, 140] (for more references see e.g. [138, 117]). Further details on this topic can be found in Sec. 4.2.

Lately the application of NRG in the framework of Dynamical Mean-Field Theory (DMFT) [24] has turned into an active field of research. DMFT is a tool for the investigation of lattice models like the Hubbard or the Kondo lattice models. These models are interesting in as much as they can provide a clue e.g. to the understanding of high-$T_c$ superconductivity [1, 2], or explain the behavior of heavy fermion compounds [4, 3]. DMFT maps the lattice model onto an effective impurity model which is then to be solved self-consistently. For its flexibility and high resolution at low-energies, NRG is becoming more and more popular as the impurity solver in DMFT studies [120, 121, 24, 122, 123, 124, 139, 85]. Another exciting new direction is the cluster dynamical mean-field theory (CDMFT) [141] that maps the lattice model onto a cluster of impurities. CDMFT outgrew from the need to resolve not only temporal but also spatial correlations in lattice models, a possibility which is ruled out in DMFT. CDMFT combined with NRG is a promising candidate for providing better resolution than present CDMFT studies that use e.g. exact diagonalization [142, 143] for solving the periodic two-impurity Anderson model. This is one of the simplest models that can capture the competition between the Kondo screening of the localized moments by conduction electrons and their ordering due to the so-called Ruderman–Kittel–Kasuya–Yoshida interaction, and thus might give insight into the properties of Kondo lattice models and possibly to heavy fermion physics.

### 2.4.1 Reduction from 3D to 1D for the Anderson model

This part contains the derivation that leads from the three-dimensional (3D) Anderson impurity Hamiltonian defined in discrete $\vec{k}$-space to a one-dimensional (1D) form in continuous energy space. This 1D form is the starting point of the next two Subsections, 2.4.2 and 2.4.3, where via approximations and unitary transformations we obtain the Hamiltonian which appears in the NRG calculations. The derivation presented is largely built on Ref. [56].

Eq. (2.3) is equivalent to the form

$$\mathcal{H}_A = -\frac{U}{2} + \sum_{\vec{k}} \epsilon(\vec{k})\, c^\dagger_\mu(\vec{k})\, c_\mu(\vec{k}) + \left(\epsilon_d + \frac{U}{2}\right) d^\dagger_\mu d_\mu + \frac{U}{2}\left(d^\dagger_\mu d_\mu - 1\right)^2 + \sum_{\vec{k}} \left(t(\vec{k})\, c^\dagger_\mu(\vec{k})\, d_\mu + h.c.\right) . \quad (2.14)$$

In going from the lattice to the continuum limit we make the substitutions:

$$\sum_{\vec{k}} \;\rightarrow\; \int d^3k \, \frac{V}{(2\pi)^3} \,, \tag{2.15}$$

$$\sqrt{\frac{V}{(2\pi)^3}} \, c(\vec{k}) \;\rightarrow\; \psi(\vec{k}) \,, \tag{2.16}$$

with $V$ the volume of the system. After dropping the constant term from the impurity part of Eq. (2.14) these substitutions lead to

$$\mathcal{H}_A \;=\; \int d^3k \, \epsilon(\vec{k}) \, \psi^\dagger_\mu(\vec{k}) \, \psi_\mu(\vec{k}) \;+\; \left(\epsilon_d + \frac{U}{2}\right) \, d^\dagger_\mu d_\mu \;+\; \frac{U}{2} \left(d^\dagger_\mu d_\mu - 1\right)^2 + \sqrt{\frac{V}{(2\pi)^3}} \int d^3k \, \left(t(\vec{k}) \, \psi^\dagger_\mu d_\mu \;+\; h.c.\right) \,, \tag{2.17}$$

with

$$\left\{\psi^\dagger_\mu(\vec{k}),\; \psi_\nu(\vec{k}')\right\}_+ \;=\; \delta_{\mu,\nu} \, \delta(\vec{k} \;-\; \vec{k}') \,. \tag{2.18}$$

Now we expand $\psi_\mu(\vec{k})$ in terms of spherical waves as[2]

$$\psi_\mu(\vec{k}) \;\equiv\; \frac{1}{k} \sum_{l,m,\mu} a_{lm\mu}(k) \; Y_l^m(\hat{k})^* \,, \tag{2.21}$$

$$a_{lm\mu}(k) \;=\; k \int d\Omega_{\hat{k}} \; Y_l{}^m(\hat{k}) \; \psi_\mu(\vec{k}) \,, \tag{2.22}$$

where $Y_l^m(\hat{k})$ are the spherical harmonics with $\hat{k}$ and $k$ the direction and the length of $\vec{k}$, respectively, and $d\Omega_{\hat{k}}$ is the integral measure on the unit sphere with the normalization $\int d\Omega_{\hat{k}} \;=\; 4\pi$. These relations imply that

$$\left\{a^\dagger_{lm\mu}(k),\; a_{l'm'\nu}(k')\right\}_+ \;=\; \delta_{l,l'} \; \delta_{m,m'} \; \delta_{\mu,\nu} \, \delta(k \;-\; k') \,. \tag{2.23}$$

[2] From the Fourier transform of $\psi(\vec{k})$:

$$\Psi_\mu(\vec{r}) \;=\; \int d^3k \; \exp(i\vec{k}\vec{r}) \; \psi_\mu(\vec{k}) \,, \tag{2.19}$$

$a_{lm\mu}(k)$ can be expressed as

$$a_{lm\mu}(k) \;=\; \int_0^\infty dr \, r^2 \, k \, j_l(kr) \, i^l 4\pi \int d\Omega_{\hat{r}} \; Y_l^m(\hat{r}) \, \Psi_\mu(\vec{r}) \,, \tag{2.20}$$

with $j_l(kr)$ the spherical Bessel functions of the first type [104] and $\hat{r}$ and $r$ are the direction and the length of $\vec{r}$, respectively. The general form of the functions $j_l(kr)$ allows the appearance of the factor $1/k$ in Eq. (2.21).

Now we make a transition to an isotropic dispersion relation: $\epsilon(\vec{k}) \rightarrow \epsilon(k) \equiv \epsilon(|\vec{k}|)$ and hopping: $t(\vec{k}) \rightarrow t(k) \equiv t(|\vec{k}|)$ . These assumptions reduce the terms of the Hamiltonian to

$$\int d^3k\, \epsilon(\vec{k})\, \psi^\dagger_\mu(\vec{k})\, \psi_\mu(\vec{k}) \;=\; \sum_{lm} \int dk\, \epsilon(k)\, a^\dagger_{lm\mu}(k)\, a_{lm\mu}(k)\,, \tag{2.24}$$

$$\sqrt{\frac{V}{(2\pi)^3}} \int d^3k\, \left( t(\vec{k})\, \psi^\dagger_\mu d_\mu \,+\, h.c. \right) \;=\; \sqrt{\frac{V}{2\pi^2}} \int dk\, k \left( t(k)\, a^\dagger_{00\mu}(k)\, d_\mu \,+\, h.c. \right) . \tag{2.25}$$

Here we have used the explicit from $1/\sqrt{4\pi}$ of $Y^0_0$ . From now on we deal only with the $s$-channel part of the kinetic energy. We also pass over to work in energy space by introducing

$$a_\mu(\epsilon) \;\equiv\; \left[ \frac{d\epsilon(k)}{dk} \right]^{-1/2} a_{00\mu}(k)\,, \quad \text{where} \quad \epsilon \,=\, \epsilon(k)\,, \tag{2.26}$$

thus

$$\left\{ a^\dagger_\mu(\epsilon),\, a_\nu(\epsilon') \right\}_+ \;=\; \delta_{\mu,\nu} \left[ \frac{d\epsilon(k)}{dk} \right]^{-1} \delta(k \,-k') \,=\, \delta(\epsilon \,-\epsilon')\,. \tag{2.27}$$

As we are interested in the low-energy properties of the system, we impose a UV cut-off by considering only energies in an interval of $2D_F$ length around the Fermi level, $E(k) \in [\epsilon_F \,-\, D_F,\, \epsilon_F \,+\, D_F]$ . This interval is the conduction band, and $D_F$ is called the bandwidth. This way we obtain the forms

$$\int dk\, \epsilon(k)\, a^\dagger_{00\mu}(k)\, a_{00\mu}(k) \,=\, \int dk\, \epsilon(k) \frac{d\epsilon(k)}{dk}\, a^\dagger_\mu(\epsilon)\, a_\mu(\epsilon) \,=\, \int_{-D_F}^{D_F} d\epsilon\, \epsilon\, a^\dagger_\mu(\epsilon)\, a_\mu(\epsilon)\,, \tag{2.28}$$

$$\begin{aligned} &\sqrt{\frac{V}{2\pi^2}} \int dk\, k \left( t(k)\, a^\dagger_\mu(k)\, d_\mu \,+\, h.c. \right) \\ &\qquad = \sqrt{\frac{V}{2\pi^2}} \int dk\, k \left( t(k) \left( \frac{d\epsilon(k)}{dk} \right)^{1/2} a^\dagger_\mu(\epsilon)\, d_\mu \,+\, h.c. \right) \\ &\qquad = \int_{-D_F}^{D_F} d\epsilon\, [\rho(\epsilon)]^{1/2} \left( t(\epsilon)\, a^\dagger_\mu(\epsilon)\, d_\mu \,+\, h.c. \right) , \end{aligned} \tag{2.29}$$

on applying the definition of the conduction electron density of states (DOS)

$$\rho(\epsilon) \,\equiv\, \sum_{\vec{k}'} \delta(\epsilon \,-\, \epsilon(\vec{k}')) \,\rightarrow\, \frac{V}{(2\pi)^3} \int d^3k'\, \delta\left( \epsilon \,-\, \epsilon(\vec{k}') \right) \,=\, \frac{V}{2\pi^2}\, k^2 \left[ \left. \frac{d\epsilon(k)}{dk} \right|_{\epsilon(k)=\epsilon} \right]^{-1} . \tag{2.30}$$

To further simplify the situation we ignore the energy-dependence of $\rho(\epsilon)$ and $t(\epsilon)$ and replace them by their values at the Fermi surface: $\rho \equiv \rho(0)$ and $t \equiv t(0)$ .[3] Furthermore we start to

[3]The energy-dependence of $\rho(\epsilon)$ and $t(\epsilon)$ can also be taken into account in the NRG calculations, as it is shown in Appendix B.

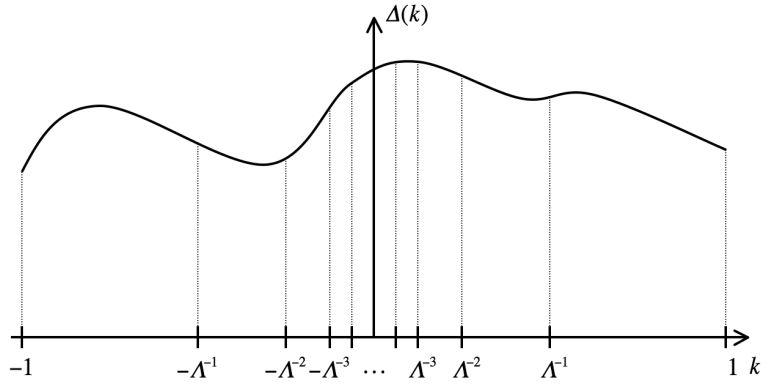


Figure 2.2: Logarithmic partitioning of the conduction band and a hybridization function.

measure energies in units of the bandwidth, $D_F$, by changing $\epsilon$ to $\mathcal{E} \equiv \epsilon/D_F$ and using the operators $a_\mu(\mathcal{E}) \equiv \sqrt{D_F}\, a_\mu(\epsilon)$ which makes $\left\{a^\dagger(\mathcal{E}),\, a(\mathcal{E}')\right\} = \delta(\mathcal{E} - \mathcal{E}')$. In terms of these operators the dimensionless version of the Hamiltonian is

$$\frac{\mathcal{H}_A}{D_F} = \left[\int_{-1}^{1} d\mathcal{E}\; \mathcal{E}\; a_\mu^\dagger(\mathcal{E})\; a_\mu(\mathcal{E}) \;+\; \frac{1}{D_F}\left(\epsilon_d + \frac{U}{2}\right)\; d_\mu^\dagger d_\mu \;+\; \frac{U}{2D_F}\left(d_\mu^\dagger d_\mu - 1\right)^2 + \left(\frac{\Delta}{\pi D_F}\right)^{1/2} \int_{-1}^{1} d\mathcal{E}\; \left(a_\mu^\dagger(\mathcal{E})\; d_\mu \;+\; h.c.\right)\right] , \quad (2.31)$$

with $\Delta = \pi\, \rho\, t^2$ the hybridization parameter introduced earlier.

### 2.4.2 Logarithmic discretization

Let us divide the $\mathcal{E}$-space interval $[-1,\, 1]$ into a sequence of intervals as in Fig. 2.2. The $n^{th}$ interval for positive $\mathcal{E}$'s is $\left(\Lambda^{-(n+1)},\, \Lambda^{-n}\right]$ with $\Lambda > 1$ the discretization parameter. Now let us define in each interval a complete set of orthonormal functions, the sine and cosine functions with appropriate frequencies, as

$$\psi_{np}^{\pm}(\mathcal{E}) \equiv \begin{cases} \frac{1}{\sqrt{l_n}}\, \exp\left(\pm\, i\, \omega_n\, p\, \mathcal{E}\right) , & \text{if } \Lambda^{-(n+1)} < \pm\,\mathcal{E} \leq \Lambda^{-n} , \\ 0 , & \text{elsewhere,} \end{cases} \quad (2.32)$$

with $n \in \{0, 1, 2, \dots\}$ the interval index, $p \in \mathbb{Z}$ the Fourier harmonic index, the superscript $\pm$ distinguishing the positive and negative $\mathcal{E}$ intervals, and $\omega_n$ is given by

$$\omega_n \equiv \frac{2\pi}{l_n} , \quad (2.33)$$

with $l_n$ the length of the $n^{th}$ interval

$$l_n \equiv \Lambda^{-n} - \Lambda^{-(n+1)} . \quad (2.34)$$

We Fourier series expand $a_\mu(\mathcal{E})$ in terms of these complete basis sets given in each interval as

$$a_\mu(\mathcal{E}) = \sum_{np} \left[a_{np\mu}\, \psi_{np}^{+}(\mathcal{E}) \;+\; b_{np\mu}\, \psi_{np}^{-}(\mathcal{E})\right] , \quad (2.35)$$

with

$$a_{np\mu} = \int_{-1}^{1} d\mathcal{E} \; \left[\psi^{+}_{np}(\mathcal{E})\right]^{*} a_{\mu}(\mathcal{E}) \,, \tag{2.36}$$

$$b_{np\mu} = \int_{-1}^{1} d\mathcal{E} \; \left[\psi^{-}_{np}(\mathcal{E})\right]^{*} a_{\mu}(\mathcal{E}) \,. \tag{2.37}$$

These expansion modes form a complete set of independent, discrete, electron operators satisfying the anticommutation relations

$$\left\{a^{\dagger}_{np\mu},\; a_{n'p'\mu'}\right\}_{+} = \delta_{n,n'}\,\delta_{p,p'}\,\delta_{\mu,\mu'} \,, \tag{2.38}$$

$$\left\{b^{\dagger}_{np\mu},\; b_{n'p'\mu'}\right\}_{+} = \delta_{n,n'}\,\delta_{p,p'}\,\delta_{\mu,\mu'} \,. \tag{2.39}$$

Thus, in terms of these operators we have the following contributions to $\mathcal{H}_A^{kin}$

$$\int_{-1}^{1} d\mathcal{E}\; \mathcal{E}\; a^{\dagger}_{\mu}(\mathcal{E})\; a_{\mu}(\mathcal{E}) = \frac{1 \,+\, \Lambda^{-1}}{2} \sum_{np} \Lambda^{-n} \left(a^{\dagger}_{np\mu}\; a_{np\mu} \;-\; b^{\dagger}_{np\mu}\; b_{np\mu}\right) + \frac{1 \,-\, \Lambda^{-1}}{2\pi i} \sum_{n,p\neq p'} \frac{\Lambda^{-n}}{p' \,-\, p} \left(a^{\dagger}_{np\mu} a_{np'\mu} \;-\; b^{\dagger}_{np\mu} b_{np'\mu}\right) \exp\left[\frac{2\pi i\,(p' \,-\, p)}{1 \,-\, \Lambda^{-1}}\right] . \tag{2.40}$$

As

$$\int_{-1}^{1} d\mathcal{E}\; a_{\mu}(\mathcal{E}) = \left(1 \,-\, \Lambda^{-1}\right)^{1/2} \sum_{n} \Lambda^{-n/2} \left(a_{n0\mu} \,+\, b_{n0\mu}\right) \,, \tag{2.41}$$

the impurity couples directly only to $a_{n0\mu}$ and $b_{n0\mu}$. If $\Lambda$ is close to 1, then the second sum on the RHS of Eq. (2.40) may be neglected. Even for larger values of $\Lambda$ the following approximation consists in the neglect of the terms containing $a_{np}$ and $b_{np}$ for $p \neq 0$

$$\frac{\mathcal{H}_A}{D_F} = \frac{1 \,+\, \Lambda^{-1}}{2} \sum_{n} \Lambda^{-n} \left(a^{\dagger}_{n\mu}\; a_{n\mu} \;-\; b^{\dagger}_{n\mu}\; b_{n\mu}\right) + \frac{1}{D_F} \left(\epsilon_d + \frac{U}{2}\right) d^{\dagger}_{\mu} d_{\mu} + \frac{U}{2D_F} \left(d^{\dagger}_{\mu} d_{\mu} - 1\right)^2 + \left(\frac{2\,\Delta}{\pi\; D_F}\right)^{1/2} \left(f^{\dagger}_{0\mu} d_{\mu} \;+\; h.c.\right) \,, \tag{2.42}$$

with

$$f_{0,\mu} \equiv \frac{1}{\sqrt{2}} \int_{-1}^{1} d\mathcal{E}\; a_{\mu}(\mathcal{E}) = \left(\frac{1 \,-\, \Lambda^{-1}}{2}\right)^{1/2} \sum_{n} \Lambda^{-n/2} \left(a_{n\mu} \,+\, b_{n\mu}\right) \,, \tag{2.43}$$

with $a_{n\mu} \equiv a_{n0\mu}$, $b_{n\mu} \equiv b_{n0\mu}$. The factor $1/\sqrt{2}$ has been introduced to have $\left\{f_{0,\mu},\; f^{\dagger}_{0,\nu}\right\}_{+} = \delta_{\mu,\nu}$.

### 2.4.3 Conversion to a hopping form

Here we show how $\mathcal{H}_A^{kin}$, or in fact how the free part of any one-dimensional Hamiltonian can be converted into a nearest neighbor hopping form. In Eq. (2.42) the impurity is coupled only to the $f_0$ electron operator. It is convenient to make a unitary transformation from $\{a_{n\mu}, b_{n\mu}\}$ to a new orthonormal set $\{f_{n,\mu}\}$ with $f_0$ given by Eq. (2.43). Since the conduction electron kinetic energy is diagonal in $\{a_{n\mu}, b_{n\mu}\}$, its transformations in general result in a non-diagonal form. We insist on having a kinetic energy which comprises only nearest neighbor hoppings, i.e. that $f_{n,\mu}$ is coupled only to $f_{(n\pm1),\mu}$. More precisely we require the conduction electron kinetic energy part of the Hamiltonian to be of the form

$$\frac{\mathcal{H}_A^{kin}}{D_F} \;=\; \frac{1 \,+\, \Lambda^{-1}}{2} \sum_{n=0}^{\infty} \Lambda^{-n/2}\, \xi_n \left( f_{n,\mu}^\dagger f_{(n+1),\mu} \,+\, h.c. \right) \,. \tag{2.44}$$

We write the unitary transformation in the following real, orthogonal form (to ease the notation, and since electrons with different spins do not couple, we omit spin indices)

$$f_n \;=\; \sum_m \left( u_{nm} a_m \,+\, v_{nm} b_m \right) \,, \tag{2.45}$$

with $u_{nm}$ and $v_{nm}$ being real numbers. It follows that the inverse transformation is

$$a_m \;=\; \sum_n u_{nm}\, f_n \,, \tag{2.46}$$

$$b_m \;=\; \sum_n v_{nm}\, f_n \,. \tag{2.47}$$

The coefficients $u_{0m}$ and $v_{0m}$ are already defined as

$$u_{0m} \;=\; v_{0m} \;=\; \left( \frac{1 \,-\, \Lambda^{-1}}{2} \right)^{1/2} \Lambda^{-m/2} \,. \tag{2.48}$$

The further coefficients can be determined recursively. It turns out that for constant hybridization

$$\xi_n \;=\; \frac{1 \,-\, \Lambda^{-n-1}}{\left(1 \,-\, \Lambda^{-2n-1}\right)^{1/2} \left(1 \,-\, \Lambda^{-2n-3}\right)^{1/2}} \,. \tag{2.49}$$

For the details of the derivation see Appendix B or Ref. [30].

### 2.4.4 Solution of the Wilson chain

To solve $\mathcal{H}_A \,/\, D_F$ Wilson defined a sequence of Hamiltonians as

$$\mathcal{H}_A^N \;=\; \Lambda^{(N-1)/2} \left[ \sum_{n=0}^{N-1} \Lambda^{-n/2}\, \xi_n \left( f_{n,\mu}^\dagger f_{(n+1),\mu} \,+\, h.c. \right) \,+\, \tilde{E}_d\, d_\mu^\dagger d_\mu \right.$$
$$\left. +\, \tilde{U} \left( d_\mu^\dagger d_\mu - 1 \right)^2 \,+\, \tilde{\Delta}^{1/2} \left( f_{0\mu}^\dagger d_\mu \,+\, h.c. \right) \right] \,, \tag{2.50}$$

with

$$\tilde{E}_d = \frac{2}{1 + \Lambda^{-1}} \frac{1}{D_F} \left( \epsilon_d + \frac{U}{2} \right) , \tag{2.51}$$

$$\tilde{U} = \frac{2}{1 + \Lambda^{-1}} \frac{U}{2D_F} , \tag{2.52}$$

$$\tilde{\Delta} = \left( \frac{2}{1 + \Lambda^{-1}} \right)^2 \frac{2\,\Delta}{\pi\, D_F} . \tag{2.53}$$

Then $\mathcal{H}_A$ can be recovered as the limit

$$\mathcal{H}_A = \lim_{N \to \infty} \frac{\left(1 + \Lambda^{-1}\right)\, D_F}{2} \Lambda^{-(N-1)/2}\, \mathcal{H}_A^N . \tag{2.54}$$

The $\mathcal{H}_A^N$'s are diagonalized iteratively, and their low-energy spectrum is presumed to describe the physics of $\mathcal{H}_A$ on the energy scale $\approx D_F\, \Lambda^{-(N-1)/2}$.

### 2.4.5 Mapping the Kondo model from 3D to 1D

In the rest of the thesis we shall mostly be dealing with the two-channel Kondo model instead of the Anderson model. For clarity here we show how to map the Kondo interaction from 3D to the Wilson chain. The reason why we discussed the Anderson model first or that we discussed it at all is that it is a more general model which involves the Kondo model as a limiting case. Furthermore certain derivations, like the one in Appendix B for the energy-dependent DOS exists in the literature only for the Anderson model, and we intend to be exhaustive.

The multi-channel, spin-half Kondo model (MCK) consists of an impurity with a magnetic moment $S = \frac{1}{2}$ immersed in a Fermi liquid (FL) of $N$ types of electrons (labeled by the flavor or channel index $\alpha \in \{1, \ldots, N\}$), and interacting with them through an exchange interaction. In discrete $k$-space this Hamiltonian takes on the form

$$\mathcal{H}_{MCK} = \sum_{\alpha,\mu} \sum_{\vec{k}} \epsilon(\vec{k})\; c^\dagger_{\alpha\mu}(\vec{k}) c_{\alpha\mu}(\vec{k}) \;+\; \sum_{\alpha} \bar{J}_\alpha \sum_{\mu,\nu} \sum_{\vec{k},\vec{k}'} \vec{S}\; c^\dagger_{\alpha\mu}(\vec{k}) \frac{\vec{\sigma}_{\mu\nu}}{2} c_{\alpha\nu}(\vec{k}') , \tag{2.55}$$

with $\vec{S}$ the impurity spin operator, $\vec{\sigma}$ the vector triad of Pauli matrices and in this subsection we denote all summation over discrete labels explicitly.

Taking the continuum limit as in Eqs. (2.15)-(2.16) we obtain

$$\begin{aligned} \mathcal{H}_{MCK} = & \sum_{\alpha,\mu} \int d^3k\, \epsilon(\vec{k})\; \psi^\dagger_{\alpha\mu}(\vec{k}) \psi_{\alpha,\mu}(\vec{k}) \\ & + \frac{V}{(2\pi)^3} \sum_{\alpha} \bar{J}_\alpha \sum_{\mu,\nu} \int d^3k \int d^3k'\; \vec{S}\; \psi^\dagger_{\alpha\mu}(\vec{k}) \frac{\vec{\sigma}_{\mu\nu}}{2} \psi_{\alpha\nu}(\vec{k}') . \end{aligned} \tag{2.56}$$

By making a Fourier transform

$$\Psi_{\alpha\mu}(\vec{r}) = \int d^3k\, \exp\left( i\, \vec{k}\, \vec{r} \right) \psi_{\alpha\mu}(\vec{k}) , \tag{2.57}$$

the anticommutation relations remain almost unchanged, i.e.

$$\left\{\Psi^{\dagger}_{\alpha\mu}\left(\vec{r}\right),\Psi_{\beta\nu}\left(\vec{r}'\right)\right\}_{+} \;=\; (2\,\pi)^{3}\;\delta_{\alpha,\beta}\,\delta_{\mu,\nu}\;\delta\left(\vec{r}\;-\;\vec{r}'\right)\;, \tag{2.58}$$

$$\tag{2.59}$$

in contrast to

$$\left\{\psi^{\dagger}_{\alpha\mu}\left(\vec{k}\right),\psi_{\beta\nu}\left(\vec{k}'\right)\right\}_{+} \;=\; \delta_{\alpha,\beta}\,\delta_{\mu,\nu}\,\delta\left(\vec{k}-\vec{k}'\right)\;, \tag{2.60}$$

and it becomes apparent that the coupling is local between the impurity and the conduction electrons

$$\mathcal{H}_{MCK}\;=\;\sum_{\alpha,\mu}\int d^{3}k\,\epsilon(\vec{k})\,\psi^{\dagger}_{\alpha\mu}(\vec{k})\,\psi_{\alpha\mu}(\vec{k})\;+\;\frac{V}{(2\pi)^{3}}\,\vec{S}\sum_{\alpha,\mu,\nu}\bar{J}_{\alpha}\,\Psi^{\dagger}_{\alpha\mu}\left(0\right)\,\frac{\vec{\sigma}_{\mu\nu}}{2}\,\Psi_{\alpha\nu}\left(0\right)\;. \tag{2.61}$$

Now, we expand $\Psi\left(\vec{r}\right)$ in terms of spherical waves as [104]

$$\Psi_{\alpha\mu}\left(\vec{r}\right) \;=\; \int_{0}^{\infty}dk\,k^{2}\int d\Omega_{\hat{k}}\,4\pi\sum_{l,m}i^{l}\,j_{l}(kr)\,Y_{l}^{m}(\hat{k})\,Y_{l}^{m*}(\hat{r})\,\psi_{\alpha\mu}(\vec{k}) \tag{2.62}$$

$$\;=\; \sum_{l,m}\int_{0}^{\infty}dk\,R_{kl}(r)\,Y_{l}^{m*}\left(\hat{r}\right)\;a_{lm\alpha\mu}(k)\;, \tag{2.63}$$

where $R_{kl}(r)$ are special functions (cf. Eq. (2.20)) and $a_{lm\alpha\mu}(k)$ is given as in Eq. (2.21) after tagging $\psi_{\alpha}(\vec{k})\;\rightarrow\;\psi_{\alpha\,\mu}(\vec{k})$ with an extra index $\alpha$. The probability of electrons to be found at the origin vanishes except for the $s$-wave part, i.e. $R_{kl}(0)\;=\;0$ unless $l\;=\;0$. It means that we can reduce the problem to a one-dimensional one again by considering only the following part of the electron field operator coupling to the impurity

$$\tilde{\Psi}_{\alpha,\mu}\left(r\right) \;=\; \sqrt{4\pi}\int_{0}^{\infty}dk\,\frac{\sin\left(kr\right)}{r}\,a_{00\alpha\mu}\left(k\right)\;, \tag{2.64}$$

with

$$\left\{a^{\dagger}_{lm\alpha\mu}(k),a_{l'm'\beta\nu}(k')\right\}_{+} \;=\; \delta_{l,l'}\,\delta_{m,m'}\,\delta_{\alpha,\beta}\,\delta_{\mu,\nu}\,\delta\left(k\;-\;k'\right)\;. \tag{2.65}$$

This way the following terms constitute the Hamiltonian

$$\mathcal{H}_{MCK}\;=\;\mathcal{H}^{l>0}\;+\;\mathcal{H}^{s}\;=\;\mathcal{H}^{l>0}\;+\;\sum_{\alpha,\mu}\int dk\,\epsilon(k)\,a^{\dagger}_{00\alpha\mu}(k)\,a_{00\alpha\mu}(k)$$
$$+\;\frac{V}{(2\pi)^{3}}\,\vec{S}\sum_{\alpha,\mu,\nu}\bar{J}_{\alpha}\,\tilde{\Psi}^{\dagger}_{\alpha\mu}\left(0\right)\,\frac{\vec{\sigma}_{\mu\nu}}{2}\,\tilde{\Psi}_{\alpha\nu}\left(0\right)\;, \tag{2.66}$$

where the part $\mathcal{H}^{l>0}$ describes channels other than $s$ and an isotropic dispersion relation is assumed. Again, we are interested in the long wavelength (low-energy) physics (and hence the impurity can be considered punctual) so we impose a UV cutoff, $D_{F}$, on the domain of

integration in $\epsilon$-space, i.e. we restrict $\epsilon(k)$ to the $[\epsilon_F - D_F, \epsilon_F + D_F]$ range, and change the integration variable from $k$ to $\epsilon$. So we get (by dropping the superfluous $l, m$ indices)

$$\mathcal{H}_{MCK} = \mathcal{H}^{l>0}_{MCK} + \mathcal{H}^{s}_{MCK} = \mathcal{H}^{l>0}_{MCK} + \sum_{\alpha,\mu} \int_{-D_F}^{D_F} d\epsilon\, \epsilon\, a^{\dagger}_{\alpha\mu}(\epsilon)\, a_{\alpha\mu}(\epsilon) + \vec{S} \sum_{\alpha,\mu,\nu} \bar{J}_{\alpha} \int_{-D_F}^{D_F} d\epsilon\, \sqrt{\rho(\epsilon)} \int_{-D_F}^{D_F} d\epsilon'\, \sqrt{\rho(\epsilon')}\, a^{\dagger}_{\alpha\mu}(\epsilon)\, \frac{\vec{\sigma}_{\mu\nu}}{2}\, a_{\alpha\nu}(\epsilon')\,. \quad (2.67)$$

From now on we take $\rho(\epsilon)$ to be constant $\rho \equiv \rho(0)$ in the conduction band. The dimensionless version of $\mathcal{H}^{s}_{MCK}$ reads

$$\frac{\mathcal{H}^{s}_{MCK}}{D_F} = \int_{-1}^{1} d\mathcal{E}\, \mathcal{E}\, a^{\dagger}_{\alpha,\mu}(\mathcal{E})\, a_{\alpha,\mu}(\mathcal{E}) + \vec{S} \sum_{\alpha,\mu,\nu} \bar{J}_{\alpha}\, \rho \int_{-1}^{1} d\mathcal{E} \int_{-1}^{1} d\mathcal{E}'\, a^{\dagger}_{\alpha\mu}(\mathcal{E})\, \frac{\vec{\sigma}_{\mu\nu}}{2}\, a_{\alpha\nu}(\mathcal{E}')\,, \quad (2.68)$$

with $\mathcal{E} \equiv \epsilon / D_F$. Once this has been done we can follow the prescriptions of the previous subsections to obtain a discrete approximation of $\mathcal{H}^{s}_{MCK}$ in a from suitable for NRG calculations, namely

$$\frac{2\,\mathcal{H}^{s}_{MCK}}{D_F\,(1 + \Lambda^{-1})} \approx \vec{S} \sum_{\alpha,\mu,\nu} \tilde{\mathcal{J}}_{\alpha}\, f^{\dagger}_{0,\alpha,\mu}\, \vec{\sigma}_{\mu\nu}\, f_{0,\alpha,\mu} + \sum_{n=0}^{\infty} \sum_{\alpha,\mu,\nu} t_n \left( f^{\dagger}_{n,\alpha,\mu}\, f_{n+1,\alpha,\mu} + h.c. \right), \quad (2.69)$$

with $\Lambda$ the discretization parameter, $\tilde{\mathcal{J}}_{\alpha} = 2\,\hat{J}_{\alpha}\,\left(1 + \Lambda^{-1}\right)^{-1}$, where $\hat{J}_{\alpha} = \bar{J}_{\alpha}\,\rho$ dimensionless. The $f_0$'s are anticommuting operators at the impurity site having the following form in terms of the $a_{\alpha\mu}(\epsilon)$ operators

$$f_{0,\alpha,\mu} = \frac{1}{\sqrt{2D_F}} \int_{-D_F}^{D_F} d\epsilon\, a_{\alpha\mu}(\epsilon)\,, \quad (2.70)$$

$$\left\{ f^{\dagger}_{0,\alpha,\mu}, f_{0,\beta,\nu} \right\}_{+} = \delta_{\alpha,\beta}\, \delta_{\mu,\nu}\,. \quad (2.71)$$

The second part of the Hamiltonian in Eq. (2.69) is the part of the Wilson chain that accounts for the dynamics of the electrons. The Hamiltonian of Eq. (2.69) has been used in our NRG calculations for the two-channel Kondo model described in detail in the forthcoming chapters.

# 3 Symmetries and density matrix in numerical renormalization group

Here we discuss some of the most recent conceptual improvements that took place in the field of calculating dynamical quantities with the Numerical Renormalization Group (NRG).

## 3.1 Symmetries in NRG

States and operators in "physical Hilbert spaces" are distinguished by quantum numbers. Widely encountered quantum numbers are the spin, the charge or the parity. These quantum numbers tell the transformation properties of a state or an operator under the action of some symmetry group. Wilson and his collaborators [56] realized that classifying states according to their transformation properties is important in NRG as it enhances the precision and speeds up the calculations. To extract the most accurate data possible from the NRG calculations, it is best to take into account the largest possible symmetry of the quantum impurity model. Yet NRG codes built so far could have handled only specific symmetry combinations suited for specific problems, and it has required a great deal of effort to adjust a few thousand line code to a new symmetry setup. We have overcome this difficulty by developing a flexible NRG code [25, 26] that can easily be adapted to the problem of interest and could make use of an arbitrary number and any type of discrete and compact, commuting Lie group symmetries that the impurity model may possess. For this to accomplish we have generalized the recursion relations that come up in the course of the NRG procedure, connecting subsequent iteration steps. On the following pages we refine these statements and show how an arbitrary number of discrete and compact Lie group symmetries can be used in the NRG process.

### 3.1.1 Symmetries of the one-channel Kondo model

In the NRG calculations, one uses the following approximation of the 1CK Hamiltonian introduced in [30] and discussed in detail in the previous chapter

$$H_{1CK} \;=\; \tilde{\mathcal{J}}\,\vec{S} \sum_{\mu,\nu\in\{\uparrow,\downarrow\}} f^{\dagger}_{0,\mu}\vec{\sigma}_{\mu\nu}f_{0,\nu} + \sum_{n=0}^{\infty}\sum_{\mu\in\{\uparrow,\downarrow\}} t_n\left(f^{\dagger}_{n,\mu}f_{n+1,\mu} + h.c.\right). \tag{3.1}$$

This Hamiltonian has an $\mathrm{SU}_S(2)$ symmetry, corresponding to spin rotations, i.e. it is invariant under the transformations

$$H_{1CK} \;=\; \mathcal{U}_s\, H_{1CK}\, \mathcal{U}_s^{\dagger}\,, \tag{3.2}$$

where the unitary operator $\mathcal{U}_s$ is generated by the total spin operators,

$$\mathcal{U}_s \equiv \mathcal{U}_s(\vec{\omega}_s) = e^{i\vec{\omega}_s\vec{S}_T} , \tag{3.3}$$

$$\vec{S}_T = \vec{S} + \frac{1}{2}\sum_{n=0}^{\infty}\sum_{\mu,\nu\in\{\uparrow,\downarrow\}} f^\dagger_{n,\mu}\vec{\sigma}_{\mu,\nu}f_{n,\nu} , \tag{3.4}$$

with $\vec{\omega}_S$ denoting a real, three-component vector. The Hamiltonian $H_{1CK}$ is also invariant under the action of $\mathrm{SU}_C(2)$ rotations, $\mathcal{U}_c = e^{i\vec{\omega}_c\vec{C}}$, generated by the operators $C^x = (C^+ + C^-)/2$, $C^y = (C^+ - C^-)/2i$ and $C^z$ with

$$\begin{aligned} C^+ &= \sum_{n=0}^{\infty}(-1)^n f^\dagger_{n,\uparrow}f^\dagger_{n,\downarrow} , \\ C^z &= \frac{1}{2}\sum_{n=0}^{\infty}\left(\sum_{\mu=\{\uparrow,\downarrow\}} f^\dagger_{n,\mu}f_{n,\mu} - 1\right) , \\ C^- &= \left(C^+\right)^\dagger , \end{aligned} \tag{3.5}$$

and parameterized by real, three-component vectors $\vec{\omega}_C$.

Since the spin symmetry generators commute with the charge symmetry generators, $H_{1CK}$ has a symmetry $\mathrm{SU}_S(2) \times \mathrm{SU}_C(2)$ [106, 107, 108]. Consequently, the eigenstates of the Hamiltonian form degenerate multiplets, $|i, \underline{Q}_i\ \underline{Q}^z_i\rangle$, that are classified by their multiplet label $i$, the spin and charge quantum numbers, $\underline{Q}_i \equiv \{S_i, C_i\}$,[1] and the $z$-components of the spin and charge operators, $\underline{Q}^z_i \equiv \{S^z_i, C^z_i\}$. There are at least two ways of interpreting the multiplet label. The first is that it assigns a unique index, $i$, to each multiplet. The other one is that we need this index only to distinguish multiplets with identical quantum numbers. In the following we will apply the former interpretation. Therefore the representation indices $\underline{Q}_i$ could be dropped from the labels of a state, i.e., $|i, \underline{Q}_i\ \underline{Q}^z_i\rangle \rightarrow |i, \underline{Q}^z_i\rangle$, since $\underline{Q}_i$ is determined uniquely by the multiplet label $i$ itself. However, to be more explicit, we keep this redundant label in what follows.

In the following we will refer to the quantum numbers $\underline{Q}_i$ as *representation indices*, while $\underline{Q}^z_i$ are referred to as *internal quantum numbers* of the internal basis states of a given multiplet. The representation index $\underline{Q}_i$ defines the dimension of the $i^{th}$ irreducible subspace which, in this example, is $\dim(i) = \dim(\underline{Q}_i) = (2S_i + 1)(2C_i + 1)$.

Similarly to the irreducible subspaces of the Hilbert space, operators can be organized into irreducible tensor operator multiplets [103]. One of the simplest examples is given by the impurity spin, from the components of which we can form an operator triplet as

$$\{A_m\} \equiv \left\{-\frac{1}{\sqrt{2}}\,S^+, S^z, \frac{1}{\sqrt{2}}\,S^-\right\} . \tag{3.6}$$

The components of this triplet transform under spin rotations as the eigenstates $|m\rangle$ of $S^z$, while they are invariant under charge rotations. This means that $A$ has quantum numbers $S_A = 1$ and $C_A = 0$, and the components of this operator multiplet are labeled by $S^z_A =$

[1] The eigenvalues of the operators $\vec{S}^2$ and $\vec{C}^2$ are $S(S+1)$ and $C(C+1)$, respectively.

$m, (m = 0, \pm 1)$, while the internal charge quantum number is trivially $C_A^z = 0$. Similarly to the eigenstates of the Hamiltonian, the quantum numbers of an irreducible tensor operator $B$ can be organized into a representation index vector, $\underline{b} = (S_B, C_B)$ and the components of $B$ are labeled by $\underline{b}^z = (S_B^z, C_B^z)$ taking the values $S_B^z = -S_B, -S_B + 1, \ldots, S_B$ and $C_B^z = -C_B, -C_B + 1, \ldots, C_B$. A further example for an $S = 1/2$ and $C = 1/2$ operator is formed by the four operators $\{f_{0,\uparrow}^\dagger, f_{0,\downarrow}^\dagger, f_{0,\downarrow}, -f_{0,\uparrow}\}$ (for a more details see p. 56).

The Wigner–Eckart theorem[2] tells that the matrix elements of the members of a given operator multiplet and states within two multiplets, $i$ and $j$ are related by

$$\left\langle i, \underline{Q}_i\ \underline{Q}_i^z \middle| B_{\underline{b},\underline{b}_z} \middle| j, \underline{Q}_j\ \underline{Q}_j^z \right\rangle = \langle i \parallel B \parallel j \rangle \left\langle \underline{Q}_i\ \underline{Q}_i^z \middle| \underline{b}\ \underline{b}_z; \underline{Q}_j\ \underline{Q}_j^z \right\rangle \tag{3.7}$$

where $\langle i \parallel B \parallel j \rangle$ denotes the reduced (invariant) matrix element of $B$, and the generalized Clebsch–Gordan coefficients are defined as

$$\left\langle \underline{Q}_i\ \underline{Q}_i^z \middle| \underline{b}\ \underline{b}_z; \underline{Q}_j\ \underline{Q}_j^z \right\rangle = \langle S_i\ S_i^z | S_B\ S_B^z; S_j\ S_j^z \rangle\ \langle C_i\ C_i^z | C_B\ C_B^z; C_j\ C_j^z \rangle\ , \tag{3.8}$$

with the usual SU(2) Clebsch–Gordan coefficients [103] on the right hand side. This relation is used extensively in the NRG calculations. Eq. (3.7) can be inverted as

$$\langle i \parallel B \parallel j \rangle = \frac{1}{\dim(i)} \sum_{\underline{Q}_i^z} \sum_{\underline{Q}_j^z, \underline{b}_z} \left\langle \underline{Q}_i\ \underline{Q}_i^z \middle| \underline{b}\ \underline{b}_z; \underline{Q}_j\ \underline{Q}_j^z \right\rangle^* \left\langle i, \underline{Q}_i\ \underline{Q}_i^z \middle| B_{\underline{b},\underline{b}_z} \middle| j, \underline{Q}_j\ \underline{Q}_j^z \right\rangle . \tag{3.9}$$

An important property of the unitary transformations above is that they are *local* in the sense that they decompose into unitary operators which commute with each other and act independently at different sites,

$$\mathcal{U} = \mathcal{U}_s \times \mathcal{U}_c\ , \tag{3.10}$$

$$\mathcal{U}_c = \prod_n \mathcal{U}_{c,n}\ , \tag{3.11}$$

$$\mathcal{U}_s = \prod_n \mathcal{U}_{s,n}\ . \tag{3.12}$$

This decomposition property is crucial for using symmetries in the NRG calculations, as it allows to exploit the presence of symmetries at each step of the NRG process all through the construction of the Wilson chain.

### 3.1.2 Symmetries on the Wilson chain

The symmetry considerations of Subsection 3.1.1 can be extended to general impurity Hamiltonians defined on the Wilson chain by

$$H = \mathcal{H}_0 + \sum_{n=0}^{\infty} (\tau_{n,n+1} + \mathcal{H}_{n+1})\ , \tag{3.13}$$

[2]Some of the considerations presented here do not apply to non-compact Lie groups.

where $\mathcal{H}_0$ contains the interaction between the impurity and the fermionic bath, and nearest-neighbors on the Wilson chain are coupled through the hopping terms, $\tau_{n,n+1}$. The $n^{th}$ on-site term, $\mathcal{H}_{n+1}$ describes local correlations/interactions, and it is zero for an electron-hole symmetrical band [112].

NRG solves the model defined in Eq. (3.13) by an iterative diagonalization process. The iteration steps consist in diagonalizing the set of Hamiltonians defined recursively by

$$H_0 = \mathcal{H}_0 \,, \tag{3.14}$$

$$H_n = H_{n-1} + \tau_{n-1,n} + \mathcal{H}_n \,. \tag{3.15}$$

Now let us assume that $H$, as well as every $H_n$, are invariant under the group $G$, i.e.

$$\mathcal{U}(g)\, H_n\, \mathcal{U}^{-1}(g) = H_n \,, \qquad n = 0, 1, 2, \dots \,, \tag{3.16}$$

holds for all $g \in G$ with $\mathcal{U}(g)$ an appropriate unitary representation of $G$. Furthermore, let us suppose that $G$ and correspondingly $\mathcal{U}$ can be decomposed into a direct product of $\Gamma$ subgroups $\mathcal{G}_\gamma$ $(\gamma = 1, ..., \Gamma)$, each acting independently on every lattice site,

$$G = \mathcal{G}_1 \times \mathcal{G}_2 \times \cdots \times \mathcal{G}_\Gamma \,, \tag{3.17}$$

$$\mathcal{U}(g) = \prod_{\gamma=1}^{\Gamma} \mathcal{U}_\gamma(g_\gamma) = \prod_{\gamma=1}^{\Gamma} \prod_n \mathcal{U}_{\gamma,n}(g_\gamma) \,. \tag{3.18}$$

The subgroups can also be finite, and so $\mathcal{G}_\gamma$ may denote a crystal field symmetry as well as e.g. the SU(3) group. However, some of the considerations may not apply to non-compact groups and not even to locally compact Lie groups, such as $\mathrm{SL}(2, \mathbb{C})$, since they have infinite-dimensional irreducible representations [218].

The above decomposition is not necessarily unique. Nevertheless, having obtained a specific decomposition of the symmetry, the argument of the previous subsection can be repeated with the only difference that now a total of $\Gamma$ number of quantum numbers classify the irreducible subspaces (multiplets) of the Hamiltonians $H_n$,

$$\underline{Q} = \left\{ Q^1, Q^2, ..., Q^\Gamma \right\} \tag{3.19}$$

and, by analogy to SU(2), states within the multiplet are labeled by the internal quantum numbers [3]

$$\underline{Q^z} = \left\{ Q^{1,z}, Q^{2,z}, ..., Q^{\Gamma,z} \right\} \,. \tag{3.20}$$

Similarly to the 1CK example, the dimension of a subspace $i$ depends uniquely on its quantum numbers $\underline{Q}_i$, i.e. $\dim(i) = \dim(\underline{Q}_i)$.

Operators can also be arranged into irreducible tensor operators, and an irreducible tensor operator multiplet $A$ is described by quantum numbers $\underline{a}$ accordingly, while members of the multiplet are labeled by $\underline{a}^z$ with $\underline{a}$ and $\underline{a}^z$ being $\Gamma$-component vectors. The Wigner–Eckart theorem, Eq. (3.7), applies to the general case too, with the slight modification that the generalized Clebsch–Gordan coefficients are now defined as

$$\left\langle \underline{Q}_i \, \underline{Q}_i^z \, \middle| \underline{a} \, \underline{a}^z ; \underline{Q}_j \, \underline{Q}_j^z \right\rangle \equiv \prod_{\gamma=1}^{\Gamma} \left\langle Q_i^\gamma \, Q_i^{\gamma,z} \, \middle| a^\gamma \, a^{\gamma,z} \, ; Q_j^\gamma \, Q_j^{\gamma,z} \right\rangle \,. \tag{3.21}$$

[3] For groups like SU(3), having a more complicated Cartan subalgebra, every component of the internal quantum numbers $Q^{i,z}$ is composed of several quantum numbers [103].

Now the dimension of the multiplet $i$ is given by

$$\dim(i) \equiv \prod_{\gamma=1}^{\Gamma} \dim(Q_i^\gamma) \,, \tag{3.22}$$

where $\dim(Q_i^\gamma)$ is the dimension of an irreducible representation characterized by the representation index $Q_i^\gamma$.

### 3.1.3 The role of symmetries in the diagonalization procedure

As it was scrutinized in Section 2.4, in Ref. [30] Wilson constructed approximate eigenstates of $H_n$ for a chain of length $n$ iteratively. The reason for the eigenstates being only approximate are as follows. At each iteration the dimension of the Hilbert space increases by a factor $d$, with $d$ the dimension of the local Hilbert space at a single site of the chain with site label $n > 0$. Therefore the size of the Hilbert space increases exponentially with $n$, and after a few iterations one must truncate it: Some of the states $i$ are discarded ($i \in D$), while other states are kept ($i \in K$), and are used to construct the eigenstates for $H_{n+1}$. Due to the truncation, however, these states will only be approximate eigenstates.

Symmetries are important in the diagonalization procedure. As we will argue below, in their presence the $H_n$'s are block diagonal in the representation indices, and thus the eigenvalue problem can be solved much more efficiently. For some of the physical quantities like the dynamical correlations, it turns out to be crucial to increase the number of kept states as much as possible to achieve sufficient numerical accuracy.

As discussed above, in the $n^{th}$ iteration the eigenstates (multiplets) of $H_n$ are constructed from the kept multiplets labeled by $u$ with $u \in K$ of the $(n-1)^{th}$ iteration (that are the approximate low-energy eigenstates of $H_{n-1}$) and from a complete set of *local states* (multiplets) at the $n^{th}$ site, labeled by $\mu$. In the sequel, we refer to these new approximate eigenstates $\tilde{i}$ as *new states*, and we call the kept states *block states* or *old states*.

In the presence of symmetries, each new multiplet carries representation indices $\underline{Q}_{\tilde{i}} = \{Q_{\tilde{i}}^\gamma\}$, and states within this multiplet are labeled by the internal quantum numbers $\underline{Q}_{\tilde{i}}^z = \{Q_{\tilde{i}}^{\gamma,z}\}$. Similarly, local states have quantum numbers $\underline{q}_\mu = \{q_\mu^\gamma\}$ and are further labeled by $\underline{q}_\mu^z = \{q_\mu^{\gamma,z}\}$. To construct the approximate eigenstates of $H_n$, we first construct new states from $\left|u, \underline{Q}_u \; \underline{Q}_u^z\right\rangle_{n-1}$ by adding the electrons at site $n$,

$$\left|u, \underline{Q}_u \; \underline{Q}_u^z\right\rangle_{n-1} \rightarrow \left|\mu, \underline{q}_\mu \; \underline{q}_\mu^z\right\rangle_{loc} \otimes \left|u, \underline{Q}_u \; \underline{Q}_u^z\right\rangle_{n} \,. \tag{3.23}$$

The addition of a new site corresponds to taking the tensor product of the local Hilbert space with that of the block states. Taking the tensor product constraints the group elements of all groups in the direct product decomposition of $G$ to be the same for all sites in a given transformation, just as it is written in Eq. (3.18). We use the Clebsch–Gordan coefficients to build from the block (old) and from the local states the new states that transform as irreducible multiplets under the symmetry transformations, $\mathcal{U}(g)$. From a given block state, $u$, and a local

state, $\mu$, we can form several new multiplets labeled by $\tilde{i}$ by the construction

$$\left|\tilde{i}, \underline{Q}_{\tilde{i}}\ \underline{Q}^z_{\tilde{i}}\right\rangle_n \equiv \sum_{\underline{Q}^z_u, \underline{q}^z_\mu} \left\langle \underline{Q}_{\tilde{i}}\ \underline{Q}^z_{\tilde{i}} \middle| \underline{q}_\mu\ \underline{q}^z_\mu; \underline{Q}_u\ \underline{Q}^z_u \right\rangle^* \left|\mu, \underline{q}_\mu\ \underline{q}^z_\mu\right\rangle_{loc} \otimes \left|u, \underline{Q}_u\ \underline{Q}^z_u\right\rangle_{n-1},$$

$$(\tilde{i} \leftarrow u, \mu \text{ with } u \in \mathrm{K}). \quad (3.24)$$

In this way, every new state $\tilde{i}$ "remembers" its parent states. The multiplets of Eq. (3.24) will be referred to as the *canonical basis* from now on. The vector space spanned by this basis can be decomposed into irreducible subspaces being invariant under the action of $G$. Their dimensions are determined by the representation indices $\underline{Q}_{\tilde{i}}$. Schur's lemmas [103] tell us that since $H_n$ is scalar under the group $G$, it has a block-diagonal structure, i.e. it connects only irreducible subspaces with the same representation indices

$$_n\left\langle \tilde{i},\ \underline{Q}_{\tilde{i}}\ \underline{Q}^z_{\tilde{i}}\ \middle|\ H_n\ \middle|\ \tilde{j},\ \underline{Q}_{\tilde{j}}\ \underline{Q}^z_{\tilde{j}} \right\rangle_n = {}_n\left\langle \tilde{i} \parallel H_n \parallel \tilde{j}\right\rangle_n \delta_{\underline{Q}_{\tilde{i}}, \underline{Q}_{\tilde{j}}} \delta_{\underline{Q}^z_{\tilde{i}}, \underline{Q}^z_{\tilde{j}}}. \quad (3.25)$$

Thus $H_N$ is diagonalized by a block-diagonal unitary transformation, $\mathcal{O}^{[n]}_{\tilde{i},i}$

$$\left|i, \underline{Q}_i\ \underline{Q}^z_i\right\rangle_n = \sum_{\tilde{i}} \mathcal{O}^{[n]}_{\tilde{i},i} \left|\tilde{i}, \underline{Q}_{\tilde{i}}\ \underline{Q}^z_{\tilde{i}}\right\rangle_n \delta_{\underline{Q}_i, \underline{Q}_{\tilde{i}}} \delta_{\underline{Q}^z_i, \underline{Q}^z_{\tilde{i}}}, \quad (3.26)$$

$$H_n \left|i, \underline{Q}_i\ \underline{Q}^z_i\right\rangle_n = E^n_i \left|i, \underline{Q}_i\ \underline{Q}^z_i\right\rangle_n, \quad (3.27)$$

with $E^n_i$ the eigenenergies of $H_n$. Here, $\mathcal{O}$ is a block-diagonal matrix, and its columns in a given symmetry sector are just the eigenvectors of the corresponding submatrix of ${}_n\langle \tilde{i} \parallel H_n \parallel \tilde{j}\rangle_n$ in the canonical basis. In the upcoming iteration, some of these multiplets will be kept, those of the lowest energy, and form the block states of the $(n+1)^{th}$ iteration, while the rest are discarded.

In the iteration step outlined above, the matrix elements ${}_n\langle \tilde{i} \parallel H_n \parallel \tilde{j}\rangle_n$ are needed, with $H_n = H_{n-1} + \tau_{n-1,n} + \mathcal{H}_n$. The matrix elements of $H_{n-1}$ follow from Eq. (3.24) and from the fact that the block states are the eigenstates of $H_{n-1}$. They are given by

$${}_n\left\langle \tilde{i} \parallel H_{n-1} \parallel \tilde{j}\right\rangle_n = E^{n-1}_u\, \delta_{\tilde{i},\tilde{j}}, \quad (3.28)$$

where $u$ is the state from which the state $\tilde{i}$ has been constructed. Similarly, the matrix elements of $\mathcal{H}_n$ are given by

$${}_n\left\langle \tilde{i} \parallel \mathcal{H}_n \parallel \tilde{j}\right\rangle_n = \varepsilon^n_\mu\, \delta_{\tilde{i},\tilde{j}}, \quad (3.29)$$

where $\varepsilon^n_\mu$ is just the expectation value of $\mathcal{H}_n$ with local states within the multiplet $\mu$. Finally, to compute the matrix elements of the hopping $\tau_{n-1,n}$, we use the fact that $\tau_{n-1,n}$ can always be decomposed as[4]

$$\tau_{n-1,n} = \sum_\alpha h^{[n-1]}_\alpha \sum_{\underline{c}^z} \left[ C^{[n-1]}_{\alpha;\underline{c},\underline{c}^z} \left(C^{[n]}_{\alpha;\underline{c},\underline{c}^z}\right)^\dagger + H.c. \right]. \quad (3.30)$$

[4]For a proof, see the first part of the proof in Appendix D.

Here $C^{[n-1]}_{\alpha;\underline{c},\underline{c}^z}$ denotes a *creation operator multiplet* at site $n-1$ that has quantum numbers $\underline{c}$, and the $h^{[n-1]}_\alpha$'s are the hopping amplitudes between sites $n-1$ and $n$. The index $\alpha$ in the equation above labels various "hopping operators". Here is an example: If we treat the 1CKM using only U(1) symmetries we have two hopping operators, $\alpha \in \{1,2\}$, corresponding to $C^{[n]}_1 = f^\dagger_{n,\uparrow}$ and $C^{[n]}_2 = f^\dagger_{n,\downarrow}$. However, if we use the spin SU(2) symmetry, then $\alpha = 1$ and $C^{[n]}_1 = \left\{ f^\dagger_{n,\uparrow}, f^\dagger_{n,\uparrow} \right\}$.

For the reduced matrix elements of $\tau_{n-1,n}$ we obtain the following formula upon using Eq. (3.24) and the decomposition in Eq. (3.30)

$$
\begin{aligned}
{}_n\left\langle \tilde{i} \parallel \tau_{n-1,n} \parallel \tilde{j} \right\rangle_n &= \sum_\alpha h^{[n-1]}_\alpha \, {}_{n-1}\left\langle u \parallel C^{[n-1]}_\alpha \parallel v \right\rangle_{n-1} \, {}_{loc}\left\langle \nu \parallel C^{[n]}_\alpha \parallel \mu \right\rangle^*_{loc} \\
&\times D\left(\alpha, \underline{c}, \underline{Q}_{\tilde{i}}, \underline{Q}_{\tilde{j}}, \underline{Q}_u, \underline{Q}_v, \underline{q}_\mu, \underline{q}_\nu\right) \delta_{\underline{Q}_{\tilde{i}},\underline{Q}_{\tilde{j}}} \delta_{\underline{Q}^z_{\tilde{i}},\underline{Q}^z_{\tilde{j}}} + H.c. \,, \qquad (\tilde{i} \leftarrow \mu, u;\ \tilde{j} \leftarrow \nu, v) \,.
\end{aligned}
\tag{3.31}
$$

Here the state $\tilde{i}$ has been constructed from the kept state $u$ of the previous iteration and from the local state $\mu$, while $\tilde{j}$ has been constructed from $v$ and $\nu$. The functions $D\left(\alpha, \underline{c}, \underline{Q}_{\tilde{i}}, \underline{Q}_{\tilde{j}}, \underline{Q}_u, \underline{Q}_v, \underline{q}_\mu, \underline{q}_\nu\right)$ denote group theoretical factors and can be expressed as

$$
\begin{aligned}
D\left(\alpha, \underline{c}, \underline{Q}_{\tilde{i}}, \underline{Q}_{\tilde{j}}, \underline{Q}_u, \underline{Q}_v, \underline{q}_\mu, \underline{q}_\nu\right) &= \mathrm{sgn}(C,\ \mu) \sum_{\underline{c}^z} \sum_{\underline{Q}^z_u,\, \underline{Q}^z_v} \sum_{\underline{q}^z_\mu,\, \underline{q}^z_\nu} \left\langle \underline{Q}_{\tilde{i}} \underline{Q}^z_{\tilde{i}} \middle| \underline{q}_\mu\, \underline{q}^z_\mu; \underline{Q}_u \underline{Q}^z_u \right\rangle \\
&\times \left\langle \underline{Q}_{\tilde{i}} \underline{Q}^z_{\tilde{i}} \middle| \underline{q}_\nu\, \underline{q}^z_\nu; \underline{Q}_v \underline{Q}^z_v \right\rangle^* \left\langle \underline{Q}_u \underline{Q}^z_u \middle| \underline{c}\, \underline{c}^z; \underline{Q}_v \underline{Q}^z_v \right\rangle \left\langle \underline{q}_\nu \underline{q}^z_\nu \middle| \underline{c}\, \underline{c}^z; \underline{q}_\mu \underline{q}^z_\mu \right\rangle^* \,,
\end{aligned}
\tag{3.32}
$$

with $\underline{Q}^z_{\tilde{i}}$ chosen arbitrarily. The sign function $\mathrm{sgn}(C,\mu) = \pm 1$ arises as one commutes the creation operators implicitly present in the local state $\mu$, over the operator $C^{[n-1]}$, and it is negative if $C^{[n]}_\alpha$ is a fermionic operator and the local state $\mu$ contains an odd number of fermions, otherwise it is positive. The local matrix elements, ${}_{loc}\langle \mu \parallel C^{[n]}_\alpha \parallel \nu \rangle_{loc}$ are the same for all sites and can easily be determined, while ${}_{n-1}\langle u \parallel C^{[n-1]} \parallel v \rangle_{n-1}$ can be computed from the previous iteration, recursively. In fact, for any operator $A$, acting only on sites $m < n$, and whose matrix elements are known in the iteration $n-1$, we have the recursion relation

$$
{}_n\left\langle \tilde{i} \parallel A \parallel \tilde{j} \right\rangle_n = {}_{n-1}\langle u \parallel A \parallel v \rangle_{n-1} \, F\left(\underline{a}, \underline{Q}_{\tilde{i}}, \underline{Q}_{\tilde{j}}, \underline{Q}_u, \underline{Q}_v, \underline{q}_\mu\right) \, \delta_{\underline{q}_\mu,\underline{q}_\nu} \,,
\tag{3.33}
$$

where we can express the factor $F\left(\underline{a}, \underline{Q}_{\tilde{i}}, \underline{Q}_{\tilde{j}}, \underline{Q}_u, \underline{Q}_v, \underline{q}_\mu\right)$ using Eq. (3.9) and Eq. (3.22) as

$$
\begin{aligned}
F\left(\underline{a}, \underline{Q}_{\tilde{i}}, \underline{Q}_{\tilde{j}}, \underline{Q}_u, \underline{Q}_v, \underline{q}_\mu\right) &= \mathrm{sgn}(A,\ \mu) \left\langle \underline{Q}_{\tilde{i}}\, \underline{Q}^z_{\tilde{i}} \middle| \underline{a}\, \underline{a}^z; \underline{Q}_{\tilde{j}}\, \underline{Q}^z_{\tilde{j}} \right\rangle^{-1} \\
&\times \sum_{\underline{Q}^z_u, \underline{Q}^z_v} \sum_{\underline{q}^z_\mu} \left\langle \underline{Q}_{\tilde{i}}\, \underline{Q}^z_{\tilde{i}} \middle| \underline{q}_\mu\, \underline{q}^z_\mu; \underline{Q}_u\, \underline{Q}^z_u \right\rangle \left\langle \underline{Q}_{\tilde{j}}\, \underline{Q}^z_{\tilde{j}} \middle| \underline{q}_\mu\, \underline{q}^z_\mu; \underline{Q}_v\, \underline{Q}^z_v \right\rangle^* \left\langle \underline{Q}_u\, \underline{Q}^z_u \middle| \underline{a}\, \underline{a}^z; \underline{Q}_v\, \underline{Q}^z_v \right\rangle
\end{aligned}
\tag{3.34}
$$

where the choice of $\underline{Q}^z_{\tilde{i}}, \underline{Q}^z_{\tilde{j}}$ and $\underline{a}^z$ is almost arbitrary. The only condition that has to be met is that the generalized Clebsch–Gordan coefficient $\left\langle \underline{Q}_{\tilde{i}}\, \underline{Q}^z_{\tilde{i}} \middle| \underline{a}\, \underline{a}^z; \underline{Q}_{\tilde{j}}\, \underline{Q}^z_{\tilde{j}} \right\rangle$ should be non-vanishing.

As only a small fraction of theses on NRG [113, 114, 115, 116, 117, 118] have been written recently without displaying the numerical values of some matrix elements, we exemplify the above procedure in Appendix C by including the reduced matrix elements and the block states of the $0^{th}$ iteration together with the local states in the 1CK model using the group $\mathrm{SU}_S(2) \times \mathrm{SU}_C(2)$.

## 3.2 Density matrix numerical renormalization group

One drawback of the algorithm described in Section 3.1 is that the eigenstates of $H_n$ constructed this way do not form a complete basis on the Wilson chain of length $n$, since states descendant from the discarded states of the previous iteration are missing. This deficiency does not effect the low-energy spectrum, or the thermodynamic quantities but for the spectral functions it leads to spectral sum rule violation and poor asymptotics. A remedy for these problems supplements the original NRG scheme with two concepts: a complete basis of the Wilson chain combined with the reduced density matrix. It was developed in the series of the papers [86, 87, 88, 89]. This extension of NRG bears the name of Density Matrix Numerical Renormalization Group (DM-NRG). Our contribution to this line of research was the incorporation of non-Abelian symmetries into DM-NRG [90], which turns out to be an important element in DM-NRG as well as far as the asymptotics of spectral functions and the performance are concerned. On the coming few pages we explain the DM-NRG algorithm from the perspective of symmetries.

### 3.2.1 Complete basis on the Wilson chain

As it was shown in Ref. [87] it is possible to construct a complete basis of the Wilson chain and compute the matrix elements, that come up in the NRG algorithm, in this basis. The benefit of this procedure is the exact fulfillment of spectral sum rules obeyed by spectral functions [88, 89]. The construction goes as follows.

Let us consider a Wilson chain of length $N$, and construct approximate eigenstates of $H_n$ with $n < N$ that, however, are extended to *all sites* of the chain,

$$\left| i, \underline{Q}_i \; \underline{Q}_i^z \right\rangle_n \to \left| i, \underline{Q}_i \; \underline{Q}_i^z; e \right\rangle_n \; . \tag{3.35}$$

In this equation $e$ labels the $d^{N-n}$ independent 'environment' states living at the last $N-n$ sites of the chain. The precise form of these environment states is not important, only their degeneracy will play an important part. The iterative construction from Section 3.1 carries over to these states too. By construction, discarded states (together with their environment state) form a complete basis set:

$$\mathbb{1} = \sum_{n=0}^{N} \sum_{i \in \mathrm{D}} \sum_{e} \sum_{\underline{Q}_i^z} \left| i, \underline{Q}_i \, \underline{Q}_i^z; e \right\rangle_{n\,n} \left\langle i, \underline{Q}_i \, \underline{Q}_i^z; e \right| , \tag{3.36}$$

where $i \in D$ refers to the fact that *only discarded states* appear in the sum. In Eq. (3.36) in the last iteration at $n = N$ all states are considered discarded. We remark that, in the actual calculations, discarded states do not appear until the iteration $M > 0$ where the first truncation is carried out. Fig. 3.1 illustrates the structure of this complete basis. In the formulation of the DM-NRG algorithm making use of non-Abelian symmetries we shall use several times the completeness relation Eq. (3.36).

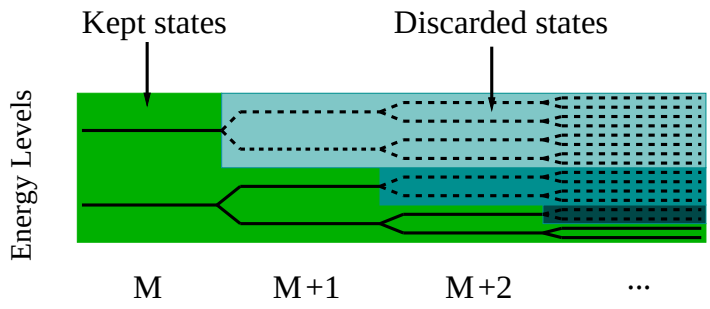


Figure 3.1: A complete basis of a Wilson chain represented as the exponentially increasing number of energy levels belonging to the successive iterations. Continuous/dashed lines represent kept, low-energy/discarded, high-energy levels, respectively. For the consecutive iteration steps the distances between the levels illustrate how the energy resolution of NRG gets exponentially subtler.

### 3.2.2 Reduction of the density matrix using symmetries

In the DM-NRG procedure on a Wilson chain of length $N$, the equilibrium density matrix is approximated by [89]

$$\rho = \sum_{n=0}^{N} \rho^{[n]} \tag{3.37}$$

$$\rho^{[n]} = \sum_{i \in D, \underline{Q}_i^z, e} \frac{e^{-\beta E_i^n}}{\mathbb{Z}} \left| i, \underline{Q}_i \, \underline{Q}_i^z; e \right\rangle_{n\,n} \left\langle e; i, \underline{Q}_i \, \underline{Q}_i^z \right| , \tag{3.38}$$

with $\beta = 1/T$ the Boltzmann factor and

$$\mathbb{Z} = \sum_{n=0}^{N} \sum_{i \in D, \underline{Q}_i^z} e^{-\beta E_i^n} d^{N-n} \tag{3.39}$$

the partition function.[5] In Eq. (3.39) the factor $d^{N-n}$ accounts for the degeneracy of the environment states in iteration $n$, i.e. for the local degrees of freedom at sites $m > n$. Since the eigenenergies do not depend on the internal quantum numbers, the expression for the partition function can be simplified to

$$\mathbb{Z} = \sum_{n=0}^{N} \sum_{i \in D} \dim(i) \, e^{-\beta E_i^n} d^{N-n} , \tag{3.40}$$

with the use of Eq. (3.22).

The concept of the reduced density matrix [86, 88, 89] arises naturally as one starts to calculate Green's functions with NRG. More precisely, the quantity that shows up in the calculations is

[5] Different approximations also exist in the literature, e.g. the one in Ref. [87] where the approximation of the density matrix comes only from the last iteration.

the *truncated reduced density matrix*, defined as

$$R^{[n]} \;=\; \mathop{\mathrm{Tr}}_{\{e_n\}} \left\{ \sum_{m>n} \rho^{[m]} \right\} , \tag{3.41}$$

where one traces over the environment states $e_n$ at sites $m > n$. This truncated reduced density matrix satisfies the recursion relations

$$\begin{aligned} R^{[N]} &= \rho^{[N]} , \\ R^{[n-1]} &= \sum_{i\in D} \frac{e^{-\beta E_i^{n-1}} d^{N-n+1}}{\mathbb{Z}} \left| i, \underline{Q}_i \; \underline{Q}_i^z \right\rangle_{n-1\; n-1} \left\langle i, \underline{Q}_i \; \underline{Q}_i^z \right| \\ &\quad + \mathop{\mathrm{Tr}}_{\mathrm{site}\; n} \left\{ R^{[n]} \right\} . \end{aligned} \tag{3.42}$$

Note that the environment variable is missing in the first term of the second expression since it has been traced over. The first term accounts for the contribution of discarded states, while the second term has matrix elements between the kept states only.

To construct the matrix elements of $R^{[n]}$, we first show by induction that $R^{[n]}$ is scalar under symmetry operations. This is clearly true for the first term in Eq. (3.42). To show that the second term is also invariant, we simply need to use the locality property of the symmetry transformations, i.e. that on the first $n$ sites $U(g) \equiv L(g)V(g)$, where $L(g)$ transforms the local states on site $n$, while $V(g)$ transforms states at sites $0 \le m \le n-1$, and clearly, $L$ and $V$ commute with each other. Therefore, because of the invariance of the trace under cyclic permutations of the operators, we have

$$\mathop{\mathrm{Tr}}_{\mathrm{site}\; n} \left\{ L\, V\, R^{[n]}\, V^+\, L^+ \right\} = \mathop{\mathrm{Tr}}_{\mathrm{site}\; n} \left\{ V\, R^{[n]}\, V^+ \right\} = V \mathop{\mathrm{Tr}}_{\mathrm{site}\; n} \left\{ R^{[n]} \right\} V^+ = U \mathop{\mathrm{Tr}}_{\mathrm{site}\; n} \left\{ R^{[n]} \right\} U^+ . \tag{3.43}$$

However, since $U\, R^{[n]}\, U^+ = R^{[n]}$ by assumption, we obtain that

$$\mathop{\mathrm{Tr}}_{\mathrm{site}\; n} \left\{ R^{[n]} \right\} \;=\; U \mathop{\mathrm{Tr}}_{\mathrm{site}\; n} \left\{ R^{[n]} \right\} U^+ , \tag{3.44}$$

implying that

$$U\, R^{[n-1]}\, U^+ = R^{[n-1]} \tag{3.45}$$

for $R^{[n-1]}$, too. This equation means that $R^{[n]}$ is *scalar* [6] and therefore, we have

$${}_n\left\langle i, \underline{Q}_i \; \underline{Q}_i^z \right| R^{[n]} \left| j, \underline{Q}_j \; \underline{Q}_j^z \right\rangle_n \;=\; {}_n\langle i \parallel R^{[n]} \parallel j\rangle_n \, \delta_{\underline{Q}_i, \underline{Q}_j} \, \delta_{\underline{Q}_i^z, \underline{Q}_j^z} . \tag{3.46}$$

The matrix elements ${}_n\langle i \parallel R^{[n]} \parallel j\rangle_n$ between discarded states simply derive from the first term in Eq. (3.42). To perform the trace in Eq. (3.42) and to construct the explicit relation between the kept matrix elements of $R^{[n-1]}$ and $R^{[n]}$, first, we rotate $R^{[n]}$ to the canonical basis

$${}_n\left\langle \tilde{i} \parallel \tilde{R}^{[n]} \parallel \tilde{j} \right\rangle_n \;=\; \mathcal{O}^{[n]}_{\tilde{i},i} \; {}_n\langle i \parallel R^{[n]} \parallel j\rangle_n \left(\mathcal{O}^{-1}\right)^{[n]}_{j\tilde{j}} . \tag{3.47}$$

[6] An alternative proof is presented in Appendix D for the case when every $\mathcal{G}_\gamma$ is an SU(2) group.

Then, using the fact that $\underset{\text{site } n}{\text{Tr}}\left\{R^{[n]}\right\}$ is diagonal in the (internal) symmetry quantum numbers, we can trace over the local states at site $n$ using the recursion relation Eq. (3.24) to obtain the matrix elements between the kept states $u, v \in K$ as

$$ {}_{n-1}\langle u \parallel R^{[n-1]} \parallel v\rangle_{n-1} = \widetilde{\sum_{\tilde{i},\tilde{j},\underline{q}_\mu,\mu}} \frac{\dim(\tilde{i})}{\dim(u)} {}_n\langle \tilde{i} \parallel \tilde{R}^{[n]} \parallel \tilde{j}\rangle_n \delta_{\underline{Q}_{\tilde{i}},\underline{Q}_{\tilde{j}}} . \tag{3.48} $$

The tilde over the sum indicates that in the summation over $\tilde{i}$ and $\tilde{j}$ only those states are considered which have been constructed from $u$ ($\tilde{i} \leftarrow \mu, u$) and $v$ ($\tilde{j} \leftarrow \mu, v$) in Eq. (3.24), respectively. This is expression applies to any type of discrete and compact Lie group symmetry. An alternative proof for the case of only SU(2) symmetries is given in Appendix D.

### 3.2.3 Spectral function computation with DM-NRG

In terms of the reduced density matrix we give a general relation for the retarded Green's function of two local operators, that act only at the impurity and/or the zeroth site of the Wilson chain. The notion of retarded Green's function is introduced in Appendix A, for convenience here we repeat its definition for two irreducible tensor operators

$$ G^R_{A_{\underline{a},\underline{a}_z},B^\dagger_{\underline{b},\underline{b}_z}}(t) = -i\left\langle\left[A_{\underline{a},\underline{a}_z}(t), B^\dagger_{\underline{b},\underline{b}_z}(0)\right]\right\rangle \Theta(t) . \tag{3.49} $$

By symmetry considerations and as it is shown below, the Green's function is non-zero only if the operators $A$ and $B$ transform according to the same representation i.e.

$$ G^R_{A_{\underline{a},\underline{a}_z},B^\dagger_{\underline{b},\underline{b}_z}}(t) = G^R_{A,B^\dagger}(t)\, \delta_{\underline{a},\underline{b}}\, \delta_{\underline{a}_z,\underline{b}_z} , \tag{3.50} $$

and it is independent of the value of $\underline{a}_z$ and correspondingly of $\underline{b}_z$. Note that in this expression the representation index $\underline{b}$ and its labels $\underline{b}_z$ are the quantum numbers that characterize the operator $B$ and not $B^\dagger$.

In the reduced density matrix formalism we can generalize the procedure outlined in Ref. [88, 89] even in the presence of non-Abelian symmetries to obtain the following form for the Laplace transform of the Green's function

$$ \begin{aligned} G^R_{A,B^\dagger}(z) = &\sum_{n=0}^{N} \sum_{i\in D,K} \sum_{(j,k)\notin(\mathrm{K,K})} {}_n\langle i \parallel R^{[n]} \parallel j\rangle_n \\ &\times \left[ \frac{{}_n\langle k \parallel A^\dagger \parallel j\rangle^*_n\, {}_n\langle k \parallel B^\dagger \parallel i\rangle_n}{z + E^n_j - E^n_k} \frac{\dim(k)}{\dim(\underline{a})} - \xi \frac{{}_n\langle j \parallel B^\dagger \parallel k\rangle_n\, {}_n\langle i \parallel A^\dagger \parallel k\rangle^*_n}{z - E^n_i + E^n_k} \frac{\dim(i)}{\dim(\underline{a})} \right] . \end{aligned} \tag{3.51} $$

Here the second sum is over all the multiplets $i, j, k$ of the given iteration subject to the restriction that $j, k$ do not belong to kept states at the same time and no summation is needed for states within the multiplets. We note that the irreducible matrix elements of $R^{[n]}$ are identical with the original ones since $R^{[n]}$ is invariant under all symmetry transformations, i.e. it is a rank 0 object with respect to all symmetries. In Eq. (3.51) $\dim(\underline{a}) = \prod_{\gamma=1}^{\Gamma} \dim(a^\gamma)$ is the

number of operators belonging to the same operator multiplet $A_{\underline{a},\underline{a}_z}$. The coefficients with the dimensions of the corresponding irreducible subspaces arise in the following way when summing over the internal quantum numbers [104]

$$\begin{aligned}
&\delta_{\underline{Q}_i\underline{Q}_j}\,\delta_{\underline{Q}_i^z\underline{Q}_j^z}\sum_{\underline{Q}_i^z,\underline{Q}_j^z,\underline{Q}_k^z}\left\langle j,\underline{Q}_j\ \underline{Q}_j^z\right|A_{\underline{a},\underline{a}_z}\left|k,\underline{Q}_k\ \underline{Q}_k^z\right\rangle\left\langle k,\underline{Q}_k\ \underline{Q}_k^z\right|B^\dagger_{\underline{b},\underline{b}_z}\left|i,\underline{Q}_i\ \underline{Q}_i^z\right\rangle\\
&\quad=\sum_{\underline{Q}_i^z,\underline{Q}_k^z}\langle k\parallel A^\dagger\parallel j\rangle^*\left\langle\underline{Q}_k\ \underline{Q}_k^z\right|\underline{a}\ -\underline{a}_z;\underline{Q}_i\ \underline{Q}_i^z\Big\rangle\ \langle k\parallel B^\dagger\parallel i\rangle\left\langle\underline{Q}_k\ \underline{Q}_k^z\right|\underline{b}\ -\underline{b}_z;\underline{Q}_i\ \underline{Q}_i^z\Big\rangle\\
&\quad=\langle k\parallel A^\dagger\parallel j\rangle^*\ \langle k\parallel B^\dagger\parallel i\rangle\sum_{\underline{Q}_i^z,\underline{Q}_k^z}\left\langle\underline{Q}_k\ \underline{Q}_k^z\right|\underline{a}\ -\underline{a}_z;\underline{Q}_i\ \underline{Q}_i^z\Big\rangle\left\langle\underline{Q}_k\ \underline{Q}_k^z\right|\underline{b}\ -\underline{b}_z;\underline{Q}_i\ \underline{Q}_i^z\Big\rangle\\
&\quad=\langle k\parallel A^\dagger\parallel j\rangle^*\ \langle k\parallel B^\dagger\parallel i\rangle\sum_{\underline{Q}_i^z,\underline{Q}_k^z}(-)^{\underline{a}-\underline{Q}_k-\underline{Q}_i^z}\ \sqrt{\frac{\dim(k)}{\dim(\underline{a})}}\left\langle\underline{a}-\underline{a}^z\left|\underline{Q}_k\ \underline{Q}_k^z;\underline{Q}_i\ -\underline{Q}_i^z\right\rangle\right.\\
&\qquad\times\ (-)^{\underline{b}-\underline{Q}_k-\underline{Q}_i^z}\ \sqrt{\frac{\dim(k)}{\dim(\underline{b})}}\left\langle\underline{b}\ -\underline{b}^z\left|\underline{Q}_k\ \underline{Q}_k^z;\underline{Q}_i\ -\underline{Q}_i^z\right\rangle\right.\\
&\qquad=\delta_{\underline{a}\,\underline{b}}\,\delta_{\underline{a}_z\,\underline{b}_z}\,\frac{\dim(k)}{\dim(\underline{a})}\ \langle k\parallel A^\dagger\parallel j\rangle^*\ \langle k\parallel B^\dagger\parallel i\rangle\ . \qquad (3.52)
\end{aligned}$$

A similar derivation yields the coefficient in the second term. Remarkably, Eq. (3.52) and thus Eq. (3.51) contain exclusively the reduced matrix elements and the dimensions of the various multiplets. Eq. (3.52) explicitely shows that $G^R_{A,B^\dagger}(z)=0$, unless $A$ and $B$ have the same quantum numbers, i.e. $\underline{a}=\underline{b}$.

## 3.3 Comparison between NRG and DM-NRG

In this section we show the advantages of using DM-NRG as opposed to NRG, and illustrate the benefits of using non-Abelian symmetries by applying DM-NRG to the 2-Channel Kondo Model (2CKM). This model is exciting in itself as it possesses a non-Fermi liquid type of fixed point and it provides the simplest descriptions of the double dot system used recently to realize the 2-Channel Kondo (2CK) effect. This 2CK effect is very fragile and in a magnetic field we find substantial difference between the NRG and DM-NRG results. For further discussion about 2CK physics see Chapter 4 whereas for the details of the double dot experiment consult Subsection 4.2.4 and Ref. [23] in particular.

In the numerical calculations we have used the Hamiltonian Eq. (2.69) with $\alpha\in\{1,2\}$ labeling the two types of electrons. The 2CKM has an obvious $\mathrm{SU}_S(2)$ spin symmetry. Furthermore the number of electrons is conserved in both channels corresponding to a $\mathrm{U}_{C1}(1)\times\mathrm{U}_{C2}(1)$ symmetry, with $C1$ and $C2$ referring to electrons in channel $\alpha=1$ and 2, respectively. Due to the presence of electron-hole symmetry, these $\mathrm{U}_C(1)$ charge symmetries can be supplemented to $\mathrm{SU}_C(2)$ symmetries, i.e. the 2CK Hamiltonian is also invariant under $\mathrm{SU}_S(2)\times\mathrm{SU}_{C1}(2)\times\mathrm{SU}_{C2}(2)$ transformations. On the other hand, the 2CKM can be solved using U(1) symmetries exclusively, $\mathrm{U}_S(1)\times\mathrm{U}_{C1}(1)\times\mathrm{U}_{C2}(1)$. This model is thus ideal for testing our flexible code and the importance of symmetries in the NRG and DM-NRG calculations.

If a local magnetic field is coupled to the impurity spin through a term $g\mu_B BS^z$, from among the total spin generators (see Eq. (3.4)), solely $S^z_T$ will commute with the Hamiltonian. That

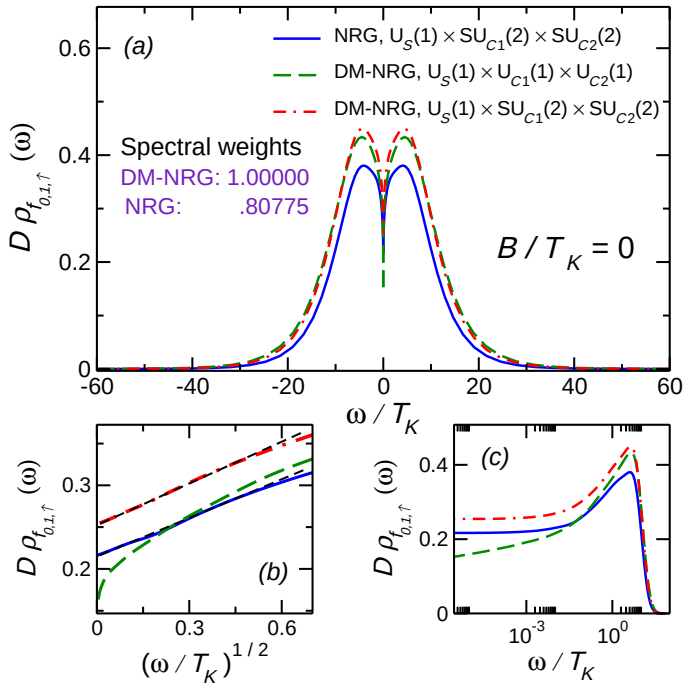


Figure 3.2: Dimensionless spectral function of $f_{0,1,\uparrow}$ normalized by $D_F$, the bandwidth cut-off, as a function of $\omega/T_K$ in the absence of magnetic field obtained with DM-NRG and with NRG using the symmetries: $\mathrm{U}_S(1) \times \mathrm{SU}_{C1}(2) \times \mathrm{SU}_{C2}(2)$ and $\mathrm{U}_S(1) \times \mathrm{U}_{C1}(1) \times \mathrm{U}_{C2}(1)$. $(a)$ Comparison between the spectral weights of the DM-NRG and NRG results: DM-NRG fulfills the sum rule entirely even when the used symmetry group and therefore the number of kept states is largely reduced. NRG violates the sum rule to over 15% if the number of kept states is $\approx 7 \times 10^4$ in each iteration. $(b)$ The same spectral functions as a function of $\sqrt{\omega/T_K}$. If a sufficient number of states is kept, i.e. when using larger symmetry groups, the expected $\sqrt{\omega}$ behavior around the 2CK fixed point is nicely recovered. $(c)$ The same spectral functions on a logarithmic scale.

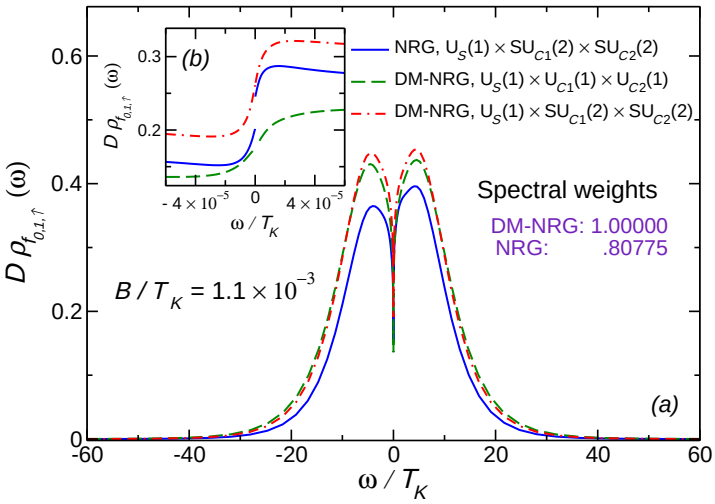


Figure 3.3: Dimensionless spectral function of $f_{0,1,\uparrow}$ normalized by $D_F$, the bandwidth cut-off, as a function of $\omega/T_K$ in the presence of magnetic field obtained with DM-NRG and with NRG using the symmetries: $\mathrm{U}_S(1) \times \mathrm{SU}_{C1}(2) \times \mathrm{SU}_{C2}(2)$ and $\mathrm{U}_S(1) \times \mathrm{U}_{C1}(1) \times \mathrm{U}_{C2}(1)$. $(b)$ On a smaller scale at $\omega = 0$ we show the smoothness of the DM-NRG data using both groups and the jump at $\omega = 0$ in the NRG results using the larger group.

is, the spin $\mathrm{SU}_S(2)$ symmetry reduces to $\mathrm{U}_S(1)$. Therefore, in a magnetic field we can either use the group $\mathrm{U}_S(1) \times \mathrm{SU}_{C1}(2) \times \mathrm{SU}_{C2}(2)$ for our calculations, or restrict ourselves to U(1) symmetries only: $\mathrm{U}_S(1) \times \mathrm{U}_{C1}(1) \times \mathrm{U}_{C2}(1)$.

As a test, we have computed the retarded Green's function, $G^R_{f_{0,\alpha,\uparrow}, f^\dagger_{0,\alpha,\uparrow}}(\omega)$, or more precisely the corresponding spectral function $\varrho_{f_{0,\alpha,\uparrow}}(\omega)$, defined by

$$\varrho_{f_{0,\alpha,\uparrow}}(\omega) \equiv -\frac{1}{\pi} \mathrm{Im}\ G^R_{f_{0,\alpha,\uparrow}, f^\dagger_{0,\alpha,\uparrow}}(\omega) \tag{3.53}$$

both in the presence and in the absence of magnetic field. All numerical results presented were obtained at zero temperature, and the dimensionless couplings were $\tilde{\mathcal{J}}_\alpha = 0.2$ in both channels and for all runs. The discretization parameter $\Lambda = 2$ was used in all cases, and for each symmetry combination we have retained a maximum of 1350 multiplets in each iteration.

In Fig. 3.2 we show data for the local fermion's spectral function in the absence of magnetic field obtained through the NRG and the DM-NRG approaches using the two symmetry groups mentioned above. The Kondo scale $T_K$ in Fig. 3.2 is the scale at which the 2CK state forms, and it is defined as the frequency where the $T$-matrix of the 2CK model drops to half of its value assumed at $\omega = 0$ at the 2CK fixed point [140]. The $T$-matrix is defined as the reducible conduction electron self-energy [29, 153]. Its imaginary part is proportional to the spectral function of the composite fermion operator. The definition of the Kondo temperature is illustrated in Fig. 4.4.

The first important test is the fulfillment of the spectral sum rules. These are always satisfied in the DM-NRG calculations independently of the symmetry group used, whereas the NRG data violate the sum rule to over 15% if the number of kept multiplets is 1350 which corresponds to $\approx 7 \times 10^4$ states taking into account states within multiplets. Fig. 3.2.$(b)$ shows that around the 2CK fixed point the $\sqrt{\omega}$ behavior, expected from conformal field theoretical calculations, [7]

[7] For the explanation of the $\sqrt{\omega}$ behavior of spectral functions around the 2CK fixed point see Subsection 4.3.3.

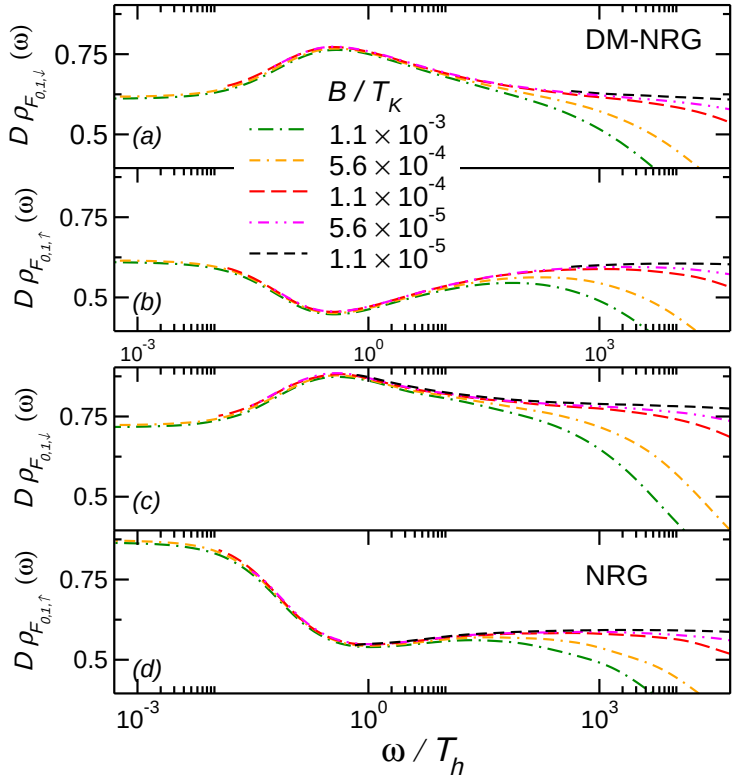


Figure 3.4: Dimensionless spectral function of the $\downarrow$- $(a),(c)$ and the $\uparrow$-spin $(b),(d)$ components of the local composite fermion operator normalized by $D_F$, the bandwidth cutoff, for sufficiently small values of $B$ as a function of $\omega/T_h$ scaled on top of each other using NRG and DM-NRG together with the group $\mathrm{U}_S(1) \times \mathrm{SU}_{C1}(2) \times \mathrm{SU}_{C2}(2)$.

is nicely recovered by both methods, but a sufficiently large number of multiplets must be kept also in the DM-NRG approach, meaning that in this case the use of the larger symmetry group is more rewarding. Fig. 3.2.$(c)$ demonstrates that, in spite of fulfilling the spectral sum rules, still the DM-NRG data do not show the expected asymptotics for low-frequencies if the number of multiplets kept is not sufficient. It is quite remarkable that only the DM-NRG procedure together with the use of non-Abelian symmetries was able to get close to the exact value of the spectral function at $\omega = 0$, $\rho_{f_{0,\alpha,\uparrow}}(\omega = 0) = 0.25$.[8] The presence of magnetic field generates a new scale [63]

$$T_h \equiv C_h \frac{B^2}{T_K} , \tag{3.54}$$

where we have fixed the somewhat arbitrary constant to $C_h \approx 60$ [91]. This scale, discussed more thoroughly in Subsection 4.3.1 (see Eq. (4.50)), is usually referred to as the renormalized magnetic field acting on the impurity, and below this scale the non-Fermi liquid physics is destroyed.

In the presence of magnetic field the sum rule is violated by the NRG approach in the positive and negative frequency ranges to a different extent, which leads to jumps at $\omega = 0$ in the spectral functions (see Fig. 3.3), while this problem is almost absent in the DM-NRG approach.

The fermion spectral functions display universal scaling in the vicinity of $T_h$ and a universal peak/dip at $T_h$ [91]. In Fig. 3.4 we show how the spectral functions of the composite fermion

[8] It can be shown that $\rho_{f_{0,\alpha,\uparrow}} = \frac{1}{2}\rho_0 = \frac{1}{4}$ at the 2CK fixed point, in the large bandwidth limit, with $\rho_0$ the unperturbed dimensionless electron DOS. Further details are provided in Chapter 4.

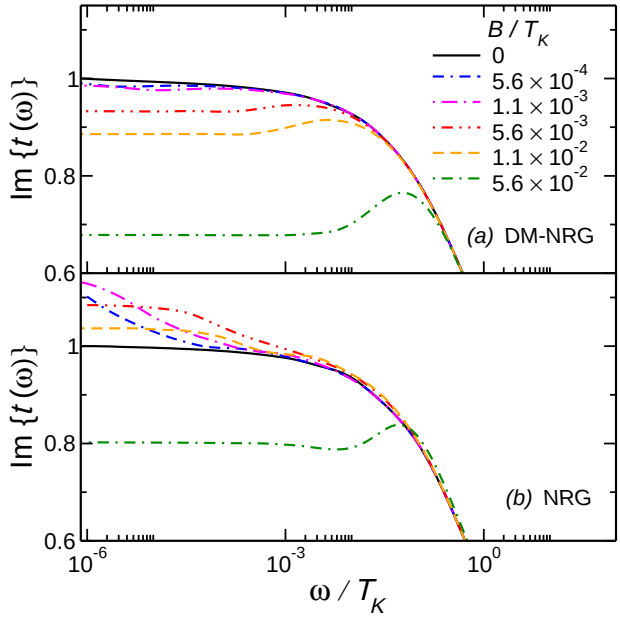


Figure 3.5: Imaginary part of the on-shell $T$-matrix using DM-NRG and NRG together with the group $\mathrm{U}_S(1) \times \mathrm{SU}_{C1}(2) \times \mathrm{SU}_{C2}(2)$ for various magnetic field values as a function of $\omega/T_K$ .

operator, $F_1^\dagger \equiv f_{0,1}^\dagger \vec{S}\vec{\sigma}$ can be scaled on top of each other using the scale $T_h$. Although, this collapse can be obtained in both approaches, there is an $\approx 20\%$ jump at $\omega = 0$ in the NRG results while the DM-NRG results are continuous there. It is possible to eliminate the jump in the NRG results by determining the phase shifts from the energy spectrum with high precision [153], but even after these corrections, the results continue to violate the sum rule and numerical errors for low-frequencies remain of the same size as before. Moreover, the 'universal' curve obtained by conventional NRG is clearly incorrect and different from the DM-NRG result.

Even more interesting is the contrast to the case of the single-channel Kondo model. There, in the presence of a small magnetic field no such universal peak presents itself. Only magnetic fields of the order of $T_K$ have influence on the low-frequency behavior of the composite fermion's spectral function and lead to the well-known splitting of the Kondo resonance [154].

Also, if we try to compute the imaginary part of the $T$-matrix of the 2CK model where the local composite fermion spectral functions for both $\uparrow$- and $\downarrow$-spin components have to be summed up, we end up with large numerical errors in the NRG results [140] (see Fig. 3.5), while DM-NRG provides satisfactory results even in this case.

It is thus clear from these examples that the DM-NRG method together with the use of lots of symmetries produces much more reliable results than NRG with non-Abelian symmetries or DM-NRG with only Abelian symmetries, and its use is needed to do computations for more delicate quantum impurity models.

## 3.4 Summary

We have developed a so-called flexible DM-NRG program [25, 26] which permits the use of an arbitrary number of Abelian and non-Abelian symmetries, and incorporates the spectral-sum preserving density matrix NRG algorithm. The DM-NRG method makes it possible to generate spectral functions that satisfy spectral sum rules with machine precision at $T = 0$. For

calculations with non-zero magnetic field the use of the DM-NRG represents a great advantage over conventional NRG methods [153], which loose spectral weights and violate spectral sum rules. Conventional methods also lead to smaller or bigger jumps in the spectral functions at $\omega = 0$ which hinder the computation of the universal scaling functions provided e.g. by the scale $T_h$ [140]. The DM-NRG method solves all these problems if a sufficient number of multiplets is kept. We have found that for more delicate quantum impurity models like the 2CK model we need to use as many symmetries as possible to perform reliable calculations and to keep the computation time within reasonable limits.

We believe that the method presented here opens up the possibility of carrying out very accurate calculations for multi-channel systems such as multi-dot devices, and even makes it possible to perform reliable DM-NRG–DMFT calculations for periodic impurity models.

# 4 Two-channel Kondo model

In this chapter we present our results about the dynamical properties of the 2-Channel Kondo Model (2CKM). In Section 4.1 we motivate our work on the 2CKM by discussing its relevance in the description of Non-Fermi Liquid (NFL) phenomena. In Section 4.2 follows further motivation with the details of the recent experiment of Potok *et al.* realizing the 2-Channel Kondo (2CK) state [23]. To gain a broader perspective this section also contains discussion about single electron transistors and the Coulomb blockade phenomenon in Subsection 4.2.2, as well as about the observation of the one-channel Kondo effect in quantum dots in Subsection 4.2.3. Section 4.3 contains our results about dynamical correlations in the 2CKM. In Subsection 4.3.1 we use boundary conformal field theory to classify the boundary highest-weight fields of the electron-hole symmetrical 2CKM by their quantum numbers and identify the relevant perturbations around the 2CK fixed point. Based on this classification the fields are then expanded in leading order in terms of the operators of the free theory. In Subsection 4.3.2 we describe the technical details of our DM-NRG calculations. In Subsections 4.3.3, 4.3.4 and 4.3.5 we study the real and the imaginary parts of the retarded Green's functions of the local fermions, the impurity spin and the local superconducting order parameters. In each of these subsections we first discuss the analytic forms of the susceptibilities in the asymptotic regions of the two-channel and single-channel Kondo scaling regimes, as they follow from scaling arguments. Then we confirm our predictions by demonstrating how the expected corrections due to the relevant perturbations and the leading irrelevant operator present themselves in the DM-NRG data. Furthermore we determine the boundaries of the 2CK scaling regimes and derive universal scaling curves connecting the FL and NFL fixed points for each operator under study. In Subsection 4.3.6 the effects of electron-hole symmetry breaking are investigated. Finally, our conclusions are drawn in Subsection 4.3.8.

## 4.1 Non-Fermi liquid behavior

Deviations from Fermi liquid-like behavior observed e.g. in the metallic state of high-temperature cuprate superconductors [1, 2], or in heavy fermion systems [3, 4] prompted experts to find out what is behind these phenomena. Two models that became paradigms for describing NFL physics are the Tomonaga–Luttinger liquid [172, 173, 179, 180, 181, 182] and the overscreened multi-channel Kondo model [174, 175, 176, 177].[1] The former one accounts for the behavior of one-dimensional interacting electron systems, while in the latter a spin degree of freedom couples to several degenerate bands of non-interacting electrons. Apart from them, the emergence of NFL physics has also been ascribed to the effect of disorder in disordered Kondo alloys [183] and possibly in doped semiconductors [184, 185]. It can also appear as a consequence of the

[1] Overscreened Kondo models are characterized by the relation $k > 2S$, with $k$ the number of electron channels (or flavors) and $S$ the value of the impurity spin.

quantum fluctuations of an order parameter or some collective modes, as is the case in the vicinity of many quantum phase transitions [176, 178].

In this chapter we study a variant of the overscreened multi-channel Kondo model, the spin-half, two-channel Kondo (2CK) model introduced by Nozières and Blandin [186], which is the simplest prototypical example of non-Fermi liquid quantum impurity models. It has been proposed to describe a variety of systems including dilute heavy fermion compounds [175], tunneling impurities in disordered metals and doped semiconductors [187, 188, 189].

The 2CKM consists of a spin-half local moment which is coupled through antiferromagnetic exchange interactions to two channels of conduction electrons (as in Eq. (2.55) with $\alpha \in \{1, 2\}$ ). Electrons in both channels try to screen the impurity spin. If the coupling of the spin to one of the channels is stronger than to the other then electrons in the more strongly coupled channel screen the spin, while the other channel becomes decoupled. However, for equal exchange couplings, the competition between the two channels leads to overscreening and results in non-Fermi liquid behavior. Among others, it is characterized by a non-trivial zero temperature residual entropy in the infinite volume limit, a square root-like temperature dependence of the differential conductance, a logarithmic divergence of the spin susceptibility and the linear specific heat coefficient at low temperatures [175]. This unusual and fragile ground state cannot be described within the framework of Nozières' Fermi liquid theory [70].

From the experimental point of view the 2CK along with the two-impurity Kondo physics are two leading candidates for creating NFL phenomena and studying them in a well-controlled way. Indeed, the observation of the 2CK state in a double dot system proposed by Oreg and Goldhaber-Gordon [149] has recently been achieved [23]. Although these measurements were restricted quantities, like the voltage dependence of the differential conductance at non-zero temperatures, dynamical quantities also reflect the vicinity of the 2CK fixed point (see Section 4.3). In fact, apart from maybe the scattering states Bethe ansatz [198], theories are lacking to calculate properties out-of-equilibrium like the voltage dependence of the differential conductance in the strong coupling regime. However, one can take hints from scaling analyses and assume that the differential conductance as a function of the source-drain voltage in the setup discussed in Subsection 4.2.4 should follow the same power law behavior as the function of frequency or temperature. Therefore to motivate our studies of the 2CKM from the experimental perspective we present the details of this experiment in Section 4.2.

Being a prototypical example of non-Fermi liquid models, the 2CKM has already been investigated with a number of methods. These include non-perturbative techniques like the Bethe Ansatz, which gives full account of the thermodynamic properties [63, 64], boundary conformal field theory [27], which describes the vicinity of the fixed points, and NRG [110, 190]. Other less powerful approximate methods such as the Yuval–Anderson approach [111], Abelian bosonization [28], large-$f$ expansion [73, 191], and the non-crossing approximation [72] have also been used to study the 2CKM successfully.

Despite this extensive work, little has been published about *dynamical* correlation functions such as the spin susceptibility, local charge and superconducting susceptibilities. Even the detailed properties of the $T$-matrix, or in other terms the reducible self-energy have only been computed earlier using conformal field theory, which is rather limited in energy range, and by the non-crossing approximation, which is not well-controlled and is unable to describe the Fermi liquid cross-over [193, 194]. It was also possible to compute some of the dynamical correlation functions in case of extreme spin anisotropy using Abelian bosonization results [28], though

these calculations reproduce only partly the generic features of the spin-isotropic model [195].

Local correlations in the two-channel Anderson model around its non-Fermi liquid fixed point have already been investigated to a certain extent with the use of NRG, although in the absence of channel anisotropy and magnetic field [196, 197]. However, a thorough NRG analysis of the zero temperature $T$-matrix of the 2CKM has been carried out only very recently [140, 192], and the $T \neq 0$ analysis still needs to be done.

Our aim was to fill this gap by giving a comprehensive analysis of the local correlation functions at zero temperature using NRG. However, in the vicinity of the rather delicate two-channel Kondo fixed point, the conventional NRG method fails and its further developed version, the density matrix-NRG (see Chapter 3) needs to be applied. Furthermore, a rather large number of multiplets must be kept to achieve good accuracy. We have therefore calculated the real and the imaginary parts of various local correlation functions with the spectral sum conserving DM-NRG method, where we use non-Abelian symmetries in a flexible way [90].

To identify the relevant perturbations around the NFL fixed point we apply boundary conformal field theory (see Subsection 4.3.1). Then we systematically study how the vicinity of fixed points and the introduction of relevant perturbations such as a finite channel anisotropy or a finite magnetic field influence the form of dynamical response functions at zero temperature. We mainly focus on the strong coupling regime of the 2CK model and the universal cross-over functions in the proximity of this region induced by an external magnetic field or channel anisotropy. These cross-over functions, describing the cross-over from the non-Fermi liquid fixed point to a Fermi liquid fixed point, as well as the response functions can currently be computed reliably at all energy scales only with NRG. However, we shall be able to use the results of boundary conformal field theory, more precisely, the knowledge of the operator content of the two-channel Kondo fixed point and the scaling dimensions of the various perturbations around it, to make very general statements on the analytic properties of the various Green's functions.

## 4.2 Observation of the two-channel Kondo effect

Here we present the particulars of the experiment of Potok *et al.* [23]. To facilitate the understanding and give a broader view we talk about quantum dots and their usage in single electron transistors, and related phenomena like the Coulomb blockade and the single-channel Kondo effect. Then we turn our attention to the specific double dot setup that was used to justify the feasibility of the 2CK state.

### 4.2.1 Quantum dots

In common electric circuits as e.g. in nanosize transistors[2] on a memory chip the current is carried by a huge number of electrons without the quantization of charge playing a role. However in the last two decades or so, it became possible to fabricate nanosize devices and electric circuits with increased sensitivity that operate on the principle of charge and energy quantization. Such a mesoscopic device is e.g. a single electron transistor (SET) [158, 203] whose essential constituents are a few electrons on a small island connected to the rest of the world only through tunneling barriers. This small droplet of electrons is also called quantum dot (QD) or artificial atom [167, 169, 156, 157, 161], and the rest of the world could mean leads or other quantum dots.

[2] now with a length of 45 nm by Intel®

Apart from their use e.g. in LED's, solar cells and possibly in quantum computing, they serve as a playground to study a profusion of phenomena. Here we focus on their low-energy transport properties and especially on their displaying the one- and the two-channel Kondo effects [151, 23].

Quantum dots have been created in a number of ways. One is by applying negative voltage to metallic gate electrodes on top of a semiconducting heterostructure, such as GaAs/AlGaAs, which contains a two-dimensional electron gas (2DEG) at the interface [144, 145, 146, 147, 148, 151]. Applying negative voltages leads to the depletion of the 2DEG underneath the gates and can be used to confine electrons in a quasi-2D region of a length of the order of a hundred nanometers. The gate electrodes and thus the size and the shape of the dot are tailored by lithographic patterning. Another possibility instead of using gate electrodes is etching a predefined geometry into the structure. In each case this arrangement is called lateral quantum dot.

Vertical quantum dots are another common type for experimental purposes [164, 165, 166]. There the dot corresponds to a few nanometer thick disc (e.g. of InGaAs) in a layered double barrier heterostructure, and the electrons are confined by the edges of this disc. The tunneling barriers could be made of thin AlGaAs films acting as insulators, and the leads of doped GaAs situated at the top and the bottom. Such a structure can for instance be grown by molecular beam epitaxy [168].

In semiconductors the de Broglie wavelength is relatively large. It is of the order of a few tens of nanometers and hence comparable to the size of the QD which makes quantization effects such as the discreteness of the excitation spectrum appreciable at low-temperatures. Thus one characteristic energy scale of a QD is the average level spacing $\delta E$ in its spectrum. It scales with $L$ the linear extent of the dot and the electron DOS $\rho$ in 2D as [170, 202]

$$\delta E \simeq \frac{1}{\rho L^2} \propto \frac{E_F}{(k_F L)^2}, \tag{4.1}$$

with the area of the QD approximated by $L^2$. As the electron DOS in metals is larger than in semiconductors, it is possible to fabricate metallic QD's with quasi-continuous spectrum made of Al for example. They are called metallic grains or islands.

Another relevant energy scale is $E_C$, the charging energy of the dot, which is roughly the energy required to add one electron to the dot and stems from the Coulomb interaction between dot electrons [155]. A crude estimate for it is

$$E_C \simeq \frac{e^2}{\varepsilon_0 L}, \tag{4.2}$$

with $e$ the electron charge and $\varepsilon_0$ the dielectric constant.

In semiconducting QD's $E_C$ is usually orders of magnitude larger than $\delta E$. Typically $E_C$ is in the range of $1 - 10$ meV corresponding to $10 - 100$ K whereas $\delta E$ is between $2 - 100$ $\mu$eV, i.e. between 25 mK $-$ 1 K. So for the one-electron phenomena to become observable one needs to go below the temperature set by $E_C$. The charging energy, as it is calculated in Subsection 4.2.2, is inversely proportional to the capacitance of the dot. Thus with a control over the smallness of the dot the one-electron phenomena is experimentally accessible. In the following Subsection 4.2.2 we derive the charging energy of the single electron transistor shown in Fig. 4.1, and then discuss some qualitative features of electron transport through the dot.

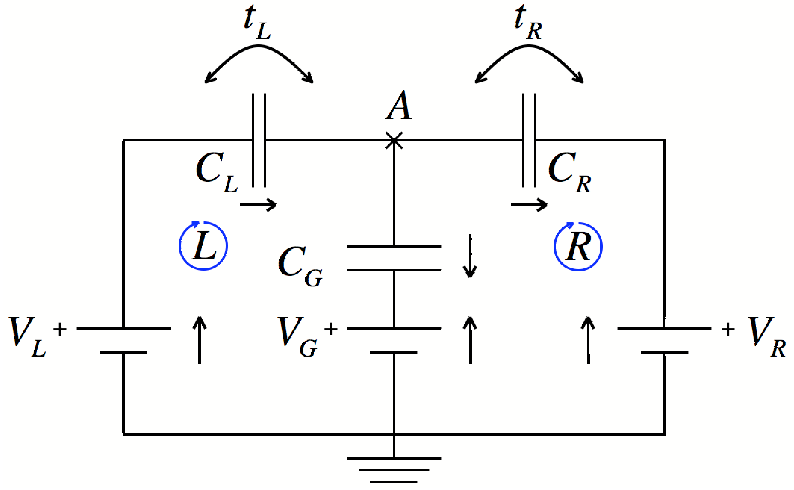


Figure 4.1: Single electron transistor

### 4.2.2 Charging energy and Coulomb blockade in a single electron transistor

First we calculate the electrostatic energy of the system shown in Fig. 4.1 which is the electric circuit equivalent of the single electron transistor with a QD in the center coupled to left ($L$) and right ($R$) leads, or by analogy with field-effect transistors corresponding to the source and drain. When the tunnel junctions are well characterized by the capacitances $C_L$ and $C_R$, we can describe the Coulomb interaction between the dot electrons by the classical electrostatic energy. To promote better understanding and as it is a frequently used formula, next follows its derivation taken from Refs. [162, 163].

The total energy of the system (after the last tunneling) is given by its electrostatic energy and the work done by the voltage sources. Now we calculate only the electrostatic part. The Lagrangian of the system reads

$$\mathscr{L}_{SET}^{elstat}\left(\phi_G, \dot{\phi}_G\right) \;=\; \frac{1}{2}\left(C_G\,\dot{\phi}_G^2 \,+\, C_L\,\dot{\phi}_L^2 \,+\, C_R\,\dot{\phi}_R^2\right), \tag{4.3}$$

with $C_L, C_R$ and $C_G$ the capacitances and $\phi_L, \phi_R$ and $\phi_G$ the corresponding phases with their orientations chosen as in Fig. 4.1. These phases have been introduced to make connection with the Lagrangian formalism. Their time derivative is the voltage difference between the two sides of the corresponding capacitor [163].

In loops $L$ and $R$ the loop rule constrains the variables as

$$V_L \,+\, \dot{\phi}_L + \dot{\phi}_G \,-\, V_G \;=\; 0\,, \tag{4.4}$$
$$V_G \,-\, \dot{\phi}_G + \dot{\phi}_R \,-\, V_R \;=\; 0\,, \tag{4.5}$$

which leave us with only one independent variable denoted to be $\phi_G$ in Eq. (4.18). Now we change this to be the phase at point $A$ where the dot is located

$$\dot{\phi}_A \;\equiv\; V_L \,+\, \dot{\phi}_L\,, \tag{4.6}$$

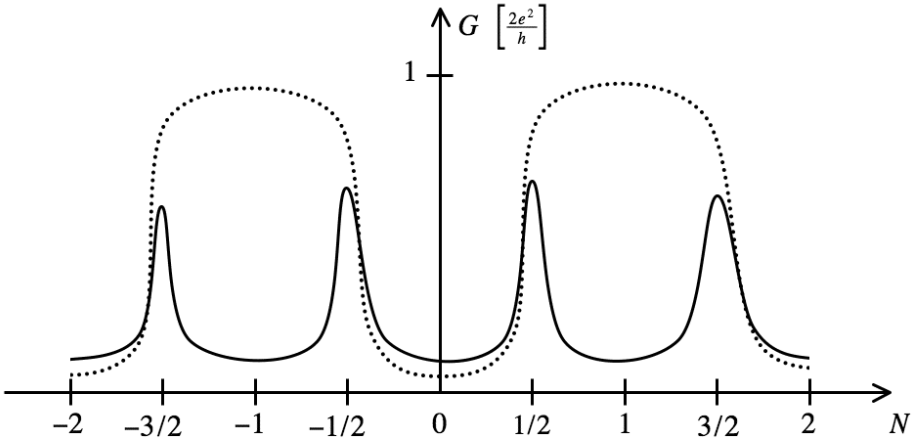


Figure 4.2: Conductance through the quantum dot in the single electron transistor as the function of $N$ for the regime $k_B T_K \ll k_B T \ll E_C$ (solid line), and for $T \ll T_K$ (dotted line).

and reexpress $\mathscr{L}_{SET}^{elstat}$ in terms of it as

$$\mathscr{L}_{SET}^{elstat}\left(\phi_A, \dot{\phi}_A\right) \;=\; \frac{1}{2}\left(C\,\dot{\phi}_A^2 \,-\, 2\,e\,N\,\dot{\phi}_A \,+\, C_G\,V_G^2 \,+\, C_L\,V_L^2 \,+\, C_R\,V_R^2\right), \qquad (4.7)$$

with the notations $C \equiv C_L + C_R + C_G$ the total dot capacitance, $e\,N \equiv C_L\,V_L + C_R\,V_R + C_G\,V_G$ the external charge and $e$ the absolute value of the electron charge. As we see, $N$ can be tuned continuously e.g. by the changing gate voltage $V_G$.

By performing a Legendre transformation we obtain the Hamiltonian from $\mathscr{L}_{SET}^{elstat}$ as

$$\mathscr{H}_{SET}^{elstat}\,(\phi_A, Q_A) \,=\, \frac{\partial \mathscr{L}}{\partial \dot{\phi}_A}\,\dot{\phi}_A \,-\, \mathscr{L} \,=\, \frac{1}{2}\left[\frac{(Q_A \,+\, e\,N)^2}{C} \,-\, C_G\,V_G^2 \,-\, C_L\,V_L^2 \,-\, C_R\,V_R^2\right]$$
$$\equiv\, E_C\,(n \,-\, N)^2 \,-\, \frac{1}{2}\left(C_G\,V_G^2 \,+\, C_L\,V_L^2 \,+\, C_R\,V_R^2\right) \,\equiv\, \mathscr{H}_C(n, N) \,+\, cst\,, \quad (4.8)$$

where the charge on the dot $Q_A \equiv \frac{\partial \mathscr{L}}{\partial \dot{\phi}_A} = C\,\dot{\phi}_A - e\,N$ is the variable canonically conjugate to $\phi_A$. Thus the term $\mathscr{H}_C(n, N) \equiv E_C\,(n - N)^2$ accounts for the Coulomb interaction, with $n$ the excess electron number on the dot: $-\,e\,n \equiv Q_A$. Note that in Eq. (4.8) we have not included the work done by the voltage sources which is needed to transport back the electrons after tunneling through the circuit to retain the equilibrium. The factor $E_C \equiv e^2 / 2\,C$ is called the charging energy. It takes $\approx E_C + \delta E$ amount of energy to charge the dot by one electron as compared to its ground state, where $n$ assumes the value of the integer closest to $N$. So by tuning $V_G$ we can adjust the chemical potential, $\mu$ of the QD at will. This classical description permits the understanding of the Coulomb blockade phenomenon, and explains why it is called a transistor [159, 160].

To simplify the situation let us assume a symmetric setup with $C_L = C_R$ and $V/2 \equiv V_L = -\,V_R$. A transport voltage $V$ can be switched on to drive current through the dot. For small

capacitance $C$, low temperature and transport voltage, and weak coupling or hybridization, $\Delta$ (see Eq. (2.31)) between the dot and the leads: $k_B T, eV, \Delta \ll E_C$, the Coulomb interaction between the dot electrons is dominant. As it is depicted in Fig. 4.2, the transport is not suppressed only near the charge degeneracy points of the dot described by the condition $\mathscr{H}_C(n,N) = \mathscr{H}_C(n+1,N)$, that is when $N$ is half-integer. Here at finite $V$ and weak coupling, $\Delta \ll k_B T$ the transport is dominated by first order processes called sequential tunneling, meaning that when one electron enters the dot, one must leave it before the next one could enter.

By raising $V$ and keeping $V_G$ fixed, the level structure of the dot can be mapped, since the appearance of new levels in the transport window, $[\mu - eV/2,\ \mu + eV/2,]$, corresponds to the opening up of new tunneling channels.[3]

For $N$ not a half-integer, i.e. in the Coulomb blockade regimes the transport is suppressed, and the number of dot electrons, $n$ is set by the gate voltage. The system is called transistor since by tuning the gate voltage the current can be switched on and off,—although doubts have been raised whether such single electron transistors would ever replace the conventional field-effect transistors [171]. For fixed $V$ and with increasing $V_G$ the dot gets filled up in a step-like fashion, (if the steps do not get smeared out by the temperature and the hybridization between the dot and the leads). Consequently the current, $I$ and the differential conductance, $G \equiv lim_{V\to 0}\, \partial I/\partial V$ show a periodic structure as a function of $V_G$. There are peaks in the conductance, separated approximately by the period $\Delta V_G \approx e/C + \delta E/(2e)$, which covers the activation energy needed to reach the next level in the dot. This period can be used to measure $E_C$ when $\delta E \ll E_C$. The resonance widths are approximately given by $\max(\Delta, k_B T)$. When $\delta E \ll k_B T \ll E_C$, in the Coulomb blockade regimes the sequential tunneling is suppressed, but other processes such as elastic and inelastic co-tunneling and higher order processes are still possible and give rise to a finite conductance [204]. As we lower the temperature below the level spacing, $k_B T \ll \delta E$ the inelastic tunneling processes, which would leave behind electron-hole excitations in the dot, die out and the transport properties strongly depend on the parity of the number of dot electrons (see Fig. 4.2).

This qualitative picture can be made quantitative on applying e.g. the real-time transport theory [206] which can be used to perform systematic diagrammatic expansion in non-equilibrium situations, and which can even account for e.g. resonant tunneling with an arbitrary number of tunneling events beyond zeroth order or co-tunneling [208]. Still for odd number of dot electrons under appropriate circumstances, below a certain temperature, called the Kondo temperature $(T_K)$, strong, so-called Kondo correlations could develop. There the higher order tunneling processes dominate the transport properties.

### 4.2.3 Kondo effect in a single electron transistor

The canonical model for localized electrons – such as e.g. dot electrons in case of weak coupling to the environment – interacting with delocalized electrons – like conduction electrons in leads – is the Anderson model [51] (see Eq. (2.3)). To adjust this model to the description of a SET we introduce two types of operators $c^\dagger_{\mu,\alpha}(\vec{k})$ that create spin-$\mu$ conduction electrons with standing wave wavefunction in lead $\alpha = L, R$, and write the tunneling part as

$$\mathcal{H}^t_A \;=\; \sum_{i,\mu,\alpha\in\{L,R\},\vec{k}} t_\alpha \left( c^\dagger_{\mu,\alpha}(\vec{k})\, d_{i,\mu} \;+\; h.c. \right) , \tag{4.9}$$

[3] In this situation the current may even get suppressed with increasing $V$ due to the coupling between the levels.

where $d_i^\dagger$ creates an electron to the $i^{th}$ level of the QD. Realizing that from the even and odd combinations

$$\psi_{\mu,e}(\vec{k}) \equiv \frac{t_L\, c_{\mu,L}(\vec{k}) \,+\, t_R\, c_{\mu,R}(\vec{k})}{t} \tag{4.10}$$

$$\psi_{\mu,o}(\vec{k}) \equiv \frac{t_R\, c_{\mu,L}(\vec{k}) \,-\, t_L\, c_{\mu,R}(\vec{k})}{t} \tag{4.11}$$

with $t = \sqrt{t_L^2 + t_R^2}$, only the even channel couples to the dot electrons, makes the calculations simpler, since due to the mixing between the $L$ and $R$ lead electrons the problem can be handled by an effective single-channel description.[4] In the impurity or dot part of the Hamiltonian we can take into account several types of intradot interactions. Now we consider only the Coulomb repulsion besides the non-interacting part

$$\mathcal{H}_A^d = \sum_{i,\mu} \epsilon_i\, n_{i,\mu} + \frac{U}{2} \sum_{\{i,\mu\}\neq\{j,\nu\}} n_{i,\mu}\, n_{j,\nu}\,, \tag{4.12}$$

with $n_{i,\mu} \equiv d_{i,\mu}^\dagger d_{i,\mu}$. Clearly, the average level spacing of the dot is coded in the level distribution, $\epsilon_i$, whereas $U = 2\,E_C$ and when $e\,V < k_B\,T$ the Fermi level can be estimated by that of the left or right leads, since then $\epsilon_{F,L} \approx \epsilon_{R,L}$. The dot-lead tunneling amplitude can also be tuned e.g. in lateral QD's by changing the voltage on the gates that created the tunneling barriers in the 2DEG.

As it has already been mentioned in Section 2.2, the Anderson model in its local moment regime can be shown to correspond to an effective Kondo model. This regime is characterized by an odd number of impurity or dot electrons and by the relations written down in Eq. (2.9). This correspondence was first established in the paper of Schrieffer and Wolff [54], and was later refined by Kehrein [55]. Based on it it was predicted already in 1988 [205, 207] that by tuning the temperature and the SET parameters: $E_C$, $\delta E$ and the tunneling barriers appropriately, the Kondo effect should be observable in quantum dots in the form of an enhanced conductance in the Coulomb blockade valleys with odd number of dot electrons. This enhanced conductance, which can even reach the unitary limit, $2\,e^2/h$, can be comprehended as follows.

At sufficiently low temperatures (or frequencies) with odd number of dot electrons, it is enough to take into account only the singly occupied level closest to the Fermi surface in order to gain an effective description. In this regime second order elastic co-tunneling processes could still occur where an incoming electron with a spin alignment different from that of the dot spin gets scattered through a virtual excited dot state. Due to the spin degeneracy in the ground state of the isolated dot these processes may flip the dot spin or leave it unchanged, but in any case lower the energy of the system. This implies that anti-parallel spin alignment between the dot and the lead electrons is favored and thus hints at an antiferromagnetic exchange coupling in the effective Kondo Hamiltonian. Perturbation theory in the exchange coupling shows that below a certain energy scale the spin-flip scattering processes dominate and lead to divergent scattering amplitude in leading order [32]. The energy scale where this divergence sets in is called the Kondo temperature, $T_K$.

As it was first suggested by Anderson's poor man's scaling analysis [57] and later got numerical confirmation by Wilson's NRG [30], in the low-frequency limit the single-channel Kondo model

[4] Note that the odd channel can be omitted only for $V \to 0$, that is in equilibrium.

evolves toward a fixed point where the effective exchange interaction between the localized spin and the conduction electrons is infinitely strong. This manifests itself in the screening of the dot spin and a formation of a singlet many-body ground state meaning that the unpaired dot electron and a conduction electron form a spin singlet with a binding energy $\approx k_B T_K$ .[5]

Based on the picture above, Nozières was the first to realize that the low-energy system properties can be understood in terms of Landau's Fermi liquid theory [70] which presumes that the low-lying excitations of the system can be mapped to that of a non-interacting one.[6] It hinges on that below $T_K$ the spin of the dot disappears from the problem leaving behind a structureless local scattering potential. This indicates the appearance of a resonance, the so-called Kondo or Abrikosov–Suhl resonance [69, 217, 216] in the $d$-electron spectral function at the Fermi level in the electron-hole symmetrical case.

Our next goal is to obtain the maximal possible conductance through the dot. More precisely we are only able to calculate the linear conductance, that is one more reason why we have assumed a vanishing source-drain voltage initially. In case of the single-impurity Anderson model the linear conductance is given by the Landauer formula generalized for local interactions as [215]

$$G = \frac{e^2}{h} \int d\epsilon \left( -\frac{df(\epsilon)}{d\epsilon} \right) 4\,\pi^2\,\rho(\epsilon)\,\frac{|t_L|^2\,|t_R|^2}{|t_L|^2 + |t_R|^2}\,\varrho_d(\epsilon)\,, \tag{4.15}$$

with $f(\epsilon)$ the Fermi distribution, $\rho(\epsilon)$ the lead electron DOS and $\varrho_d(\epsilon)$ the $d$-level spectral function. At $T = 0$ this formula simplifies considerably. By knowing that below $T_K$ in the $d$-level spectral function the so-called Kondo resonance develops at the Fermi level which in the large bandwidth limit can be approximated by a Lorentzian peak as

$$\varrho_d(\epsilon) = \frac{1}{\pi}\,\frac{\Delta}{(\epsilon - \epsilon_F)^2 + \Delta^2}\,, \tag{4.16}$$

with $\Delta$ the hybridization defined as previously, we get that the linear conductance reaches its maximum $2\,e^2/h$ for $|t_L| = |t_R|$ at $T = 0$ at the Fermi level. The value of $\varrho_d(\epsilon_F)$ can

[5] The value of $T_K$ can be estimated e.g. by using the poor man's scaling approach [58]. Such an estimate is useful in the experiments when setting the temperature.

[6] Related to the previous footnote is that another possibility is to extract $T_K$ from the susceptibility of the impurity spin. At weak-coupling, i.e. at high frequencies the impurity is essentially free, decoupled from the conduction electrons which leads to an impurity susceptibility $\propto \omega^{-1}$, which is called Curie–Weiss susceptibility. On the other hand for low-temperatures Fermi liquid theory predicts a linear frequency-dependence. We can read out $T_K$ as the crossover energy scale matching these two types of behaviors.

The following simple calculation shows that the free spin susceptibility is indeed of Curie–Weiss form. Consider a system with two spin states: $S_z = \pm\frac{1}{2}$. If the Hamiltonian is simply given by $-\mu H S_z$ with $\mu = g\mu_B$ : the magnetic moment, $g$ : the gyromagnetic constant, $\mu_B = e\,\hbar/(2mc)$ : the Bohr magneton, and $H$ the magnetic field, then the magnetization, $M$ at temperature $T$ is

$$M = \mu\,\frac{\mathrm{Tr}\,\{S_z\,\exp[\mu\,H\,S_z\,/\,(k_B\,T)]\}}{\mathrm{Tr}\,\{\exp[\mu\,H\,S_z\,/\,(k_B\,T)]\}} = \frac{\mu}{2}\tanh\left(\frac{\mu\,H}{2\,k_B\,T}\right) \tag{4.13}$$

thus the susceptibility ($\chi \equiv \frac{\partial M}{\partial H}\big|_{H\,=\,0}$) is

$$\chi = \frac{\mu^2}{4\,k_B\,T}\,. \tag{4.14}$$

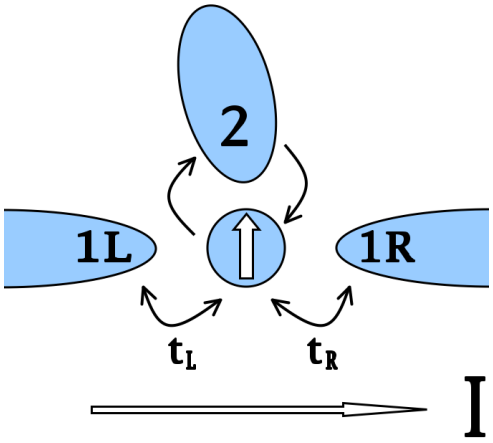


Figure 4.3: The double dot device (left) and its electric circuit equivalent (below) that was used to justify the existence of the 2CK state. The small dot in the center couples to a large dot (2) and to a left and a right lead ( $1L$ and $1R$ ) via the hopping amplitudes, $t_L$ and $t_R$. The small dot has a large level spacing ( $\delta E_s$ ), and the large dot is characterized by a vanishing level spacing ( $\delta E_l$ ). The temperature is set so that both dots are in the Coulomb blockade regime and $\delta E_l \ll T \ll \delta E_s$. As a result, only spin exchange is possible between the dots.

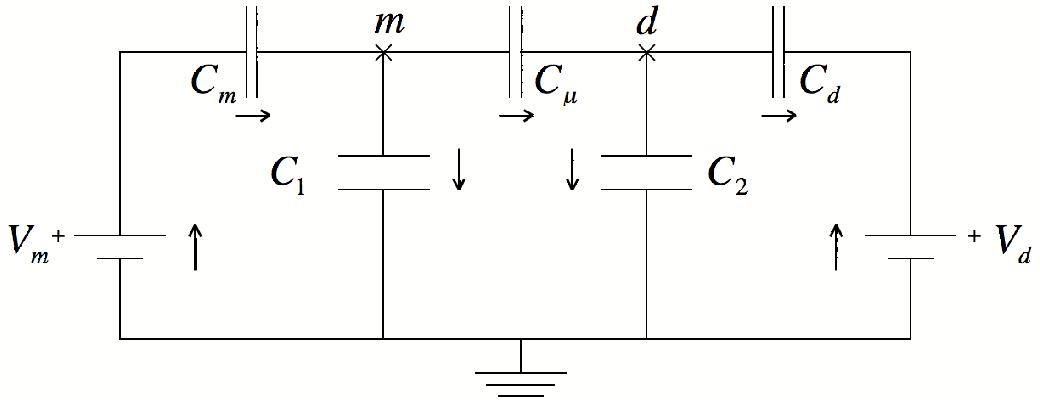


also be obtained from scattering theory by applying Friedel's sum rule [105], which relates the single-particle scattering phase shifts, $\delta_\mu(\epsilon)$ to the number of displaced electrons, $N$ due to the screening of the dot spin

$$\delta_\uparrow(\epsilon_F) + \delta_\downarrow(\epsilon_F) \;=\; \pi N\,. \tag{4.17}$$

In the case of one spin-half unpaired dot electron $N = 1$ and when there is no magnetic field $\delta_\uparrow(\epsilon_F) = \delta_\downarrow(\epsilon_F) = \pi/2$.

The first observation of the Kondo effect in QD's had to be waited until 1998 [151], whereas reaching the unitary limit was first reported in Ref. [209] in 2000.

### 4.2.4 Two-channel Kondo effect in a double dot system

Unlike the 1CK effect, the 2CK effect is not expected to occur in metals with magnetic impurities because its being unstable to channel anisotropy and other perturbations that are usually present (see Subsection 4.3.1). Recently a single electron transistor was designed and built to justify the existence of the 2CK state [149, 23]. The setup is depicted in Fig. 4.3. It consists of a small dot coupled to a large dot and to two leads. The spin of the small dot in the center plays the role of the impurity, whereas in the appropriate temperature domain, the large dot and the even combination of left and right lead electrons (cf. Eq. (4.10)) correspond to two independent

screening channels. Clearly, the large dot has to be large enough so that it has a relatively small level spacing and thus can operate as a conduction electron reservoir. That is the temperature must be in the range $\delta E_l \ll T \ll \delta E_s$, with $\delta E_l$ and $\delta E_s$ the level spacing of the large and small dot, respectively. The temperature needs to be set so that both dots are in the Coulomb blockade regime, and thus no mixing occurs between the screening channels. In this arrangement only spin exchange is possible between the small dot and the screening channels.

It is instructive to determine the electrostatic part of the Hamiltonian of this double dot system. It can be expressed much the same way as it was done in Subsection 4.2.2 for a simpler single electron transistor, therefore we do not present the details of the calculations only the initial conditions and the conclusions.

The electric circuit equivalent of the setup is shown in Fig. 4.3. The Lagrangian is given by

$$\mathscr{L}_{DD}^{elstat}\left(\phi_m, \dot{\phi}_m, \phi_d, \dot{\phi}_d\right) \;=\; \frac{1}{2} \sum_{i \in \{1,2,\mu,m,d\}} C_i \, \dot{\phi}_i^2 \,, \tag{4.18}$$

with $C_i$ and $\phi_i$ the corresponding capacitances and phases. The large and small dots are located at $m$ and $d$, respectively. We assume $C_m$ to be much larger than the other capacitances to have a quasi-continuous spectrum in the large dot. Due to the loop rules there are two independent variables which we choose to be the two phases at the islands $m$ and $d$, as eventually we would like to express the Hamiltonian in terms of the accumulated excess charges, $n_d$ and $n_m$ on the islands of the small and the large dots. By inspection it turns out the dominant energy scale is the charging energy of the small dot. Additionally there will be subleading terms in the electrostatic energy that describe the charging energy of the large dot and the interaction between the two dots due to their coupling via the capacitor $\mu$

$$\mathscr{H}_{DD}^{elstat}(n_d, n_m) \;=\; \frac{e^2}{2\,\tilde{C}_d} \left(n_d - N_d\right)^2 + E_{sl}\left(n_d, n_m\right) \,, \tag{4.19}$$

with $\tilde{C}_d \equiv C_\mu + C_2 + C_d$ the total capacitance of the small dot, and $N_d \equiv C_d\, V_d/e$. The rest of the Hamiltonian assumes the usual non-interacting Anderson Hamiltonian form with possible tunneling only between the small dot and leads and between the small and large dots.

When the temperature is lowered below the charging energy of the large dot then only spin exchange is possible between the small dot and the appointed screening channels. It is crucial that in this setup one has a precise control over the coupling between the small dot and the two screening channels. Thus it is possible to fine-tune the gate voltages so as to equalize the exchange couplings for the two channels and produce 2CK physics. The 2CK physics presents itself in the specific form of the linear conductance, $G$. Based on conformal field theory, for temperatures below $T_K$ in the regime $e\,V \;<\; k_B\,T$ $G$ should display quadratic voltage dependence, whereas for approximately $3\,k_B\,T \;<\; e\,V$ [193], it should switch to a square root-like voltage dependence (see Fig. 4.5).

## 4.3 Dynamical correlations in the two-channel Kondo model

### 4.3.1 Operator spectrum of the 2CK fixed point

To start our conformal field theoretical investigations we get back to the $s$-channel part of the Hamiltonian in Eq. (2.66) for the two-channel case

$$\mathcal{H}^s_{2CK} \;=\; \sum_{\alpha,\mu}\int dk\,\epsilon(k)\,a^\dagger_{\alpha\mu}(k)\,a_{\alpha\mu}(k) \;+\; \frac{V}{(2\pi)^3}\,\vec{S}\sum_{\alpha,\mu,\nu}\bar{J}_\alpha\,\tilde{\Psi}^\dagger_{\alpha\mu}(0)\,\frac{\vec{\sigma}_{\mu\nu}}{2}\,\tilde{\Psi}_{\alpha\nu}(0)\;. \quad (4.20)$$

This Hamiltonian possesses various symmetries. To see it, it is worth introducing left- and right-moving fermion fields for $r \geq 0$ as

$$\psi_{L/R,\alpha,\mu}(r) \;\equiv\; \int_{-D_F/v_F}^{D_F/v_F} dk\,e^{ipkr}\,a_{\alpha,\mu}\,(k+k_F)\;, \quad (4.21)$$

with $\epsilon_F = v_F\,k_F$ [7] and $p = \pm$ for right- and left-movers, respectively. In terms of these fields (suppressing channel and spin indices)

$$\tilde{\Psi}(r) \;\approx\; \frac{\sqrt{\pi}}{i\,r}\,\Big[e^{ik_Fr}\psi_R(r) \,-\, e^{-ik_Fr}\psi_L(r)\Big]\;, \quad (4.22)$$

(cf. Eq. (2.64)). Since $\psi_R(0) = \psi_L(0)$, $\lim_{r\to 0}\tilde{\Psi}(r)$ exists. We extend the fields to negative space coordinates as $\psi_L(-x) \equiv \psi_R(x)$. Next we linearize the dispersion around $\epsilon_F$: $\epsilon(k) = v_F\,(k - k_F)$ and express the free part of the Hamiltonian solely in terms of $\psi_L$ as

$$\mathcal{H}^{free}_{2CK} \;\approx\; iv_F\sum_{\alpha,\mu}\int_{-\infty}^{\infty}\frac{dx}{2\pi}\,\psi^\dagger_{L,\alpha,\mu}(x)\,\partial_x\,\psi_{L,\alpha,\mu}(x)\;, \quad (4.23)$$

whereas the interaction part becomes

$$\mathcal{H}^{int}_{2CK} \;\approx\; \vec{S}\,v_F\sum_{\alpha,\mu,\nu}\hat{J}_\alpha\,\psi^\dagger_{L,\alpha,\mu}(0)\;\frac{\vec{\sigma}_{\mu\nu}}{2}\,\psi_{L,\alpha,\nu}(0)\;, \quad (4.24)$$

with $\hat{J}_\alpha = \bar{J}_\alpha\,k_F^2\,V\,/\,(2\pi^2\,v_F) = \bar{J}_\alpha\,\rho(0)$ being the dimensionless coupling as before.[8] In the following we suppress the index $L$ : $\psi_{L,\alpha,\nu} \to \psi_{\alpha,\nu}$, since right-moving fields will not appear in the formulas. Then the total spin operators $\mathscr{J}^i$ defined as

$$\mathscr{J}^i \;\equiv\; S^i \,+\, \int\frac{\mathrm{d}x}{2\pi}\,J^i(x)\;, \quad (4.25)$$

$$J^i(x) \;\equiv\; \frac{1}{2}\sum_{\alpha,\mu}:\psi^\dagger_{\alpha,\mu}(x)\sigma^i_{\mu,\nu}\psi_{\alpha,\nu}(x):\;, \quad (4.26)$$

commute with the Hamiltonian and satisfy the standard SU(2) algebra,

$$\big[\mathscr{J}^i,\mathscr{J}^j\big] = i\epsilon^{ijk}\,\mathscr{J}^k\;, \quad (4.27)$$

[7] Throughout the calculations we use units of $\hbar = k_B = 1$.
[8] From now on we use units of $v_F = 1$.

(cf. Eq. (3.4)). In Eq. (4.26) we introduced the normal ordering $: \ldots :$ with respect to the non-interacting Fermi sea to set the energy of the filled Fermi sea to zero. In a similar way we can define the "charge spin" (or isospin) density operators, for the channels $\alpha = 1, 2$ respectively as

$$\begin{aligned} C^+_\alpha(x) &\equiv \psi^\dagger_{\alpha\downarrow}(x)\psi^\dagger_{\alpha\uparrow}(x)\,, \\ C^z_\alpha(x) &\equiv \frac{1}{2}\sum_\mu : \psi^\dagger_{\alpha,\mu}(x)\,\psi_{\alpha,\mu}(x) :\,, \\ C^-_\alpha(x) &\equiv \psi_{\alpha\uparrow}(x)\,\psi_{\alpha\downarrow}(x)\,, \end{aligned} \tag{4.28}$$

with $C^\pm_\alpha(x) \equiv C^x_\alpha(x) \pm i\, C^y_\alpha(x)$ , and the corresponding symmetry generators

$$\mathscr{C}^i_\alpha \equiv \int \frac{\mathrm{d}x}{2\pi}\, C^i_\alpha(x) \qquad (i = x, y, z)\,. \tag{4.29}$$

The generators $\mathscr{C}^i_\alpha$ , which are related to the electron-hole symmetry [106, 107, 108], and satisfy the same SU(2) algebra as the $\mathscr{J}^i$'s,

$$\left[\mathscr{C}^i_\alpha, \mathscr{C}^j_\beta\right] = i\delta_{\alpha\beta}\,\epsilon^{ijk}\mathscr{C}^k_\beta\,, \tag{4.30}$$

and they also commute with the Hamiltonian (cf. Eq. (3.5)). Thus the Hamiltonian $\mathcal{H}^s_{2CK}$ has a symmetry $\mathrm{SU}_{C1}(2) \times \mathrm{SU}_{C2}(2) \times \mathrm{SU}_S(2)$ in the charge and spin sectors for arbitrary couplings, $\hat{J}_\alpha$ .[9]

The same way as it was discussed in Subsection 3.1.2, these symmetries can be used to label every multiplet in the Hilbert space and every operator multiplet by the eigenvalues $\vec{\mathscr{J}}^{\,2} = J\,(J+1)$ and $\vec{\mathscr{C}}^{\,2}_\alpha = C_\alpha\,(C_\alpha+1)$ .

In the presence of a local magnetic field, i.e. when a term

$$\mathcal{H}_{magn} = -\,g\,\mu_B\,B\,S^z \tag{4.31}$$

is added to $\mathcal{H}^s_{2CK}$ , the symmetry of the system breaks down to $\mathrm{SU}_{C1}(2) \times \mathrm{SU}_{C2}(2) \times \mathrm{U}_S(1)$ , with the symmetry $\mathrm{U}_S(1)$ corresponding to the conservation of the $z$-component of the spin, $\mathscr{J}^z$ .[10]

For $\hat{J}_1 = \hat{J}_2 = \hat{J}$ and in the absence of an external magnetic field, the Hamiltonian, $\mathcal{H}^s_{2CK}$ possesses a dynamically generated energy scale, the so-called Kondo temperature,

$$T_K \approx D_F\, e^{-1/\hat{J}}\,. \tag{4.32}$$

At this scale perturbative expansions around the free fermion fixed point blow up and the system crosses over to another regime characterized by another fixed point. The definition of $T_K$ is somewhat arbitrary. We define $T_K$ to be the energy $\omega$ at which for $\hat{J}_1 = \hat{J}_2$ the spectral function of the composite fermion drops to half of its value assumed at $\omega = 0$ . The reason for this choice is that the composite fermion spectral function is proportional to the reducible self-energy of the conduction electrons which can be related to measurable quantities, e.g. it

[9] This group is a non-trivial subgroup of the $\mathrm{Sp}(4) \times \mathrm{SU}_S(2)$ group which is also a symmetry of the 2CKM for equal exchange coupling as it was established in the paper of Affleck *et al.* [65].

[10] From now on we use units where we set $g\,\mu_B \equiv 1$ .

determines the differential conductance of the double dot device depicted in Fig. 4.3, as it is discussed in Subsection 4.3.7. (for further details see the end of this Section and Fig. 4.4). For $B = 0$ and $\hat{J}_1 = \hat{J}_2$, below $T_K$ the physics is governed by the so-called two-channel Kondo fixed point.

The physics of the two-channel Kondo fixed point and its vicinity can be captured using conformal field theory. The two-channel Kondo finite size spectrum and its operator content has first been obtained using boundary conformal field theory by Affleck and Ludwig [27]. However, instead of charge SU(2) symmetries, Affleck and Ludwig used flavor SU(2) and charge U(1) symmetries to obtain the fixed point spectrum [27]. The generators of the flavor SU(2) symmetry are

$$\mathscr{T}^i = \int \frac{dx}{2\pi} T^i(x)\,, \tag{4.33}$$

$$T^i(x) = \frac{1}{2}\sum_{\alpha,\beta,\mu} :\psi^\dagger_{\alpha,\mu}(x)\sigma^i{}_{\alpha\beta}\psi_{\beta,\mu}(x):\,, \tag{4.34}$$

with $T^i(x)$ the flavor density operators. The use of charge SU(2) symmetries, however, has a clear advantage over the flavor symmetry when it comes to performing NRG calculations: While the channel anisotropy violates the flavor symmetry, it does not violate the charge SU(2) symmetries. Therefore, even in the channel anisotropic case, we have three commuting SU(2) symmetries. If we switch on a local magnetic field, only the spin SU(2) symmetry is reduced to its U(1) subgroup. Using charge symmetries permits much more precise calculations, and in fact using them is necessary to obtain accurate enough spectral functions, especially in the presence of magnetic field.

To understand the fixed point spectrum and the operator content of the 2CKM, let us outline the boundary conformal field theory in this $\mathrm{SU}_{C1}(2) \times \mathrm{SU}_{C2}(2) \times \mathrm{SU}_S(2)$ language. First, we remark that the spin density operators, $J^i(x)$ satisfy the $\mathrm{SU}(2)_{k=2}$ Kac–Moody algebra of level $k = 2$ [109, 27],

$$\begin{aligned}\left[J^i(x), J^j(x')\right] &= \frac{k}{2}\,\delta^{ij}\;\delta'(x-x') \\ &+ \;i\,2\pi\;\delta(x-x')\,\epsilon^{ijk}\,J^k(x)\,,\end{aligned} \tag{4.35}$$

while the charge density operators, $C^i_\alpha(x)$ satisfy the Kac-Moody algebra of level $k = 1$:

$$\begin{aligned}\left[C^i_\alpha(x), C^j_\beta(x')\right] &= \frac{k}{2}\delta^{ij}\delta_{\alpha\beta}\;\delta'(x-x') \\ &+ \;i\,2\pi\;\delta_{\alpha\beta}\delta(x-x')\epsilon^{ijk}C^k_\alpha(x)\,.\end{aligned}$$

We can use these current densities and the Sugawara construction to write the kinetic part of the Hamiltonian as

$$\mathcal{H}^{free}_{2CK} = \mathscr{H}_{C1} + \mathscr{H}_{C2} + \mathscr{H}_S + \mathscr{H}_I\,, \tag{4.36}$$

$$\mathscr{H}_{C\alpha} = \frac{1}{3}\int \frac{\mathrm{d}x}{2\pi} :\vec{C}_\alpha(x)\vec{C}_\alpha(x):\,,$$

$$\mathscr{H}_S = \frac{1}{4}\int \frac{\mathrm{d}x}{2\pi} :\vec{J}(x)\vec{J}(x):\;.$$

| $C_1$ | $C_2$ | $J$ | $I$ | $E_{\text{free}}$ |
|---|---|---|---|---|
| 0 | 0 | 0 | $\mathbb{1}$ | 0 |
| $\frac{1}{2}$ | 0 | $\frac{1}{2}$ | $\sigma$ | $\frac{1}{2}$ |
| 0 | $\frac{1}{2}$ | $\frac{1}{2}$ | $\sigma$ | $\frac{1}{2}$ |
| $\frac{1}{2}$ | $\frac{1}{2}$ | 1 | $\mathbb{1}$ | 1 |
| $\frac{1}{2}$ | $\frac{1}{2}$ | 0 | $\epsilon$ | 1 |

| $C_1$ | $C_2$ | $J$ | $I$ | $E_{\text{2CKM}}$ |
|---|---|---|---|---|
| 0 | 0 | $\frac{1}{2}$ | $\mathbb{1}$ | 0 |
| $\frac{1}{2}$ | 0 | 0 | $\sigma$ | $\frac{1}{8}$ |
| 0 | $\frac{1}{2}$ | 0 | $\sigma$ | $\frac{1}{8}$ |
| $\frac{1}{2}$ | $\frac{1}{2}$ | $\frac{1}{2}$ | $\mathbb{1}$ | $\frac{1}{2}$ |
| $\frac{1}{2}$ | 0 | 1 | $\sigma$ | $\frac{5}{8}$ |
| 0 | $\frac{1}{2}$ | 1 | $\sigma$ | $\frac{5}{8}$ |
| $\frac{1}{2}$ | $\frac{1}{2}$ | $\frac{1}{2}$ | $\epsilon$ | 1 |

Table 4.1: Left: Primary fields and the corresponding finite size energies at the free fermion fixed point for anti-periodic boundary conditions. States are classified according to the group $\mathrm{SU}_{C1}(2) \times \mathrm{SU}_{C2}(2) \times \mathrm{SU}_S(2)$ and the Ising model. The excitation energies $E_{\text{free}}$ are given in units of $2\pi/L$, with $L$ the size of the chiral fermion system. Right: Finite size spectrum at the two-channel Kondo fixed point.

In $\mathcal{H}_{2CK}^{free}$, the first two terms describe the charge sectors, and have central charge $c = 1$, while $\mathscr{H}_S$ describes the spin sector, and has central charge $c = 3/2$. The last term corresponds to the coset space, and must have central charge $c = 1/2$, since the free fermion model has central charge $c = 4$. This term can thus be identified as the critical Ising model [200], having primary fields $\mathbb{1}, \sigma, \epsilon$ with scaling dimensions $0, 1/16, 1/2$, respectively. We can then carry out the conformal embedding in the usual way, by comparing the finite size spectrum of the free Hamiltonian with that of Eq. (4.36), and identifying the allowed primary fields in the product space. The fusion rules obtained this way are listed on the left side of Table 4.1. The finite size spectrum at the two-channel Kondo fixed point can be derived by fusing with the impurity spin (which couples to the spin sector only) following the operator product expansion of the Wess–Zumino–Novikov–Witten model, $1/2 \otimes 0 \to 1/2$, $1/2 \otimes 1/2 \to 0 \oplus 1$, $1/2 \otimes 1 \to 1/2$ (see RHS of Table 4.1). Finally, the operator content of the fixed point can be found by performing a second fusion with the spin. The results of this double fusion are presented in Table 4.3.1. In Table 4.3.1 the leading irrelevant operator, $\vec{\mathscr{J}}_{-1}\vec{\phi}_s$, is also included; although it is not a primary field [27], close to the 2CK fixed point, this operator will also have impact on the form the correlation functions.

Conformal invariance binds the long-time behavior of the correlators of the primary fields, $\phi(\tau)$ to be

$$\lim_{\tau \to \infty} \langle \phi(\tau)\phi(0) \rangle \quad \propto \quad \frac{1}{\tau^{2\,x}}\,, \tag{4.37}$$

with $x$ the scaling dimension of $\phi$ [200, 6, 210]. This would mean no or logarithmic $\omega$-dependence around the 2CK fixed point at low-frequencies for the correlators of the primary fields. However, as we shall see, this behavior is modified by the presence of irrelevant perturbations which eventually result in a power law-like behavior.

What remains is to identify the scaling operators in terms of the operators of the non-interacting theory, or more precisely in terms of the local operators acting at the zeroth site of the Wilson chain. There are only five simple operators, $\vec{S}$ and $f_{0,\alpha,\mu}$ that satisfy this criterium,

but out of them, based on simple combinatorics, we can form all together 139 different local irreducible tensor operators not including the identity. In the following we do not consider all of them. Based on naive power counting among others we leave out the operators with $x < 0$, where $x$ is the dimensionality (in powers of momentum) of the corresponding coupling of the interaction described by the operator.[11] These interactions are termed to be non-renormalizable and are naively ignored on approaching the 2CK fixed point assuming that they are irrelevant, as they become less important in the limit of low-energies, i.e. using Weinberg's theorem or due to a theorem of Polchinski [201]. Every composite operator with more than two local fermions belongs to this family.

In general, an operator of the non-interacting theory can be written as an infinite series in terms of the scaling operators and their descendants. Apart from the Ising sector, which is hard to identify, we can tell by looking at the various quantum numbers of the operators acting on the Wilson chain, which primary fields could be present in them. In this way, we can identify, e.g. $\vec{\phi}_s$ as the spin operator $\vec{S}$. Thus the spin operator can be expressed as

$$\vec{S} \;=\; A_s\,\vec{\phi}_s + \dots \tag{4.38}$$

where the dots stand for all the less relevant operators that are present in the expansion of $\vec{S}$, and some high-frequency portions which are not properly captured in the expansion above. The weight, $A_s$ can be determined by matching the decay of the spin-spin correlation function at short and long times. This way we get $A_s \sim 1/\sqrt{T_K}$ since we know that at high-frequencies the impurity spin is decoupled from the conduction electrons and thus its susceptibility follows the Curie–Weiss law (see Eq. (4.14)).

There are many operators that contain the scaling fields in their expansion. As an example, let us consider the operators $\phi_{\psi 1}^{\tau\mu}$. Here the label $\mu = \{\uparrow,\downarrow\}$ refers to the spin components of a $J = 1/2$ spinor, while $\tau = \pm$ refers to the charge spins (or isospins) of a charge $C = 1/2$ spinor. To identify the corresponding operator on the Wilson chain, we first note that $f_{0,1,\mu}^\dagger$ transforms as a spinor under spin rotations. It can easily be seen that the operator $\tilde{f}_{0,1}^\dagger \equiv i\,\sigma_y\,f_{0,1}$ also transforms as a spinor. We can then form a four-spinor out of these operators, $\gamma_1 \equiv \{f_{0,1,\mu}^\dagger, \tilde{f}_{0,1,\mu}^\dagger\}$. It is easy to show that $\gamma_1$ transforms as a spinor under $\mathrm{SU}_{C1}(2)$ rotations as well, thus $\phi_{\psi 1}^{\tau\mu}$ could be identified as $\gamma_1 = \{f_{0,1,\mu}^\dagger, \tilde{f}_{0,1,\mu}^\dagger\}$.

However, we can construct another operator, $F_1^\dagger \equiv f_{0,1}^\dagger \vec{S}\vec{\sigma}$ and its counterpart, $\tilde{F}_1^\dagger \equiv i\,\sigma_y\,F_1$, and form a four-spinor out of them: $\Gamma_1 \equiv \{F_{1,\mu}^\dagger, -\tilde{F}_{1,\mu}^\dagger\}$. This operator has the same quantum numbers as $\gamma_1$, and in fact, both operators' expansions contain $\phi_{\psi 1}^{\tau\mu}$.

The operator $\phi_\Delta^{\tau\tau'}$ is of special interest, since it is relevant at the two-channel Kondo fixed point, just like the spin. Its susceptibility therefore diverges logarithmically. Good candidates for these operators would be $\sum_{\mu\nu}\epsilon_{\mu\nu}\,\gamma_1^{\tau\mu}\,\gamma_2^{\tau'\nu}$ (with $\epsilon_{\mu\nu}$ a two by two antisymmetric matrix with the entry $\epsilon_{\uparrow\downarrow} = 1$), since these are spin singlet operators that behave as charge 1/2 spinors in both channels. The $\tau = \tau' = +$ component of this operator corresponds to the superconducting order parameter

$$\mathcal{O}_{SC} \;\equiv\; f_{0,1,\uparrow}^\dagger f_{0,2,\downarrow}^\dagger \;-\; f_{0,1,\downarrow}^\dagger f_{0,2,\uparrow}^\dagger\,, \tag{4.39}$$

while the $+-$ components describe a local operator that hybridizes the channels, $\sim f_{0,1,\mu}^\dagger\,f_{0,2,\mu}$.

[11] Of course, here we refer to the local operators on the Wilson chain prior to making them dimensionless.

| $C_1$ | $C_2$ | $J$ | $I$ | $x^{2CK}$ | scaling operators | corresponding operators |
|---|---|---|---|---|---|---|
| 0 | 0 | 1 | 1 | $\frac{1}{2}$ | $\vec{\phi}_s$ | $\vec{S}$ |
| $\frac{1}{2}$ | 0 | $\frac{1}{2}$ | $\sigma$ | $\frac{1}{2}$ | $\phi_{\psi 1}^{\tau\mu}$ | $\gamma_1 \equiv \left(f_{0,1,\mu}^\dagger\,,\ (i\sigma_y f_{0,1})_\mu\right)$<br>$\Gamma_1 \equiv \left(F_{0,1,\mu}^\dagger\,,\ -(i\sigma_y F_{0,1})_\mu\right)$ |
| 0 | $\frac{1}{2}$ | $\frac{1}{2}$ | $\sigma$ | $\frac{1}{2}$ | $\phi_{\psi 2}^{\tau\mu}$ | $\gamma_2$<br>$\Gamma_2$ |
| $\frac{1}{2}$ | $\frac{1}{2}$ | 0 | $\mathbb{1}$ | $\frac{1}{2}$ | $\phi_\Delta^{\tau\tau'}$ | $\begin{pmatrix} f_{0,1}^\dagger \vec{S}\vec{\sigma}\ i\sigma_y f_{0,2}^\dagger & -f_{0,1}^\dagger \vec{S}\vec{\sigma} f_{0,2} \\ -f_{0,1}\sigma_y\ \vec{S}\vec{\sigma}\ \sigma_y f_{0,2}^\dagger & -f_{0,1} i\sigma_y\ \vec{S}\vec{\sigma} f_{0,2} \end{pmatrix}$ |
| 0 | 0 | 0 | $\epsilon$ | $\frac{1}{2}$ | $\phi_{anis}$ | $\vec{S}(f_{0,1}^\dagger \vec{\sigma} f_{0,1} - f_{0,2}^\dagger \vec{\sigma} f_{0,2})$ |
| 0 | 0 | 0 | $\mathbb{1}$ | $\frac{3}{2}$ | $\vec{\mathscr{J}}_{-1}\vec{\phi}_s$ | $\vec{S}(f_{0,1}^\dagger \vec{\sigma} f_{0,1} + f_{0,2}^\dagger \vec{\sigma} f_{0,2})$ |

Table 4.2: Highest-weight operators and their dimensions $x^{2CK}$ at the 2CK fixed point. Operators are classified by the symmetry group $\mathrm{SU}_{C1}(2) \times \mathrm{SU}_{C2}(2) \times \mathrm{SU}_S(2)$ and the scaling operators of the Ising model. The constants $C_1$ and $C_2$ denote the charge spins (or isospins) in channels 1 and 2, respectively, while $J$ refers to the spin, and $I$ labels the scaling operators of the Ising model: $\mathbb{1}, \sigma, \epsilon$. Superscripts $\tau, \tau' = \pm$ refer to the two components of charge spinors, while $\mu = \uparrow, \downarrow$ label the components of a spin-half spinor. The operator $\vec{\mathscr{J}}_{-1}$ is the Kac–Moody raising operator which raises the scaling dimension of $\vec{\phi}_s$ by one [193].

Another candidate would be the operator, $\sum_{\mu\nu} \epsilon_{\mu\nu} \Gamma_1^{\tau\mu} \gamma_2^{\tau'\nu}$. This operator is also a local singlet, and has charge spins (or isospins) $C_1 = C_2 = 1/2$. It contains the following component of the composite superconducting order parameter

$$\mathcal{O}_{SCC} \equiv f_{0,1}^\dagger \vec{S}\,\vec{\sigma}\, i\,\sigma_y\, f_{0,2}^\dagger\,. \tag{4.40}$$

From their transformation properties it is not obvious, which one of the above superconducting order parameters has singular susceptibility. However, NRG gives a definite answer by showing that while the susceptibility of the traditional operator does not diverge as the temperature or frequency goes to zero, that of the composite order parameter does (see Subsection 4.3.5), and thus confirms what first has first been anticipated in Ref. [28]. It is thus this latter operator that can be identified as $\phi_\Delta^{\tau\tau'}$. Note that, in case of electron-hole symmetry, the composite hybridization operator

$$\mathcal{O}_{mix} \equiv f_{0,1}^\dagger \vec{S}\,\vec{\sigma}\, f_{0,2} \tag{4.41}$$

has the same singular susceptibility as $\mathcal{O}_{SCC}$ since they are both components of the same tensor operator. This is, however, not true any more away from electron-hole symmetry. Furthermore, superconducting correlations are usually more dangerous, since in the Cooper channel any small attraction may lead to ordering when a regular lattice model of two-channel Kondo impurities is considered.

The knowledge of the operator content of the 2CK fixed point enables us to describe the effects of small magnetic fields and small channel anisotropies ($\hat{J}_1 \neq \hat{J}_2$). For energies and

temperatures below $T_K$, the behavior of the model can be described by the slightly perturbed two-channel Kondo fixed point Hamiltonian. For $\hat{J}_1 \approx \hat{J}_2$ and in a small magnetic field, $B \ll T_K$, this Hamiltonian can be expressed as

$$\mathcal{H} = \mathcal{H}^*_{2CK} + D_0^{1/2}\,\kappa_0\,\phi_{anis} + D_0^{1/2}\,\vec{h}_0\,\vec{\phi}_s + D_0^{-1/2}\,\lambda_0\,\vec{\mathscr{J}}_{-1}\,\vec{\phi}_s + \dots\,. \tag{4.42}$$

Here $\mathcal{H}^*_{2CK}$ is the 2CK fixed point Hamiltonian, and $\kappa_0$ is the dimensionless coupling to the channel anisotropy field, $\phi_{anis}$, whereas the effective magnetic field, $\vec{h}_0$, couples to the "spin field", $\phi_s$. Both of them are relevant perturbations at the 2CK fixed point and they must vanish to end up with the 2CK fixed point at $\omega, T \to 0$. The third coupling, $\lambda_0$, couples to the leading irrelevant operator (see Tab. 4.3.1), which dominates the physics when $\kappa = h = 0$. The energy cut-off $D_0$ in Eq. (4.42) is a somewhat arbitrary scale: it can be though of as the energy scale below which the 2CK physics emerges, i.e. $D_0 \sim T_K$. Then the dimensionless couplings $\kappa_0$, $\lambda_0$ and $h_0$ are approximately related to the couplings of the original Hamiltonian, Eq. (2.69), as[12]

$$\kappa_0 \approx K_R \equiv 4\,\frac{\hat{J}_1 - \hat{J}_2}{(\hat{J}_1 + \hat{J}_2)^2}\,, \tag{4.43}$$

$$h_0 \approx B/T_K\,, \tag{4.44}$$

$$\lambda_0 \approx O\,(1)\,. \tag{4.45}$$

However, the arbitrary scale $D_0$ in Eq. (4.42) can be changed at the cost of changing the couplings: $D_0 \to D\,, \kappa_0 \to \kappa(D)\,,\ h_0 \to h(D)$ and $\lambda_0 \to \lambda(D)$ in such a way that the physics below $D_0$ remains unchanged. This freedom translates to scaling equations, whose leading terms follow from the conformal field theory results (see Tab. 4.3.1), and read

$$\frac{d\kappa(D)}{dl} = \frac{1}{2}\,\kappa(D) + \dots\,, \tag{4.46}$$

$$\frac{dh(D)}{dl} = \frac{1}{2}\,h(D) + \dots\,, \tag{4.47}$$

$$\frac{d\lambda(D)}{dl} = -\frac{1}{2}\,\lambda(D) + \dots\,, \tag{4.48}$$

with $l = -\log D$, and the coefficients of the leading terms on the RHS are the RG eigenvalues, $y^{2CK} \equiv 1 - x^{2CK}$ of the corresponding operator [6]. Solving these equations with the initial conditions, $D = D_0 \sim T_K$ and $h = h_0\,,\ \kappa = \kappa_0\,,\ \lambda = \lambda_0$, we can read out the energy scales at which the rescaled couplings become of the order of one,

$$T^* \propto T_K\,\kappa_0^2 \sim T_K\,\frac{(\hat{J}_1 - \hat{J}_2)^2}{(\hat{J}_1 + \hat{J}_2)^4}\,, \tag{4.49}$$

$$T_h \propto T_K\,h_0^2 \sim B^2/T_K\,. \tag{4.50}$$

At these scales the couplings of the relevant operators are so large that they can no longer be treated as perturbations. Below $T^*$ the single-channel Kondo behavior is recovered in the more

[12] See e.g. Ref. [199] for the details of the derivation of these scales where the perturbative renormalization group approach breaks down.

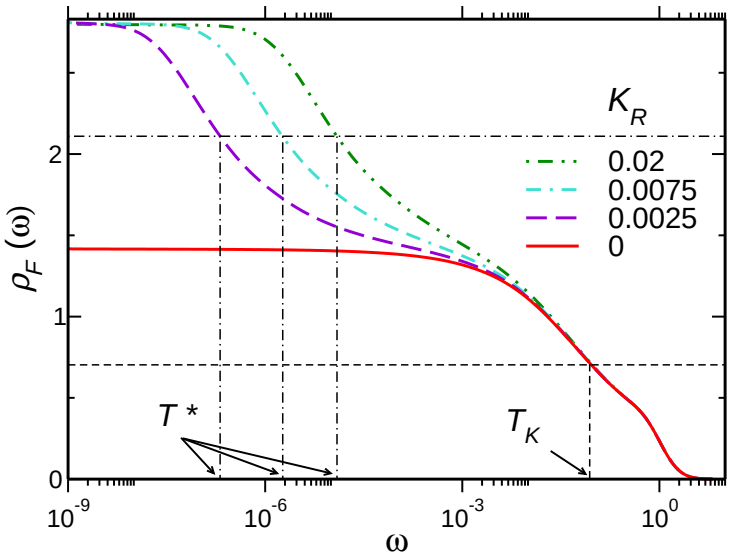


Figure 4.4: Spectral function $\varrho_F$ of the composite fermion operator, $F_{0,1,\uparrow}$ as a function of $\omega$, and the definition of the scales $T_K$ and $T^*$. $T_K$ is defined by the relation $\varrho_F(\omega = T_K, T = 0, K_R = 0) \equiv \frac{1}{2}\,\varrho_F(\omega = 0, T = 0, K_R = 0)$. For non-zero $K_R$ the scale $T^*$ is defined through $\varrho_F(\omega = T^*, T = 0, K_R) \equiv \frac{3}{4}\,\varrho_F(\omega = 0, T = 0, |K_R|)$.

strongly coupled channel, while $T_h$ can be interpreted as the scale where the impurity spin dynamics is frozen by the external field.

The prefactors in Eqs. (4.49) and (4.50) are somewhat arbitrary. They depend slightly on the precise definition one uses to extract these scales. In this thesis, we use the spectral function of the composite fermion to define the scales $T_K$ and $T^*$. We define $T_K$ to be the energy at which for $K_R = 0$ the spectral function of the composite fermion takes half of its fixed point value (i.e. the value assumed at $\omega = 0$), whereas $T^*$ is the energy at which for $K_R > 0$ it takes 75% of its fixed point value (see Fig. 4.4).

It is much harder to relate $T_h$ to a physically measurable quantity. We defined it simply through the relation, $T_h \equiv C_h\, B^2/T_K$, where the constant was chosen to be $C_h \approx 60$. This way $T_h$ corresponds roughly to the energy at which the NFL finite size spectrum crosses over to the low-frequency FL spectrum.

### 4.3.2 Details of the NRG calculations

All results presented refer to zero temperature. The NRG calculations were performed with a discretization parameter $\Lambda = 2$.

In the electron-hole symmetrical cases the sum of the dimensionless couplings was $\tilde{\mathcal{J}}_1 + \tilde{\mathcal{J}}_2 = 0.4$ for each run. We have used the symmetry group $\mathrm{SU}_{C1}(2) \times \mathrm{SU}_{C2}(2) \times \mathrm{SU}_S(2)$ in case of channel anisotropy but no magnetic field or electron-hole symmetry breaking.[13] At these calculations the maximum number of kept multiplets was 750 in each iteration. This corresponds to the diagonalization of $\approx 90$ matrices with matrix sizes ranging up to $\approx 600$, acting on the vector space of $\approx 9000$ multiplets consisting of $\approx 106000$ states.

In the presence of magnetic field we used the symmetry group $\mathrm{SU}_{C1}(2) \times \mathrm{SU}_{C2}(2) \times \mathrm{U}_S(1)$, and retained a maximum of 1350 multiplets in each iteration, that corresponds to the diagonalization of $\approx 150$ matrices with matrix sizes ranging up to $\approx 800$ acting on the vector space of

[13] The corresponding symmetry generators have been enumerated in Eqs. (3.4) and (3.5).

$\approx$ 18000 multiplets consisting of $\approx$ 73000 states.

As for the details of the DM-NRG calculations in case of electron-hole symmetry breaking caused by the term Eq. (4.82), which is briefly discussed in Subsection 4.3.6, we used the symmetry group $\mathrm{U}_{C1}(1) \times \mathrm{U}_{C2}(1) \times \mathrm{SU}_S(2)$ and retained a maximum of 2000 multiplets in each iteration, that corresponds to the diagonalization of $\approx$ 250 matrices with matrix sizes ranging up to $\approx$ 1000 acting on the vector space of $\approx$ 29000 multiplets consisting of $\approx$ 138000 states.

Next we show how the knowledge of the operator content of the two-channel Kondo fixed point help us understand the analytic structure of the various dynamical correlation functions obtained by DM-NRG.

### 4.3.3 Local fermions' spectral functions and susceptibilities

Let us first analyze the Green's function of the local fermion, $f^\dagger_{0,\alpha,\mu} \leftrightarrow \vec{\gamma}_\alpha$. The composite fermion's ( $F^\dagger_{0,\alpha,\mu} \leftrightarrow \vec{\Gamma}_{0,\alpha}$ ) Green's function [140], which is proportional to the reducible self-energy, is closely related to it through the Dyson equation. Therefore we do not discuss its analytic properties in detail but use it merely as a reference to define the various energy scales in the NRG calculations (see Fig. 4.4). Let us note, however, that in the large bandwidth limit, apart from a trivial constant shift, a minus sign and a proportionality factor, the spectral function of the local fermion is that of the composite fermion, and close to the 2CK fixed point all features of $\varrho_F$ are also reflected in $\varrho_f$.

Before we discuss the NRG results, let us examine what predictions we have for the retarded Green's function of the operator $f^\dagger_{0,\alpha,\mu}$ from conformal field theory. By looking at its quantum numbers, this operator can be identified with the operator $\phi^{+\mu}_{\psi\alpha}$ (see Tab. 4.3.1), i.e.

$$f^\dagger_{0,\alpha,\mu} = A_f \, \phi^{+\mu}_{\psi\alpha} + \dots \,, \tag{4.51}$$

with the prefactor $A_f \propto 1/\sqrt{D_F}$ with $A_f$ a complex number. The dots in the equation above indicate the series of other, less relevant operators and their descendants, which give subleading corrections to the correlation function of $f^\dagger_{0,\alpha,\mu}$. Furthermore, the expansion above holds only for the long time behavior. The short time part of the correlation function of $f^\dagger_{0,\alpha,\mu}$ is not captured by Eq. (4.51), and gives a constant to $\mathcal{G}_f(\omega)$ of the order of $\sim 1/D_F$. Thus, apart from a prefactor $A_f^2$, a constant shift and subleading terms, the Green's function of $f^\dagger_{0,\alpha,\mu}$ is that of the field $\phi^{+\mu}_{\psi\alpha}$. Using the Callan–Symanzik equations it can be shown that the Green's function of any operator of dimension $x = 1/2$ is scale invariant around the two-channel Kondo fixed point [91]. Since $\phi^{+\mu}_{\psi\alpha}$ and thus $f^\dagger_{0,\alpha,\mu}$ have a scaling dimension 1/2 at the 2CK fixed point, it follows that the dimensionless retarded Green's function, $D_F \, \mathcal{G}_f(\omega)$, is also scale invariant

$$\begin{aligned} D_F \, \mathcal{G}_f(\omega, T) &\equiv \hat{g}_f \left( \frac{\omega}{D}, \frac{T}{D}, \kappa(D), h(D), \lambda(D), \dots \right) , \\ \frac{\mathrm{d}\hat{g}_f}{\mathrm{d}l} = D \frac{\mathrm{d}\hat{g}_f}{\mathrm{d}D} &= 0 \,. \end{aligned} \tag{4.52}$$

From Eq. (4.52), we can deduce various important properties. Let us first consider the simplest case, $T = 0$ and $\kappa = h = 0$. Then setting the scale $D$ to $D_0 \sim T_K$ we have

$$\hat{g}_f^{\kappa,h,T=0}(\omega) = \hat{g}_f \left( \frac{\omega}{D_0}, \lambda_0, \dots \right) . \tag{4.53}$$

Let us now by choosing a time rescaling parameter $a > 1$ with $a^n = D_0/|\omega|$ rescale $D \to |\omega|$ in $n$ steps. By using the fixed point scaling equation (4.48) we obtain $\lambda(D)$

$$\begin{aligned} \hat{g}_f &= \hat{g}_f \left( \pm a^n \, \frac{\omega}{D_0}, a^{-n/2} \, \lambda_0, \dots \right) \\ &= \hat{g}_f \left( \pm 1, \sqrt{\frac{|\omega|}{D_0}} \; \lambda_0, \dots \right) . \end{aligned} \tag{4.54}$$

Assuming that this function is analytic in its second argument we have for $|\omega| \ll T_K$

$$\begin{aligned} \hat{g}_f^{\kappa,h,T=0}(\omega) &= \hat{g}_f\Big(\frac{\omega}{T_K}\Big) \\ &\approx g_{\pm\, f} + g'_{\pm\, f} \sqrt{\frac{|\omega|}{T_K}} + \dots , \end{aligned} \tag{4.55}$$

with $g_{\pm\, f}$ and $g'_{\pm\, f}$ some complex expansion coefficients. Here the subscripts $\pm$ refer to the cases $\omega > 0$ and $\omega < 0$, respectively. As we discussed above, the constants $g_{\pm\, f}$ depend also on the short time behavior of $\mathcal{G}_f(t)$, and are not universal in this sense. These constants are not independent of each other. They are related by the constraint that the retarded Green's function must be analytic in the upper half-plane. Furthermore, electron-hole symmetry implies that $g_{+\, f} = g_{-\, f}$ and $g'_{+\, f} = -\,(g'_{-\, f})^*$.

Relations similar to the ones above hold for the dimensionless spectral function. This is defined as

$$\hat{\varrho}_f(\omega) \equiv -\frac{1}{\pi} \, \mathrm{Im} \, \hat{g}_f(\omega) \, , \tag{4.56}$$

and assumes the following form at small frequencies in case of electron-hole symmetry,

$$\hat{\varrho}_f^{T,\kappa,h=0}(\omega) = r_f + r'_f \sqrt{\frac{|\omega|}{T_K}} + \dots \tag{4.57}$$

For $\omega \gg T_K$ the scaling dimension of the local fermion is governed by the free fermion Hamiltonian, $x_f^{free} = 1/2$, corresponding to an $\omega$-independent spectral function. Perturbation theory in $J$ amounts to logarithmic corrections of the form: $1/2 - cst\,/\,\log^2(T_K/\omega)$, as we sketched it on the left parts of Figs. 4.5 and 4.6.

For $T \neq 0$, and $\kappa = h = 0$ using similar arguments as before, but now rescaling $D \to T$ we find

$$\begin{aligned} \hat{g}_f^{\kappa,h=0}(\omega) &= \hat{g}_f \left( \frac{\omega}{T}, \frac{T}{T_K}, \lambda_0 \right) \\ &\equiv \hat{g}_f \left( \frac{\omega}{T}, 1, \sqrt{\frac{T}{D_0}} \; \lambda_0, \dots \right) . \end{aligned} \tag{4.58}$$

Then by expanding $\hat{g}_f$ we obtain the following scaling form for the low temperature behavior of the spectral function,

$$\hat{\varrho}_f^{\kappa,h=0}(\omega) = \Theta_f \left( \frac{\omega}{T} \right) + \sqrt{\frac{T}{T_K}} \; \tilde{\Theta}_f \left( \frac{\omega}{T} \right) + \dots \, , \tag{4.59}$$

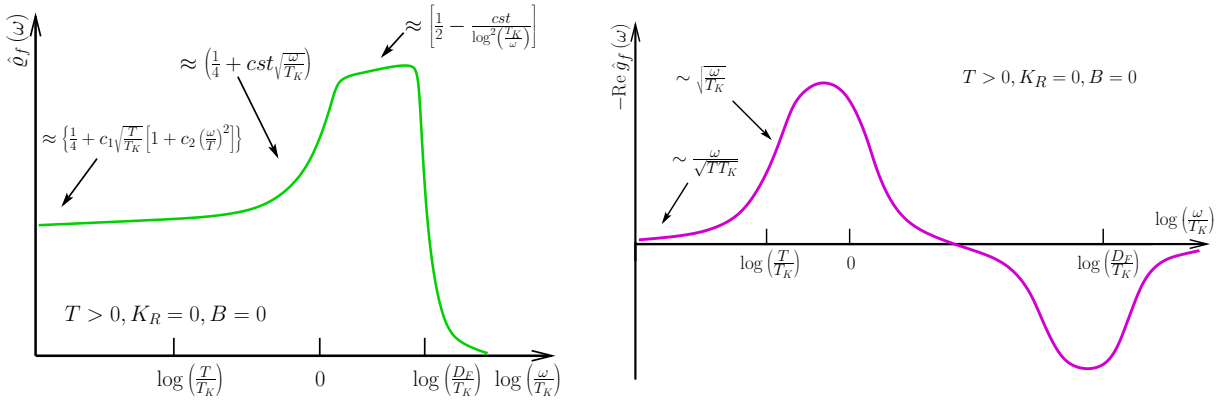


Figure 4.5: (left) Sketch of the dimensionless spectral function $\hat{\varrho}_f = D_F\,\varrho_f$ of $f^\dagger_{0,1,\sigma}$, and (right) the real part of its dimensionless Green's function, $\mathrm{Re}\,\hat{g}_f = D_F\,\mathrm{Re}\,\mathcal{G}_f$ for $T > 0$ and $K_R = 0, B = 0$ as a function of $\log(\omega/T_K)$. Asymptotics indicated for $\omega < T_K$ were derived through scaling arguments. The large $\omega$-behavior is a result of perturbation theory. The features of the spectral functions for $\omega > D_F$ are non-universal and depend on the realization of the model.

with $\Theta_f$ and $\tilde{\Theta}_f$ universal scaling functions. Note that we made no assumption about the ratio $\omega/T$, but both $\omega$ and $T$ must be smaller than $T_K$.

The asymptotic properties of $\tilde{\Theta}_f$ can be extracted by making use of the facts that $(i)$ $\hat{g}_f(\omega, T)$ must be analytic for $\omega \ll T$, $(ii)$ that Eq. (4.59) should reproduce the $T \to 0$ results in the limit $\omega \gg T$, and $(iii)$ that by electron-hole symmetry, $\hat{\varrho}_f$ must be an even function of $\omega$. The emerging asymptotic properties together with those of the other scaling functions defined later are summarized in Table 4.3.3. The asymptotic properties of the real part, $\mathrm{Re}\,\hat{g}_f$, can be extracted from those of $\hat{\varrho}_f$ by performing a Hilbert transform

$$\mathrm{Re}\,\hat{g}_f(\omega) \;=\; \mathcal{P}\int \mathrm{d}\tilde{\omega}\,\frac{\hat{\varrho}_f(\tilde{\omega})}{\omega - \tilde{\omega}} \tag{4.60}$$

with $\mathcal{P}$ the principal part. The obtained features are sketched in Fig. 4.5 for $T > 0$ and $\kappa = h = 0$.

Let us now investigate the effect of channel anisotropy, i.e. $\kappa \neq 0$ at $T = 0$ temperature and no magnetic field $h = 0$. In this case, we can rescale $D$ from its initial value $D_0$ to $D = |\omega|$ to obtain

$$\begin{aligned}\hat{\varrho}_f^{T,h=0}(\omega) \;&=\; \hat{\varrho}_f\left(1, \left(\frac{T_K}{\omega}\right)^{1/2}\kappa_0, \left(\frac{\omega}{T_K}\right)^{1/2}\lambda_0, \dots\right) \\ &=\; \mathcal{K}_f^{\pm}\left(\frac{\omega}{T^*}\right) + \sqrt{\frac{|\omega|}{T_K}}\;\tilde{\mathcal{K}}_f^{\pm}\left(\frac{\omega}{T^*}\right) + \dots\,,\end{aligned} \tag{4.61}$$

with $T^*$ the anisotropy scale defined earlier in Eq. (4.49). The superscripts $\pm$ refer to the cases of positive or negative anisotropies: the superscript "+" is used when the coupling is larger in the channel $\alpha$ where the Green's function of $f^\dagger_{0,\alpha,\mu}$ is measured. The asymptotics of the

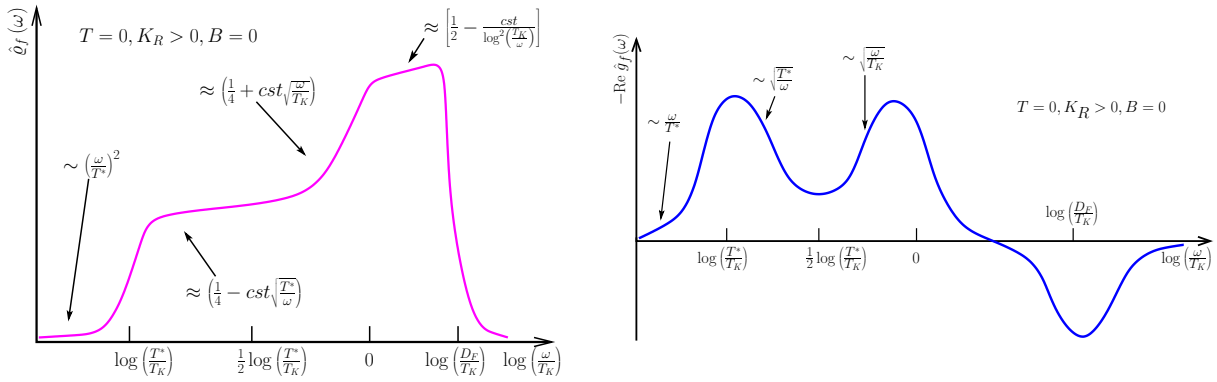


Figure 4.6: (left) Sketch of the dimensionless spectral function of $f^\dagger_{0,1,\mu}$: $\hat{\varrho}_f = D_F\ \varrho_f$, and (right) the real part of its dimensionless Green's function: $\mathrm{Re}\,\hat{g}_f = D_F\,\mathrm{Re}\,\mathcal{G}_f$ for $T = 0, K_R > 0$ and $B = 0$ as a function of $\log(\omega/T_K)$. Asymptotics indicated for $\omega < T_K$ were derived through scaling arguments. The large $\omega$-behavior is a result of perturbation theory. The features of the spectral functions for $\omega > D_F$ are non-universal.

universal functions $\mathcal{K}^\pm_f$ and $\tilde{\mathcal{K}}^\pm_f$ can be obtained through similar scaling arguments as before and they differ only slightly from those of $\Theta_f$ and $\tilde{\Theta}_f$ (see Table 4.3.3). The properties of $\hat{\varrho}^{T,h=0}_f(\omega)$ are summarized in Fig. 4.6. A remarkable feature of the spectral function is that it contains a correction $\sim \sqrt{T^*/|\omega|}$. This correction can be obtained by doing perturbation theory in the small parameter $\kappa(\omega)$ at the two-channel Kondo fixed point, and exploiting that there the long-time behavior of the three-point functions is specified by conformal invariance [200, 193]. Hence for $\omega \to 0$ the analytic form of the Fourier transform of

$$\int d\tau' \left\langle \mathcal{T}\, f^\dagger_{0,\alpha,\mu}(\tau)\, \phi_{anis}(\tau')\, f_{0,\alpha,\mu}(0)\right\rangle \tag{4.62}$$

with $\mathcal{T}$ the time-ordering operator, can easily be determined upon dimensional analysis. Thus the procedure of extracting the leading correction to the near fixed point behavior works the same way as for the leading irrelevant operator.

From the asymptotic forms in Table 4.3.3 we find that in the limit $\omega/T^* \gg 1$ in the local fermion's susceptibility a new scale, $T^{**}_f \sim \sqrt{T^* T_K}$ appears as a result of the competition between the leading irrelevant operator and the channel anisotropy [140]. Thus it is only in the regime $T^{**}_f < \omega < T_K$ that the leading irrelevant operator determines the dominant scaling behavior of the local fermion's susceptibility, i.e. we expect to see 2CK physics. The expected properties of $\hat{\rho}_f$ and that of the real part of its dimensionless Green's function $\hat{g}_f$ in the presence of channel asymmetry are shown in Fig. 4.6. And as we shall see, these analytic expectations are nicely confirmed by our NRG results.

Fig. 4.7.($a$) depicts the spectral function of $f^\dagger_{0,1,\mu}$ for several values of $K_R$ as a function of $\omega/T_K$ on a logarithmic scale. The overall scaling is very similar to the one sketched in Fig. 4.6, except that the high temperature plateau is missing; this is due to the relatively large value of $T_K$, which is only one decade smaller than the bandwidth cut-off. We chose such a large $T_K$ so that the low-frequency behavior is visible for longer before the numerical errors blow up.

| Scaling Function | Asymptotic Form | | Scaling Variable | 2CK |
|---|---|---|---|---|
| | $x \ll 1$ , | $1 \ll x$ | $x$ | Scaling Regime |
| $\Theta_f\ (x)$ | $1/4$ | $1/4$ | $\omega/T$ | $T \lessapprox \omega$ |
| $\tilde{\Theta}_f\ (x)$ | $\tilde{\theta}_f^{\,0} + \tilde{\theta}_f^{\,0\,\prime}\, x^2$ , | $\tilde{\theta}_f^{\infty}\ x^{1/2}$ | | |
| $\mathcal{K}_f^{\pm}\ (x)$ | $\kappa_{f,0}^{\pm} + \kappa_{f,0}^{\pm\,\prime}\, x^2$ , | $\kappa_{f,\infty}^{\pm} + \kappa_{f,\infty}^{\pm\,\prime}\ \left\lvert\frac{1}{x}\right\rvert^{1/2}$ | $\omega/T^*$ | $T_f^{**} \lessapprox \omega$ , $\quad T_f^{**} \propto \sqrt{T^* T_K}$ |
| $\tilde{\mathcal{K}}_f^{\pm}\ (x)$ | $\tilde{\kappa}_{f,0}^{\pm}\ \lvert x\rvert^{3/2}$ , | $\tilde{\kappa}_{f,\infty}^{\pm}$ | | |
| $\mathcal{B}_{f,\mu}\ (x)$ | $\beta_{f,\mu}^{0} + \beta_{f,\mu}^{0\,\prime}\, x^2$ , | $\beta_{f,\mu}^{\infty} + \beta_{f,\mu}^{\infty\,\prime}\ \left\lvert\frac{1}{x}\right\rvert^{1/2}$ | $\omega/T_h$ | $T_h^{**} \lessapprox \omega$ , $\quad T_h^{**} \propto \sqrt{T_h T_K}$ |
| $\tilde{\mathcal{B}}_{f,\mu}\ (x)$ | $\tilde{\beta}_{f,\mu}^{0}\ \lvert x\rvert^{3/2}$ , | $\tilde{\beta}_{f,\mu}^{\infty}$ | | |
| $\Theta_S\ (x)$ | $\theta_S^{0}\, x$ , | $\theta_S^{\infty}\ \mathrm{sgn}(x)$ | $\omega/T$ | $T \lessapprox \omega$ |
| $\tilde{\Theta}_S\ (x)$ | $\tilde{\theta}_S^{0}\, x$ , | $\tilde{\theta}_S^{\infty}\ \mathrm{sgn}(x)\ \lvert x\rvert^{1/2}$ | | |
| $\mathcal{K}_S\ (x)$ | $\kappa_S^{0}\, x$ , | $\kappa_S^{\infty}\ \mathrm{sgn}(x)\ + \kappa_S^{\infty\,\prime\prime}\, \frac{1}{x}$ | $\omega/T^*$ | $T_s^{**} \lessapprox \omega$ , $\quad T_s^{**} \propto \left(T^{*2} T_K\right)^{1/3}$ |
| $\tilde{\mathcal{K}}_S\ (x)$ | $\tilde{\kappa}_S^{\,0}\ \mathrm{sgn}(x)\ \lvert x\rvert^{1/2}$ , | $\tilde{\kappa}_S^{\infty}\ \mathrm{sgn}(x)$ | | |
| $\mathcal{B}_{S,z}\ (x)$ | $\beta_{S,z}^{0}\, x$ , | $\beta_{S,z}^{\infty} + \beta_{S,z}^{\infty\,\prime}\ \left\lvert\frac{1}{x}\right\rvert^{1/2}$ | $\omega/T_h$ | $T_h^{**} \lessapprox \omega$ , $\quad T_h^{**} \propto \sqrt{T_h T_K}$ |
| $\tilde{\mathcal{B}}_{S,z}\,(x)$ | $\tilde{\beta}_{S,z}^{0}\ \lvert x\rvert^{1/2}$ , | $\tilde{\beta}_{S,z}^{\infty}$ | | |

Table 4.3: Asymptotic behavior of the universal cross-over functions. At finite temperature, the boundary of the two-channel Kondo scaling regime is set by the temperature. At zero temperature, the various boundaries of the 2CK scaling regime derive from the competition between the leading irrelevant operator and the relevant perturbation.

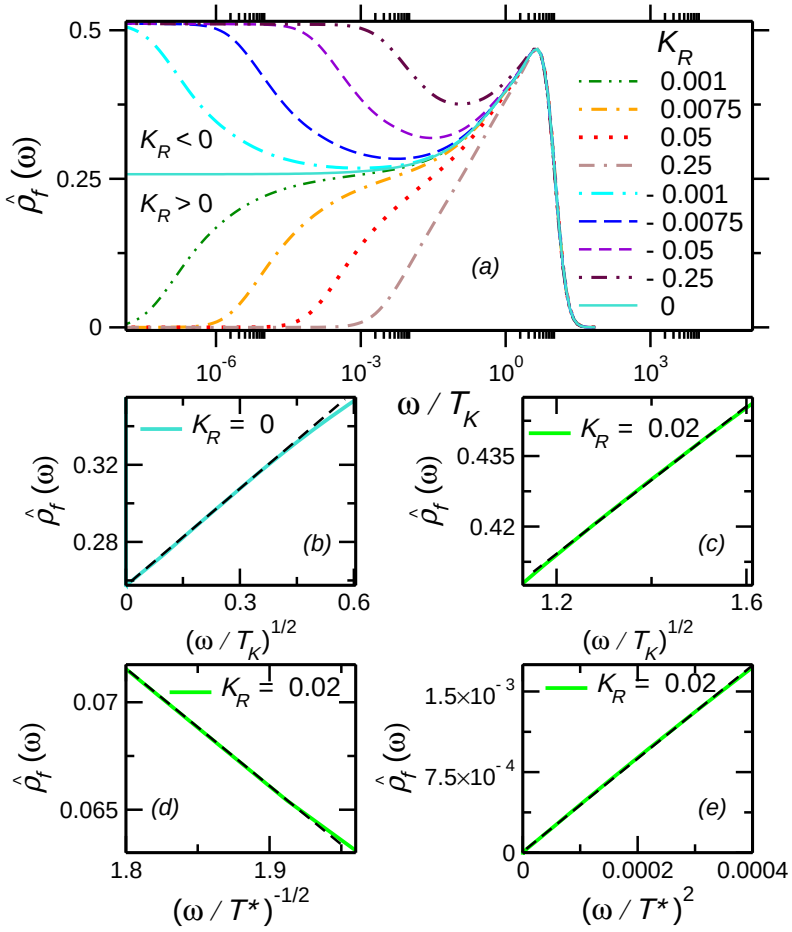


Figure 4.7: $(a)$ Dimensionless spectral function of $f_{0,1,\mu}$: $\hat{\varrho}_f(\omega) = D_F \varrho_f(\omega)$ as a function of $\omega/T_K$ for different values of $K_R$. $(b-e)$ Numerical confirmations of the low-frequency asymptotics derived through scaling arguments in Subsection 4.3.3. Dashed straight lines are to demonstrate deviations from the expected $\sqrt{\omega}$-like $(b-c)$, $1/\sqrt{\omega}$-like $(d)$ and $\omega^2$-like $(e)$ behavior. In plots $(c-e)$ $T^*/T_K = 2.4 \times 10^{-4}$.

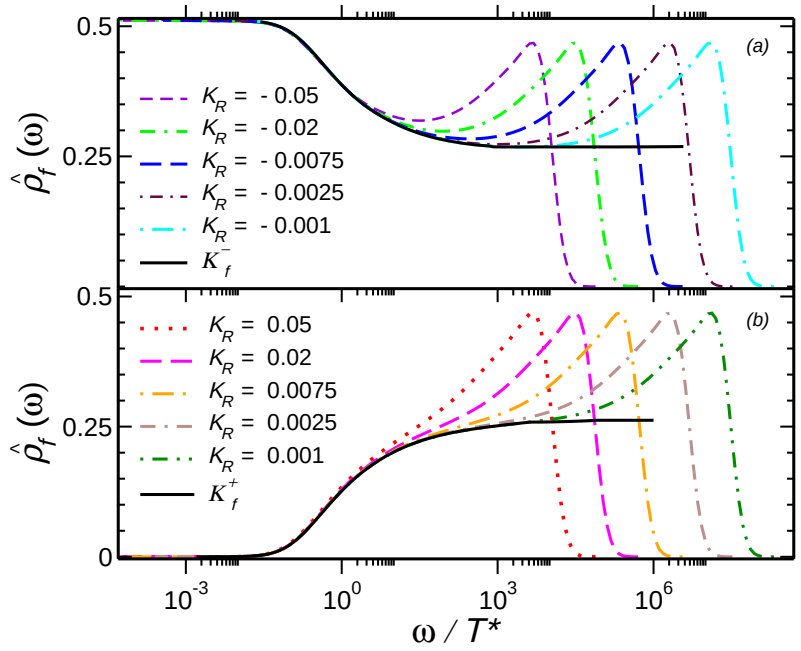


Figure 4.8: Universal collapse of the dimensionless spectral functions, $\hat{\varrho}_f = D_F \varrho_f$ (with $f$ in channel 1) to two scaling curves, $\mathcal{K}_f^{\pm}$ as a function of $\omega/T^*$ for positive $(b)$ and negative $(a)$ values of $K_R$.

Figures 4.7.$(b-e)$ are the numerical confirmations of the asymptotics stated. In all these figures dashed straight lines are to demonstrate deviations from the expected behavior. In Fig. 4.7.$(b)$ we show the square root-like asymptotics in the 2CK scaling regime for the channel symmetric case. This behavior is a consequence of the dimension of the leading irrelevant operator as it has just been discussed. In Fig. 4.7.$(c)$ the same asymptotics is shown in the same region in case of a finite channel anisotropy, whereas below them Fig. 4.7.$(d)$ demonstrates an $(1/\omega)^{1/2}$-like behavior resulting from the relevant perturbation of the 2CK fixed point Hamiltonian with channel anisotropy. In Fig. 4.7.$(e)$ the FL-like $\omega^2$-behavior is recovered below $T^*$, which is typical of fermionic operators in the 1CK scaling regimes.

In Figs. 4.8.$(a-b)$ we show the universal scaling curves, $\mathcal{K}^{\pm}$ that connect the two-channel and single-channel fixed points at low-frequencies. They were computed from runs with negative and positive values of $K_R$ and are plotted as a function of $\omega/T^*$. The universal behavior is violated for values of $K_R$ higher than the highest ones shown in Fig. 4.8, where $T^*$ becomes comparable to $T_K$.

The real parts of the local fermion susceptibilities are plotted in Fig. 4.9 for several values of $K_R$. They were obtained by performing the Hilbert transformations numerically. They should show a three-peak structure based on the analytic considerations (see Fig. 4.6). There are two low-frequency peaks clearly visible, associated with the cross-overs at $T^*$ and $T_K$. Furthermore there should be a non-universal peak at the cut-off. For relatively large channel anisotropies, where $T^* \sim T_K$, the former two peaks cannot be clearly separated in Fig. 4.9. Also, due to the large value of $T_K \sim D_F$, the peak at $\omega \sim T_K$ and the smeared singularity at the bandwidth cut-off, $\omega = D_F$ merge to a single non-universal feature in our NRG curves.

Let us now turn to the effect of a finite magnetic field, $B \neq 0$ for the case $T = 0, K_R = 0$. As $h$ and $\kappa$ scale the same way in the 2CK scaling regime, the argument concerning the $\kappa \neq 0$ case can be repeated with some distinctive features: Now, the spin $\mathrm{SU}_S(2)$ symmetry

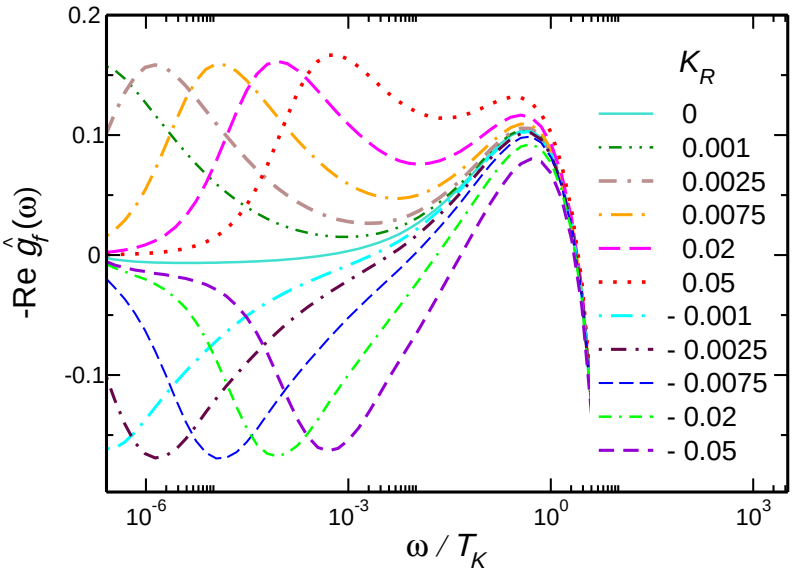


Figure 4.9: Real part of the dimensionless Green's function: $\mathrm{Re}\,\hat{g}_f = D_F \mathrm{Re}\,\mathcal{G}_f$ (with $f^\dagger$ in channel 1) as a function of $\omega/T_K$ for different values of $K_R$. From among the three peaks sketched in Fig. 4.6 only the two peaks around $T^*$ and $T_K$ are shown.

is violated, and therefore the spectral functions of $f^\dagger_{0,\alpha,\uparrow}$ and $f^\dagger_{0,\alpha,\downarrow}$ become different, and they are no longer even either. Nevertheless, due to particle-hole symmetry, they are still related through the relations

$$\begin{aligned} \hat{\rho}_{f,\uparrow}(\omega, T, \kappa, h, \dots) &= \hat{\rho}_{f,\downarrow}(-\omega, T, \kappa, h, \dots) \ , \\ \hat{\rho}_{f,\uparrow}(\omega, T, \kappa, h, \dots) &= \hat{\rho}_{f,\downarrow}(\omega, T, \kappa, -h, \dots) \ . \end{aligned} \tag{4.63}$$

We are thus free to choose the orientation of the magnetic field downwards. Then, after rescaling $D \to |\omega|$ we get

$$\hat{\varrho}^{\kappa,T=0}_{f,\mu}(\omega) = \mathcal{B}_{f,\mu}\left(\frac{\omega}{T_h}\right) + \sqrt{\frac{|\omega|}{T_K}}\ \tilde{\mathcal{B}}_{f,\mu}\left(\frac{\omega}{T_h}\right) + \dots \ , \tag{4.64}$$

where the label $\mu$ refers to the different spin components and $\mathcal{B}_{f,\mu}$ and $\tilde{\mathcal{B}}_{f,\mu}$ are yet another pair of universal cross-over functions. The asymptotic properties of the functions $\mathcal{B}_{f,\mu}$ and $\tilde{\mathcal{B}}_{f,\mu}$ are summarized in Table 4.3.3.

Fig. 4.10 shows the spectral functions $\hat{\varrho}_{f,\mu}$ as a function of $\omega/T_K$ on linear and logarithmic scales for different magnetic field values. The same curves are depicted as a function of $\omega/T_h$ in Fig. 4.11, which demonstrates the existence of the universal scaling curves, $\mathcal{B}_{f,\mu}$, i.e. that by using the scale, $T_h$ the local fermion's spectral functions can be scaled on top of each other for small enough magnetic fields. In this magnetic field region, we find a peak at $T_h$ for the spin-$\uparrow$ component of $f^\dagger$, while at the same place there is a dip for the spin-$\downarrow$ component. This remarkable feature contrasts with the 1CK case, where no such universal peak/dip occurs for small magnetic fields. In fact, the same universal features also appear for the spectral functions of the composite fermions, which were computed independently and which are proportional to the reducible conduction electron self-energies [153]. The rescaled spectral functions $\hat{\varrho}_{F,\mu}(\omega)$ have already been shown in Chapter 3 in Fig. 3.4.

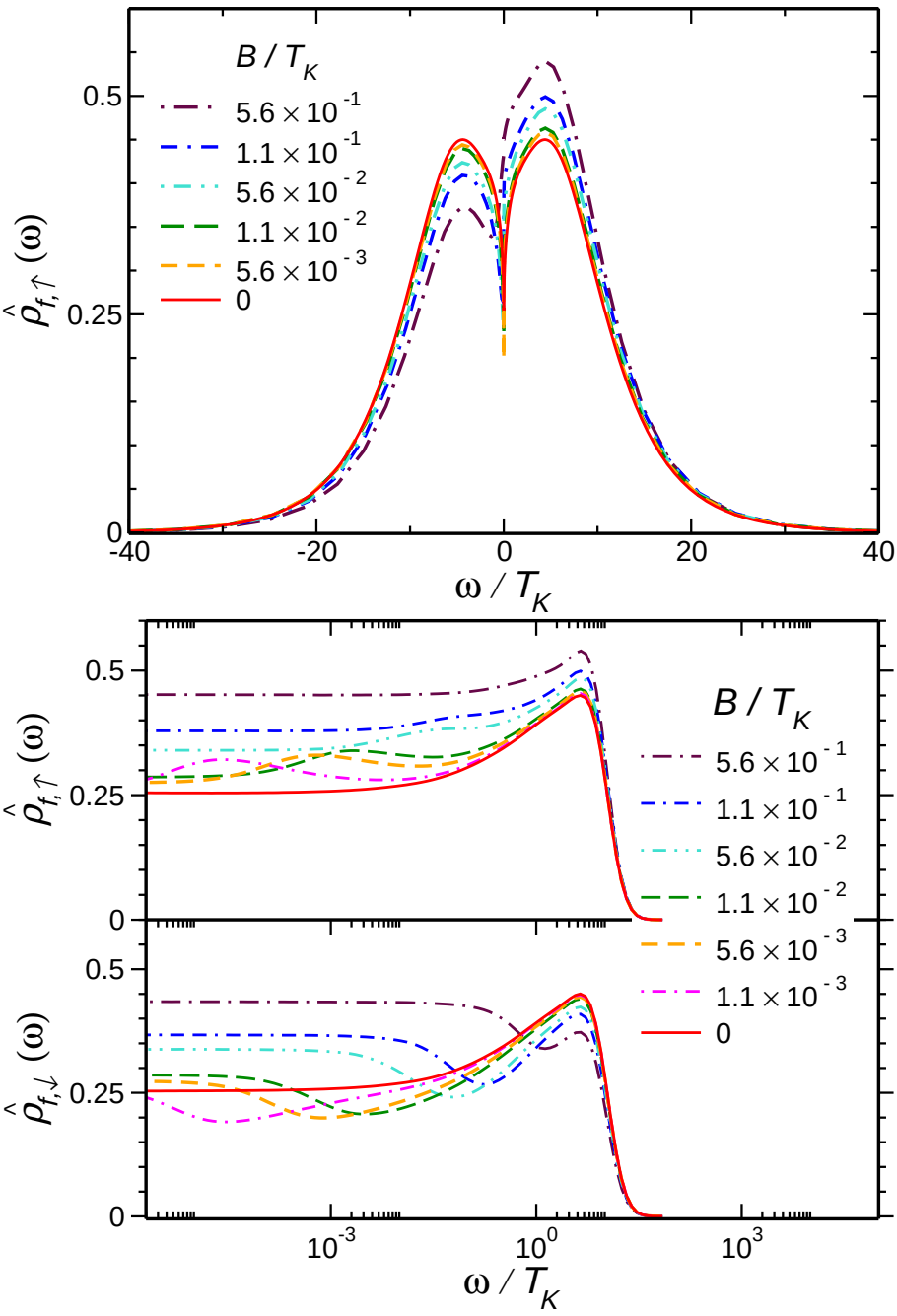


Figure 4.10: Top: Dimensionless spectral function of $f_{0,1,\uparrow}$ : $\hat{\varrho}_{f,\uparrow} = D_F\, \varrho_{f,\uparrow}$ for different values of $B$ as a function of $\omega/T_K$ on linear scale. Bottom: Dimensionless spectral function of $f_{0,1,\uparrow}$ $(a)$ and of $f_{0,1,\downarrow}$ $(b)$ for different values of $B$ as a function of $\omega/T_K$ on logarithmic scale.

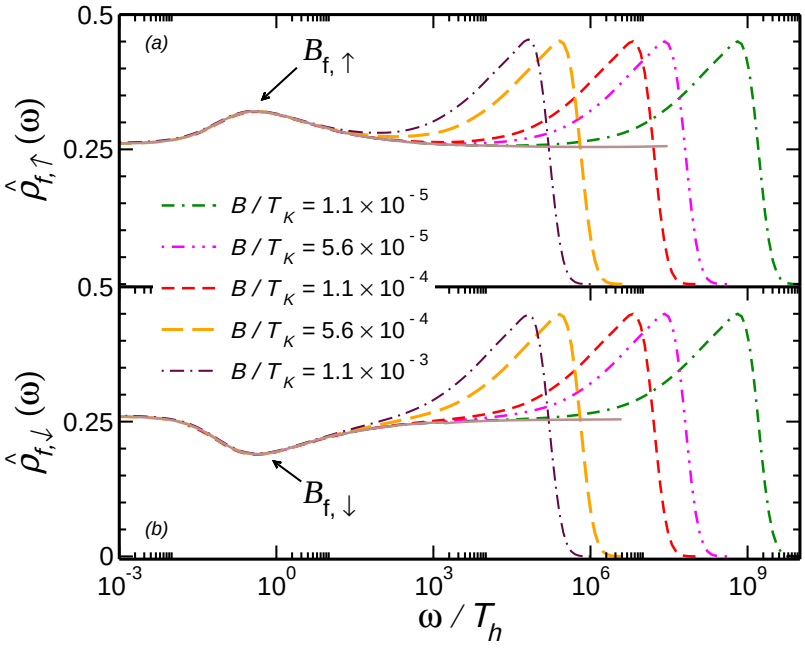


Figure 4.11: Universal collapse of the dimensionless spectral functions: $\hat{\varrho}_{f,\uparrow} = D_F \varrho_{f,\uparrow}$ and $\hat{\varrho}_{f,\downarrow} = D_F \varrho_{f,\downarrow}$ to two scaling curves: $\mathcal{B}_{f,\uparrow}$ and $\mathcal{B}_{f,\downarrow}$ for sufficiently small, non-zero values of $B$ as a function of $\omega/T_h$.

Although this numerical evidence can be obtained by conventional NRG methods not using the density matrix, this is no longer true for the sum of the local fermions spectral function over the different spin components. In fact, for this quantity universal scaling curves in the presence of magnetic field cannot be obtained using NRG because of the increase in the size of the numerical errors at low-frequencies and the mismatch between the positive and negative frequency parts of the spectral functions. The sum of the local fermion's spectral function over the two spin components is depicted in Fig. 4.12 as a function of $\omega/T_K$. Here the splitting of the Kondo resonance in the energy-dependent total scattering cross section appears as a minimum at $\omega \sim T_h$. Unfortunately, for even smaller magnetic fields the accuracy of our numerical data is insufficient to tell if the splitting of the Kondo resonance persists in the limit $B \to 0$, as conjectured in Ref. [140]. In the data with $B/T_K > 1.1 \times 10^{-4}$, there seems to be always a shallow minimum in the spectral function, and we see no indication for crossing of the curves as the magnitude of the field is reduced.

With small modifications, the analysis presented in this subsection carries over to essentially any fermionic operator that has quantum numbers $C_1 = J = 1/2$ or $C_2 = J = 1/2$ and has a finite overlap with the primary fields $\phi_{\psi 1}$ and $\phi_{\psi 2}$, only the high-frequency behavior ($\omega > T_K$) and the normalization factors change. Typically, a local operator having the same charge and spin quantum numbers as $\phi_{\psi\alpha}$ will have a finite overlap with them. However, in some cases the Ising quantum number of an operator may prevent an overlap.

### 4.3.4 Spin spectral functions and susceptibilities

In this section, we discuss the properties of the spin operator, $\vec{S}$, which is the most obvious example of a bosonic operator of spin $J = 1$ and charge quantum numbers $C_1 = C_2 = 0$ that overlaps with the scaling operator $\phi_s$. There are, however, many operators that have the

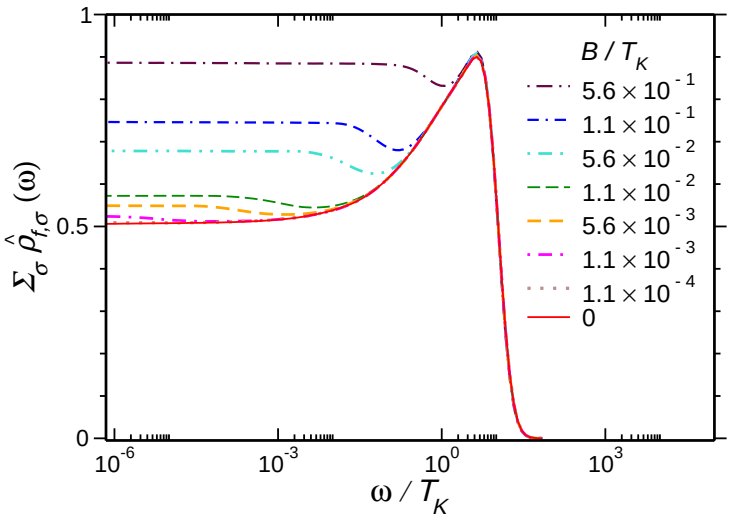


Figure 4.12: Sum of the dimensionless spectral functions: $\hat{\varrho}_{f,\uparrow} = D_F \varrho_{f,\uparrow}$ and $\hat{\varrho}_{f,\downarrow} = D_F \varrho_{f,\uparrow}$ for different values of $B$ as a function of $\omega/T_K$ .

same quantum numbers: Two examples are the so-called channel spin operator

$$\vec{S}_C \equiv f^\dagger_{0,1} \vec{\sigma} f_{0,1} - f^\dagger_{0,2} \vec{\sigma} f_{0,2} \,, \tag{4.65}$$

and a composite channel spin operator

$$\vec{S}_{CC} \equiv F^\dagger_{0,1} \vec{\sigma} f_{0,1} - F^\dagger_{0,2} \vec{\sigma} f_{0,2} \,. \tag{4.66}$$

Our discussion can be easily generalized to these operators with slight modifications.

The analysis of the spin spectral function goes along the lines of the previous subsection. First we recall that the field $\vec{\phi}_s$ appears in the expansion of the spin operator,

$$\vec{S} = A_s \, \vec{\phi}_s + \ldots \,, \tag{4.67}$$

with $A_s \sim 1/\sqrt{T_K} \sim 1/\sqrt{D_0}$. Therefore, the appropriate dimensionless scale invariant Green's function is defined as

$$\hat{g}_S \left( \frac{\omega}{D}, \frac{T}{D}, \kappa_0, h_0, \ldots \right) \equiv T_K \, G_S \left( \omega, T, \kappa_0, \ldots, D_0 \right) \,. \tag{4.68}$$

We remark that, apart from a minus sign, for bosonic correlations we identified the retarded Green's function as the *dynamical susceptibility*,

$$\chi(\omega) = - G(\omega) \,. \tag{4.69}$$

We shall not repeat here all the steps of the derivation, only summarize the main results. In the absence of magnetic field ( $h = 0$ ) the spectral function of the spin operator is odd. Furthermore, at $T = 0$ and for no anisotropy ( $\kappa = 0$ ) the spin spectral function has a discontinuity at $\omega = 0$ [175]

$$\hat{\varrho}_S^{T,h,\kappa=0}(\omega) \approx \mathrm{sgn}(\omega) \left[ r_S + r'_S \sqrt{\frac{|\omega|}{T_K}} + \ldots \right] . \tag{4.70}$$

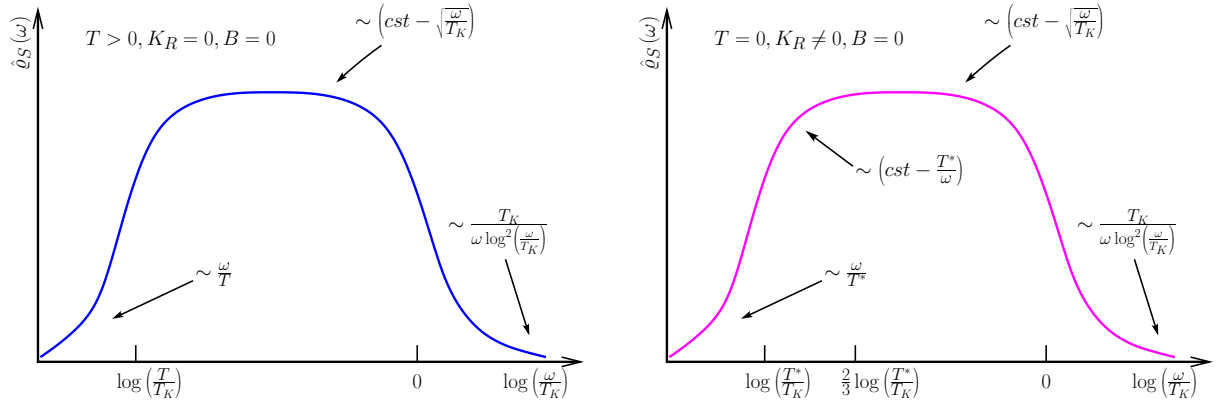


Figure 4.13: Left: Sketch of the dimensionless spectral function of $\vec{S}$: $\hat{\varrho}_S = T_K \varrho_S = T_K \,\mathrm{Im}\,\chi_S(\omega)/\pi$ for $T > 0$ and $K_R = 0, B = 0$ as a function of $\log(\omega/T_K)$. Right: Sketch of $\hat{\varrho}_S = T_K \varrho_S = T_K \,\mathrm{Im}\,\chi_S(\omega)/\pi$ for $T = 0$ and $K_R \neq 0, B = 0$ as a function of $\log(\omega/T_K)$. Asymptotics indicated for $\omega < T_K$ were derived through scaling arguments. The large $\omega$-behavior is a result of perturbation theory [214].

This jump corresponds to a logarithmically divergent dynamical susceptibility, $\mathrm{Re}\,\chi_S(\omega) = -\mathrm{Re}\,\mathcal{G}_S(\omega) \propto \ln(T_K/\omega)/T_K$.

For $\omega \gg T_K$ the impurity spin becomes asymptotically free, decoupled from the conduction electrons, therefore its $\omega$-dependence is set by its scaling dimension at the free fermion fixed point where $x_S^{free} = 0$. It has the implication that its correlation function decays as $\omega^{-1}$ corresponding to the Curie-Weiss susceptibility with logarithmic corrections present, known from Bethe Ansatz results and from perturbation theory.

At finite temperatures $T \neq 0$, but for $\kappa = h = 0$, we obtain the following scaling form for $T, \omega \ll T_K$:

$$\hat{\varrho}_S^{h,\kappa=0}(\omega) \;\equiv\; \Theta_S\left(\frac{\omega}{T}\right) + \sqrt{\frac{T}{T_K}}\;\tilde{\Theta}_S\left(\frac{\omega}{T}\right) + \ldots . \tag{4.71}$$

The asymptotic properties of the scaling functions $\Theta_S$ and $\tilde{\Theta}_S$ are listed in Table 4.3.3.

In case of finite channel anisotropy but zero temperature we obtain for $\omega \ll T_K$ the scaling form

$$\hat{\varrho}_S^{T,h=0}(\omega) \;\approx\; \mathcal{K}_S\left(\frac{\omega}{T^*}\right) + \sqrt{\frac{|\omega|}{T_K}}\;\tilde{\mathcal{K}}_S\left(\frac{\omega}{T^*}\right) + \ldots . \tag{4.72}$$

The asymptotic properties of $\mathcal{K}_S, \tilde{\mathcal{K}}_S$ are only slightly different from those of $\Theta_S, \tilde{\Theta}_S$ (see Table 4.3.3): below $T^*$ the spectral function displays analytic behavior, while the regime $\omega > T^*$ is governed by non-analytical corrections associated with the 2CK fixed point. In this regime a feature worth mentioning is the appearance of a correction, $\sim T^*/\omega$ to $\mathcal{K}_S$, more precisely, the lack of a $\sqrt{|T^*/\omega|}$ correction. This is due to the fact that the anisotropy operator is odd, while the spin operator is even with respect to swapping the channel labels. Therefore there is no first order correction to the spin-spin correlation function in $\kappa$, and the leading corrections

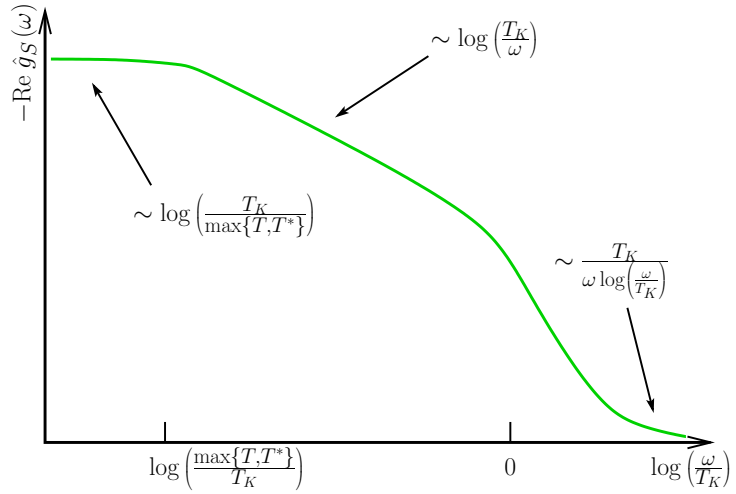


Figure 4.14: Sketch of the real part of the dimensionless Green's function of $\vec{S}$, $\mathrm{Re}\,\hat{g}_S = -T_K\ \mathrm{Re}\,\chi_S(\omega) \equiv T_K\ \mathrm{Re}\,\mathcal{G}_S(\omega)$ for $T, T^* > 0$ as a function of $\log(\omega/T_K)$.

are only of second order, i.e., of the form $\kappa^2/\omega$. From the comparison of the terms in $\mathcal{K}_S$ and $\tilde{\mathcal{K}}_S$ it also follows the existence of another cross-over scale

$$T_s^{**} \sim \left(T^{*2} T_K\right)^{1/3}, \tag{4.73}$$

that separates the regimes governed by the leading relevant and leading irrelevant operators. Here we used the subscript $s$ to indicate that this scale $T_s^{**}$ is different from the scale $T_f^{**}$ introduced in relation to the local fermion's spectral function. The asymptotic properties of $\hat{\varrho}_S \propto \chi_S(\omega)$ for $T > 0, K_R = 0$ and $T = 0, K_R \neq 0$ are sketched in the upper and lower parts of Fig. 4.13, while the behavior of the real part is presented in Fig. 4.14.

These expectations above are indeed nicely met by the NRG calculations: Fig. 4.15 shows the impurity spin spectral functions as a function of $\omega/T_K$ for various $K_R$'s and their asymptotic properties. First, in Fig. 4.15.($b$) we show a very small logarithmic $\omega$-dependence that we observed below $T_K$ at the 2CK fixed point. The amplitude of this $\log(\omega)$-dependence was reduced as we increased the number of multiplets. It appears that this behavior is not derived from the lognormal smoothing of the NRG data, and it may be due to some approximations used in the spectral sum-conserving DM-NRG procedure. In Fig. 4.15.($c$) we show the square root-like behavior around the 2CK Kondo fixed point which is attributed to the leading irrelevant operator, while Fig. 4.15.($d$) shows that first order corrections coming from the scaling of the channel anisotropy are indeed absent just as we stated above, and only second order terms appear, resulting in an $1/\omega$-like behavior. Finally, Fig. 4.15.($e$) demonstrates the linear $\omega$-dependence, which is characteristic of most bosonic operators in the proximity of an FL fixed point. All these findings support very nicely the analytical properties summarized in Table 4.3.3.

The spin spectral functions also collapse to a universal scaling curve describing the cross-over from the two-channel Kondo to the one-channel Kondo fixed points, when they are plotted against $\omega/T^{**}$. This universal data collapse is demonstrated in Fig. 4.16, where the impurity spin spectral functions are plotted for various $K_R$ values. The data collapse works up to somewhat higher anisotropy values than for the local fermions' spectral functions as it is indicated by the $K_R$-dependence of the scales $T_s^{**}$ and $T_f^{**}$.

The real part of the spin susceptibility was obtained through numerical Hilbert transformation,

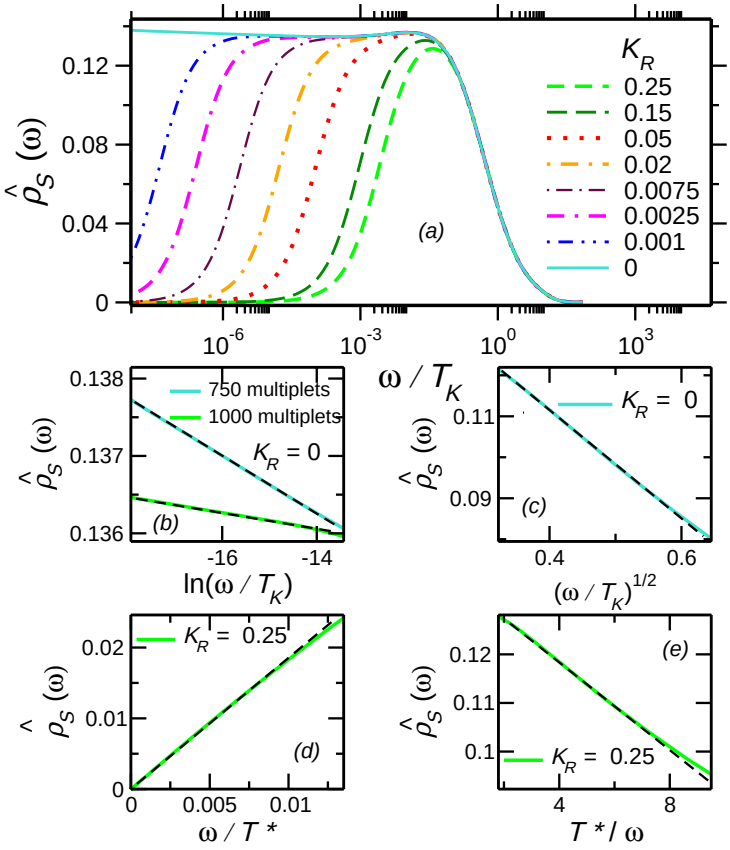


Figure 4.15: $(a)$ Dimensionless spectral function of $\vec{S}$: $\hat{\varrho}_S = T_K \varrho_S = T_K \,\mathrm{Im}\,\chi_S(\omega)/\pi$ as a function of $\omega/T_K$ for different values of $K_R$. $(b)$ Minute $\log(\omega)$-dependence at the lowest frequencies diminishing as a function of the number of kept multiplets. $(c-e)$ Numerical confirmations of the low-frequency asymptotics derived from scaling arguments in Section 4.3.4. Straight dashed lines are to demonstrate deviations from the expected $\sqrt{\omega}$-like $(c)$, $\omega$-like $(d)$, and $1/\omega$-like behavior $(e)$. In plots $(d-e)$ $T^*/T_K = 7 \times 10^{-2}$.

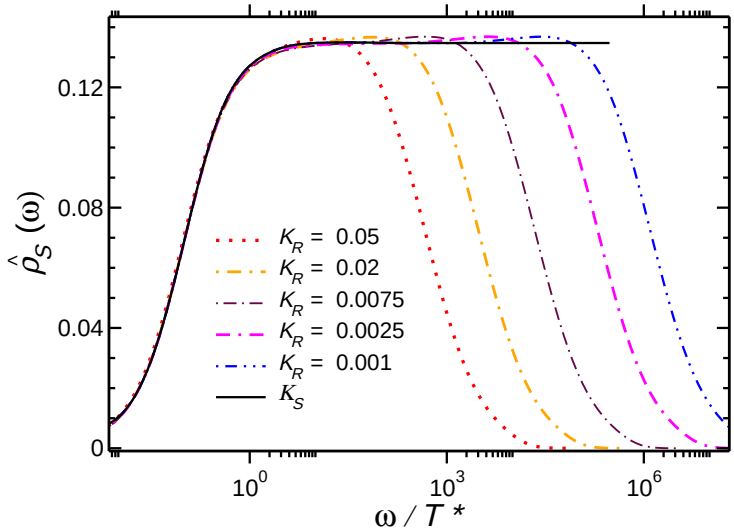


Figure 4.16: Universal collapse of the dimensionless spectral function of $\vec{S}$: $\hat{\varrho}_S = T_K \varrho_S$ to the scaling curve, $\mathcal{K}_S$ as a function of $\omega/T^*$ for sufficiently small, non-zero values of $K_R$.

and is shown in Fig. 4.17 as a function of $\omega/T_K$ for various values of $K_R$. These curves meet the expected behavior sketched in Fig. 4.14: they display a logarithmic increase at high-frequencies and saturate at values that correspond to Re $\chi_S \sim \ln(T_K/T^*) \,/\, T_K$.

Let us finally discuss the case, $T = \kappa = 0$ but $h \neq 0$. Then the components of $\vec{S}$ are distinguished by the magnetic field: The spectral function of $S^z$ has almost the same features as for finite channel anisotropies. Since $S^z$ is a hermitian operator, its spectral function remains odd and acquires the following corrections in the different scaling regimes

$$\hat{\varrho}_{S,z} \equiv \mathcal{B}_{S,z}\left(\frac{\omega}{T_h}\right) + \sqrt{\frac{|\omega|}{T_K}}\ \tilde{\mathcal{B}}_{S,z}\left(\frac{\omega}{T_h}\right) + \ldots \tag{4.74}$$

with the scaling functions $\mathcal{B}_{S,z}, \tilde{\mathcal{B}}_{S,z}$ having the asymptotic properties listed in Table 4.3.3.

Note that in this case the first order correction coming from the magnetic field does not vanish, and leads to the appearance of a cross-over scale $\sim \sqrt{T_h T_K}$.

The perpendicular components of the impurity spin have somewhat different properties. Since the operators $S^{\pm}$ are not Hermitian, and therefore their spectral functions are not symmetrical. The spectral functions of the operators $S^x$ and $S^y$ are, however, symmetrical, and their Green's functions (and susceptibilities) are related through

$$\mathcal{G}_S^x = \mathcal{G}_S^y = \frac{1}{4}\left(\mathcal{G}_S^{+-} + \mathcal{G}_S^{-+}\right) . \tag{4.75}$$

The corresponding dimensionless spectral functions, $\hat{\varrho}_s^z$ and $\hat{\varrho}_s^{\pm}$ as computed by our DM-NRG calculations are shown in Fig. 4.18 as a function of $\omega/T_K$, while the universal scaling with $\omega/T_h$ is confirmed for low-frequencies in Fig. 4.19. This scaling also turned out to be valid for values of $B$ higher than the ones for fermions (see Fig. 4.19). The scaling functions $\mathcal{B}_{S,z}$ and $\mathcal{B}_{S,\pm}$ behave very similarly. This is somewhat surprising, since the naive expectation would be to have a *resonance* in $\mathcal{B}_{S,+}$, just as in the local fermion's spectral function, that would correspond to a spin-flip excitation at the renormalized spin splitting, $T_h$.

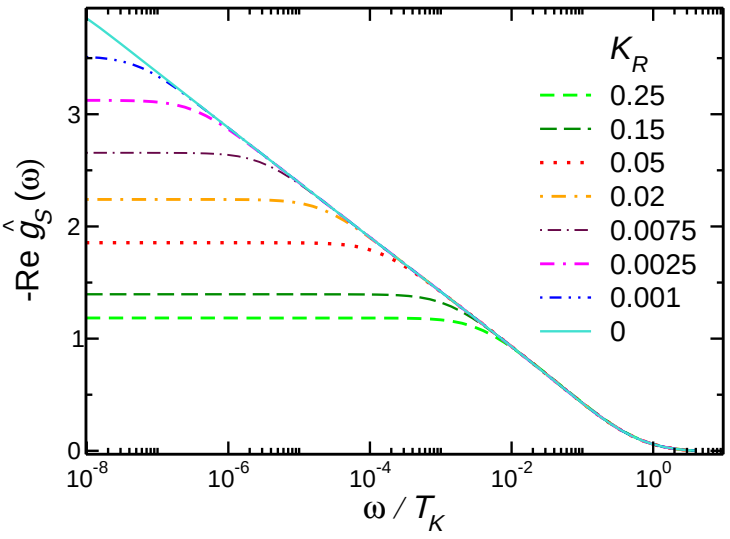


Figure 4.17: Real part of the dimensionless Green's function (susceptibility) of $\vec{S}$, $\mathrm{Re}\,\hat{g}_S = -T_K\ \mathrm{Re}\,\chi_S(\omega)$, as a function of $\omega/T_K$, for different values of $K_R$.

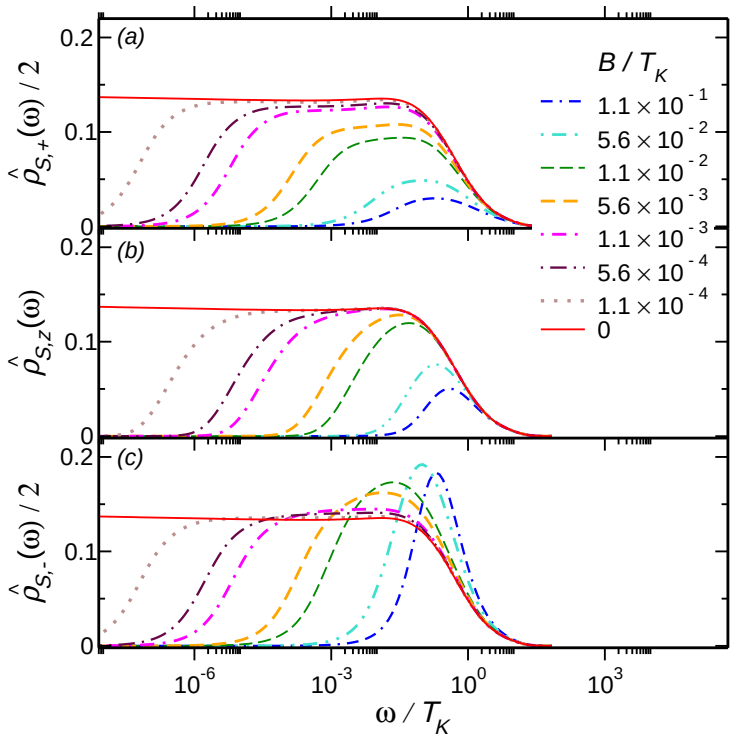


Figure 4.18: (*a*) Dimensionless spectral function of $S^+$: $\hat{\varrho}_{S,+} = T_K \varrho_{S,+}$, (*b*) of $S^z$: $\hat{\varrho}_{S,z} = T_K\, \varrho_{S,z}$ and (*c*) of $S^-$: $\hat{\varrho}_{S,-} = T_K \varrho_{S,-}$ for different values of $B$ as a function of $\omega/T_K$.

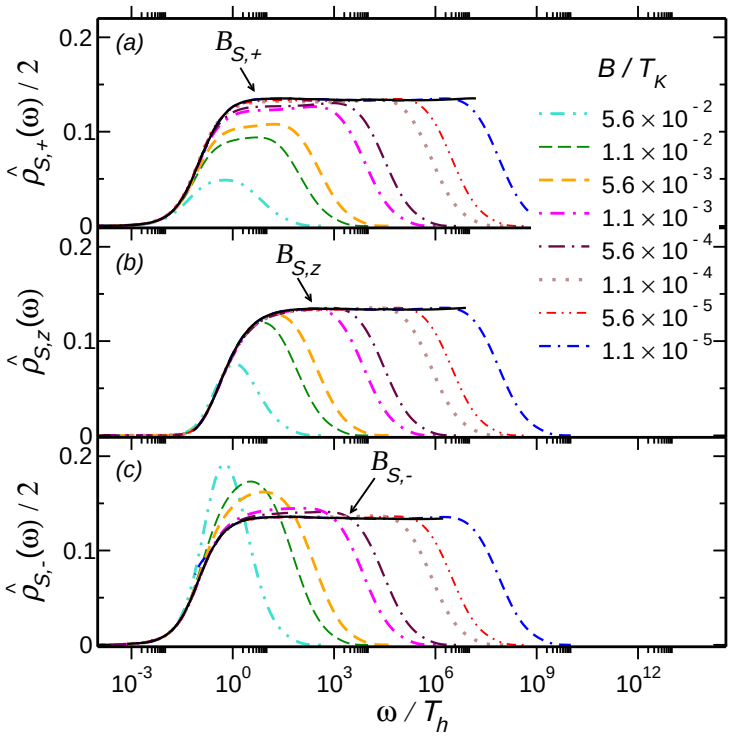


Figure 4.19: Universal collapse of $\hat{\varrho}_{S,+} = T_K \varrho_{S,+}$, $\hat{\varrho}_{S,z} = T_K \varrho_{S,z}$ and $\hat{\varrho}_{S,-} = T_K \varrho_{S,-}$ to the three scaling curves: $\mathcal{B}_{S,+}, \mathcal{B}_{S,z}$ and $\mathcal{B}_{S,-}$ for sufficiently small, non-zero values of $B$ as a function of $\omega/T_h$.

### 4.3.5 Superconducting correlations

Now let us investigate the local superconducting correlations. They deserve special attention, since many heavy fermion compounds display exotic superconducting phases that may possibly be induced by local two-channel Kondo physics [175]. The most obvious candidates for the corresponding local operators have been identified in Subsection 4.3.1, and are the local channel-asymmetric superconducting operator, $\mathcal{O}_{SC} = f^\dagger_{0,1,\uparrow} f^\dagger_{0,2,\downarrow} - f^\dagger_{0,1,\downarrow} f^\dagger_{0,2,\uparrow}$, and the composite fermion superconductor field, $\mathcal{O}_{SCC} = f^\dagger_{0,1} \vec{S}\vec{\sigma}\, i\sigma_y f^\dagger_{0,2}$.

For the composite superconductor we find the expansion,

$$\mathcal{O}_{SCC} \;=\; A_{SCC}\, \phi^{++}_{\Delta} + \ldots \tag{4.76}$$

where the expansion coefficient $A_{SCC}$ can be estimated from the high-frequency behavior of the correlation function up to logarithmic prefactors as $A_{SCC} \sim \sqrt{T_K}/D_F$. While for the impurity spin, one can exclude logarithmic corrections to the expansion coefficient $A_S$ in Eq. 4.67 based on the exact Bethe ansatz results, this is not possible for the superconducting correlation function. In fact, we know that in the expansion of the composite fermion itself the correct prefactor is $A_F \sim J/\sqrt{T_K} \sim 1/\big(\sqrt{T_K}\ln(D_F/T_K)\big)$ [153]. Therefore, similar logarithmic factors could appear in the prefactor $A_{SCC}$. Nevertheless, in the following, we shall disregard possible logarithmic corrections, and define the normalized dimensionless and scale-invariant correlation function through the relation

$$\hat{g}_{SCC}(\omega) \;\equiv\; \frac{D_F^2}{T_K}\, \mathcal{G}_{SCC}(\omega) \;=\; -\frac{D_F^2}{T_K}\, \chi_{SCC}(\omega)\,. \tag{4.77}$$

Apart from its overall amplitude and its high-frequency behavior, in the low-frequency scaling regimes the spectral function of the composite superconductor operator behaves the same way as that of $S^z$ (see Tab. 4.3.1). Therefore we merely state its asymptotics without further explanation.

In the absence of anisotropy and magnetic field, $\kappa = h = 0$, for $\omega \ll T_K$ the spectral function becomes a universal function, $\hat{\rho}_{SCC}(\omega/T)$, whose behavior is described by the scaling form

$$\hat{\varrho}^{h,\kappa=0}_{SCC}(\omega) \;\approx\; \Theta_{SCC}\left(\frac{\omega}{T}\right) + \sqrt{\frac{T}{T_K}}\, \tilde{\Theta}_{SCC}\left(\frac{\omega}{T}\right) + \ldots\,, \tag{4.78}$$

while in the presence of anisotropy, but at zero temperature and for $h = 0$, the spectral functions behave as

$$\hat{\varrho}^{T,h=0}_{SCC}(\omega) \;\approx\; \mathcal{K}_{SCC}\left(\frac{\omega}{T^*}\right) + \sqrt{\frac{|\omega|}{T_K}}\, \tilde{\mathcal{K}}_{SCC}\left(\frac{\omega}{T^*}\right) + \ldots\,. \tag{4.79}$$

Finally, in a finite magnetic field but for $\kappa = 0$ anisotropy and at $T = 0$ the spectral function assumes the following scaling form,

$$\hat{\varrho}^{\kappa=T=0}_{SCC} \;\equiv\; \mathcal{B}_{SCC}\left(\frac{\omega}{T_h}\right) + \sqrt{\frac{|\omega|}{T_K}}\, \tilde{\mathcal{B}}_{SCC}\left(\frac{\omega}{T_h}\right) + \ldots\,. \tag{4.80}$$

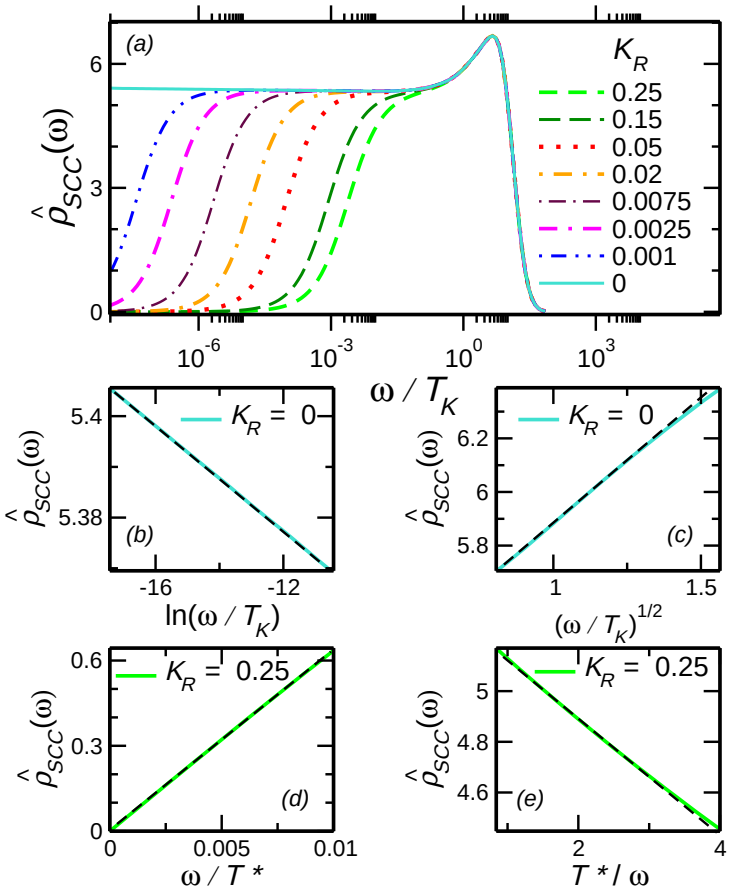


Figure 4.20: $(a)$ Dimensionless spectral function, $\hat{\varrho}_{SCC} = D_F^2/T_K \ \mathrm{Im}\ \chi_{SCC}$ of the operator $\mathcal{O}_{SCC}$, as a function of $\omega/T_K$ for different values of $K_R$. $(b)$. The very weak $\log(\omega)$-dependence at the lowest frequencies. This dependence is suppressed as we increased the number of kept multiplets. $(c-e)$ Numerical confirmations of the low-frequency asymptotics derived from scaling arguments in Subsection 4.3.5. Dashed straight lines are to demonstrate deviations from the expected $\sqrt{\omega}$-like $(c)$, $\omega$-like $(d)$ and $1/\omega$-like $(e)$ behavior. In plots $(d-e)$ $T^*/T_K = 7 \times 10^{-2}$.

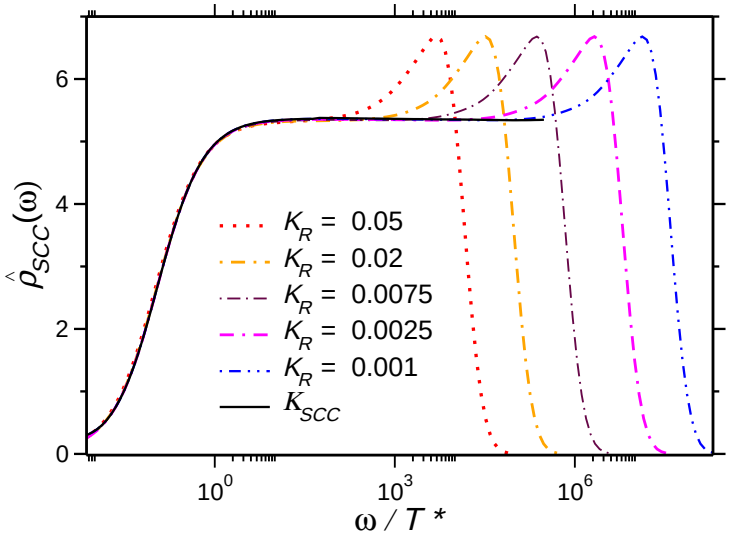


Figure 4.21: Universal collapse of $\hat{\varrho}_{SCC}$ to the scaling curve $\mathcal{K}_{SCC}$ as a function of $\omega/T^*$ for sufficiently small, non-zero values of $K_R$.

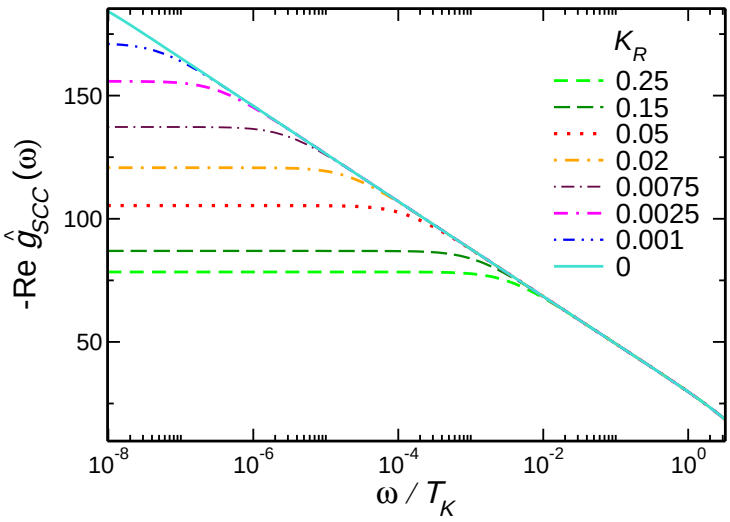


Figure 4.22: Real part of the dimensionless Green's function of $\mathcal{O}_{SCC}$: $\mathrm{Re}\,\hat{g}_{SCC} = -D_F^2/T_K \;\mathrm{Re}\,\chi_{SCC}$ as a function of $\omega/T_K$ for different values of $K_R$.

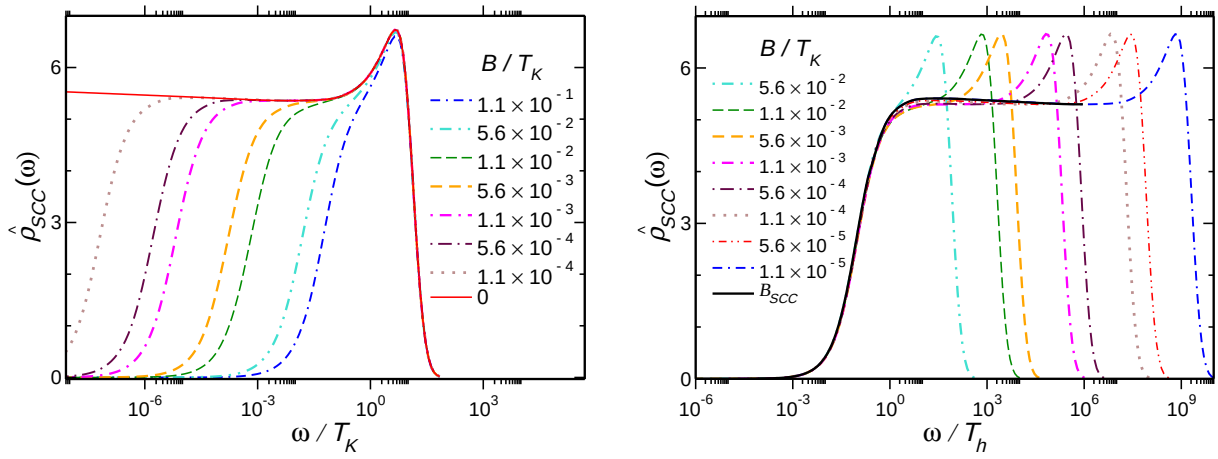


Figure 4.23: Left: Dimensionless spectral function $\hat{\varrho}_{SCC} = (D_F^2/\pi T_K)\ \mathrm{Im}\,\chi_{SCC} = -(D_F^2/\pi T_K)\ \mathrm{Im}\,\mathcal{G}_{SCC}$ of the composite superconductor operator $\mathcal{O}_{SCC}$ for different values of $B$, as a function of $\omega/T_K$. Right: Universal collapse of $\hat{\varrho}_{SCC}$ to the scaling curve $\mathcal{B}_{SCC}$ for sufficiently small, non-zero values of $B$ as a function of $\omega/T_h$.

The properties of the the various scaling functions defined above are identical to those of the corresponding spectral functions of the $S^z$ given in Table 4.3.3, therefore they have not been included in Table 4.3.3 again.

The asymptotic properties are nicely confirmed by our NRG calculations. The dependence on the anisotropy, together with the $\sim \sqrt{|\omega|}$, the $\sim 1/\omega$ and the $\sim \omega$ scaling regimes are plotted in Fig. 4.20. Here the high-frequency region, $\omega > T_K$, is also displayed, where the spectral function is roughly linear in the frequency, as dictated by the free fermion fixed point.

The universal collapse of the low-frequency part of the curves in terms of $\omega/T^*$ is shown in Fig. 4.3.5. The cross-over curve, $\mathcal{K}_{SCC}\left(\frac{\omega}{T^*}\right)$ is very similar to the spin cross-over function, $\mathcal{K}_S$, and displays a plateau at large frequencies from which it deviates as $1/\omega$, until it finally reaches the linear frequency regime below $T^*$.

Fig. 4.3.5 displays the real part of the dimensionless Green's function, that is essentially the real part of the superconducting susceptibility. This diverges logarithmically for $T^* = 0$, but for finite $T^*$'s it saturates, corresponding to a susceptibility value

$$\mathrm{Re}\,\chi_{SCC} \sim \frac{T_K}{D_F^2} \ln\left(\frac{T_K}{T^*}\right) . \tag{4.81}$$

There appears a small prefactor in front of the logarithm due to the fact that composite superconducting correlations are irrelevant at energies $\omega > T_K$, as it follows from simple power counting.

Application of a magnetic field has effects very similar to the anisotropy, as shown in the upper part of Fig. 4.23. We kept a relatively small number of multiplets therefore the small logarithmic increase at small frequencies is more visible in Fig. 4.23. As mentioned before, this increase is most likely an artifact of the spectral sum conserving approximation of Ref. [90] and it is due to the way this method redistributes spectral weights. This is based on the observation

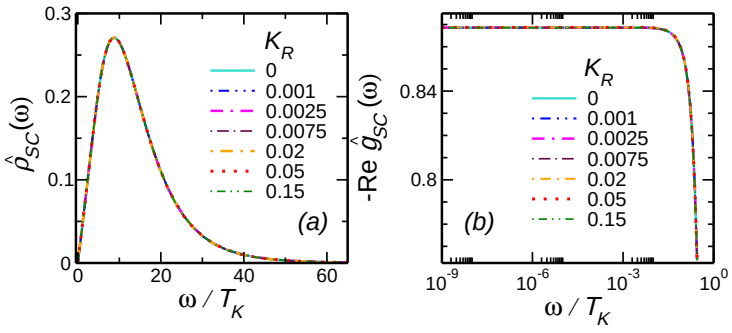


Figure 4.24: $(a)$ Dimensionless spectral function of $\mathcal{O}_{SC}$: $\hat{\varrho}_{SC} = D_F \varrho_{SC}$ as a function of $\omega/T_K$ for different values of $K_R$, and $(b)$ the real part of its dimensionless Green's function: $\mathrm{Re}\,\hat{g}_{SC} = D_F\,\mathrm{Re}\,\mathcal{G}_{SC}$.

that the slope of the logarithm diminishes if we increase the number of kept multiplets. These curves also collapse to a single universal curve as a function of $\omega/T_h$, as shown in the lower part of Fig. 4.23.

Finally, in Fig. 4.24, we show the numerically obtained spectral function and the corresponding dimensionless susceptibility of the non-composite superconductor, $\mathcal{O}_{SC} = f^\dagger_{0,1,\uparrow} f^\dagger_{0,2,\downarrow} - f^\dagger_{0,1,\downarrow} f^\dagger_{0,2,\uparrow}$. Clearly, this spectral function displays no plateau below $T_K$, but it exhibits a linear $\omega$ behavior below $T_K$, and correspondingly, the susceptibility $\mathrm{Re}\,\chi_{SC}$ remains finite for $\omega \to 0$ even in the absence of anisotropy and an external magnetic field, i.e. at the 2CK fixed point.

This implies that, although its charge and spin quantum numbers would allow it, the expansion of this operator does not contain the scaling operator $\phi^{\tau\tau'}_\Delta$. This may be due to the difference in the Ising quantum numbers, which we did not identify. Thus the dimension of the highest-weight scaling operator that appears in the expansion of $\mathcal{O}_{SC}$ is $x = 1$ and not $1/2$, as one would have naively expected it based on a simple comparison of quantum numbers. Turning on a small anisotropy or magnetic field does not influence substantially the spectral properties of the corresponding Green's function either.

### 4.3.6 Electron-hole symmetry breaking

Throughout an actual experiment the electron-hole (e-h) symmetry might not be assured. Motivated by this condition we studied the effects of e-h symmetry breaking on the local Green's functions of the 2CKM. We added a potential scattering term

$$V \sum_{\alpha,\mu} f^\dagger_{0,\alpha,\mu} f_{0,\alpha,\mu} \tag{4.82}$$

to the NRG Hamiltonian of Eq. (2.69). As this operator is marginal around the 2CK fixed point it is not expected to influence the asymptotic behavior of the spectral functions [175]. Indeed, the numerical results for the composite fermion's and local fermion's spectral functions reinforce this expectation. At the level of the finite size spectrum, this operator appears through a phase shift $\delta$, i.e. as a shift of the energy levels.

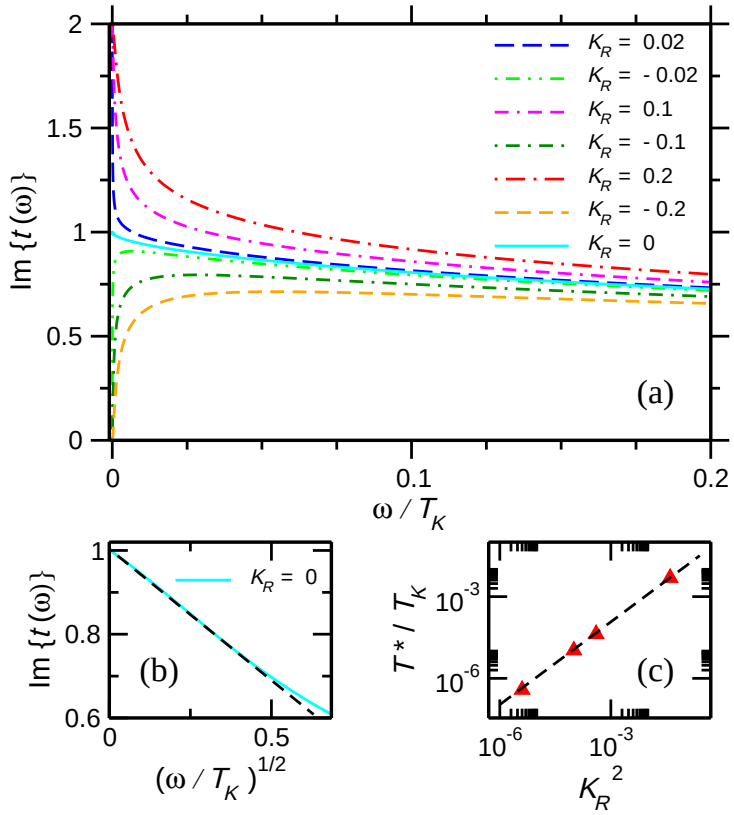


Figure 4.25: (a) Imaginary part of the eigenvalue of the on-shell T-matrix, as function of $\omega/T_K$, for several different values of the anisotropy parameter, $K_R \equiv 4(\tilde{\mathcal{J}}_1 - \tilde{\mathcal{J}}_2)/(\tilde{\mathcal{J}}_1 + \tilde{\mathcal{J}}_2)^2$. In all cases $\tilde{\mathcal{J}}_1 + \tilde{\mathcal{J}}_2 = 0.2$. Curves with $\tilde{\mathcal{J}}_1 > \tilde{\mathcal{J}}_2$ or $\tilde{\mathcal{J}}_1 < \tilde{\mathcal{J}}_2$ scale to Im $t(0) = 2$ or Im $t(0) = 0$, respectively. The critical curve corresponding to $\tilde{\mathcal{J}}_1 = \tilde{\mathcal{J}}_2$ separates these two sets of curves. (b) Im $t(\omega)$ for $\tilde{\mathcal{J}}_1 = \tilde{\mathcal{J}}_2$, as a function of $\sqrt{\omega/T_K}$. The dashed line is to demonstrate deviations from the expected $\sqrt{\omega}$-behavior. (c) $T^*$ as the function of $K_R^2$.

The upper part of Fig. 4.28 shows the universal scaling of the composite fermion's spectral function, $\hat{\varrho}_F(\omega)$ versus $\omega/T_K$ for different values of the potential scattering strength, $V$ and the exchange coupling, $\tilde{J}$ with $\tilde{J} \equiv \tilde{J}_1 = \tilde{J}_2$. We defined $T_K$ by the half width of the function $\hat{\varrho}_F(\omega)$ for each value of the $\tilde{J}, V$ parameter pair and for each positive and negative frequency range individually.

The numerical calculations manifested the expected $\sqrt{\omega/T_K}$ scaling for low-frequencies as it is demonstrated in the insets of Fig. 4.28.

For the composite fermions for low-frequencies the effect of e-h symmetry breaking manifests itself mostly in the shift of $\hat{\varrho}_F(\omega)$ by a constant.

For the local fermions we carried out the same kind of analysis and found reassuring $\sqrt{\omega/T_K}$ behavior as shown in the inset of the lower part of Fig. 4.28. For low-frequencies the above e-h symmetry violation makes the local fermions' spectral functions much more asymmetric as that of the composite fermions, whereas $\hat{\varrho}_f(0) = 0.25$ remains unchanged in accordance with the result of Affleck and Ludwig for the retarded self-energy at the 2CK fixed point [193].

### 4.3.7 Linear conductance of a double dot system

Using NRG, we have also computed the zero temperature, finite-frequency linear conductance of the double dot system discussed in Subsection 4.2.4 and depicted in Fig. 4.3. In the regime

where the system can be described by the 2CK Kondo model, we can identify the dimensionless eigenvalue of the so-called on-shell $T$-matrix, $t_\mu(\omega)$ as being proportional to the dimensionless, retarded Green's function of the composite fermion operator, $\mathcal{G}_{F,\mu}(\omega)$ [153, 192, 140]

$$t_\mu(\omega) \;=\; -\hat{J}_1^2\,\mathcal{G}_{F,\mu}(\omega)\,, \tag{4.83}$$

with $\hat{J}_1$ the Kondo exchange coupling to the even combination of the left and right lead conduction electrons. It is also known that at the 2CK fixed point, the single particle sector of the $S$-matrix of the conduction electrons vanishes [193]. Thus from the relation, $S(\omega) = 1 + i\,t(\omega)$ between the dimensionless eigenvalue of the $S$- and $T$-matrices we obtain that

$$\lim_{\omega,T\to 0} t(\omega,T) \;=\; i\,, \qquad \text{for } \hat{J}_1 \,=\, \hat{J}_2\,. \tag{4.84}$$

Furthermore in the linear response regime we can relate $\mathrm{Im}\,\{t(\omega)\}$ to the real part of the linear conductance through the Kubo formula. We get that

$$\mathrm{Re}\,\{G(\omega)\} \;=\; \frac{G_0}{8\,\omega}\sum_\mu \int d\omega'\;\mathrm{Im}\,\{t_\mu(\omega')\}\,\big[f(\omega'+\omega)-f(\omega'-\omega)\big]\,, \tag{4.85}$$

with $G_0 \equiv \frac{2e^2}{h}\,\frac{4t_L^2 t_R^2}{(t_L^2+t_R^2)^2}$ the maximal conductance through the dot and $f$ the Fermi distribution. It means that at the 2CK fixed point $G(\omega = 0) = G_0/2$. Based on the formulas above and using NRG, we have computed $\mathrm{Im}\,\{t(\omega)\}$ and $\mathrm{Re}\,\{G(\omega)\}$ for finite channel anisotropies, characterized by the anisotropy parameter now defined as $K_R \equiv 4(\tilde{\mathcal{J}}_1 - \tilde{\mathcal{J}}_2)/(\tilde{\mathcal{J}}_1 + \tilde{\mathcal{J}}_2)^2$ (with $\tilde{\mathcal{J}}_\alpha$ the value of the exchange couplings in the NRG calculations). The results of these calculation are shown in Figs. 4.25 and 4.26, and are very similar to the results for the spectral function of the local fermion operators (cf. Subsection 4.3.3), therefore we do not discuss their properties again.

### 4.3.8 Summary

In the previous subsections we analyzed the properties of the correlation functions of various local operators of the 2CK model in the presence of a channel anisotropy, external magnetic field and potential scattering. In particular, we studied numerically and analytically the correlation functions of local fermions, the impurity spin and local superconductivity operators. The selection of these operators was partially motivated by conformal field theory, which tells us the quantum numbers and scaling dimensions of the various scaling operators at the 2CK fixed point [27]. There are, however, many operators that have quantum numbers identical with the scaling fields. Here we picked operators having the right quantum numbers, and at the same time having the largest possible scaling dimension at the free fermion fixed point where the exchange coupling goes to zero. These are the operators whose spectral functions are expected to have the largest spectral weight at small temperatures, and which are therefore the primary candidates for an order parameter, when a lattice of 2CK impurities is formed, as is the case in some U- and Ce-based compounds. The operators above are, of course, also of physical interest on their own: the spectral function of $f^\dagger_{0,\alpha,\mu}$ is related to the tunneling spectrum into the conduction electron sea at the impurity site, the Green's function of $\vec{S}$ is just the dynamical spin susceptibility that can be measured in inelastic neutron scattering, and finally the local superconducting operators

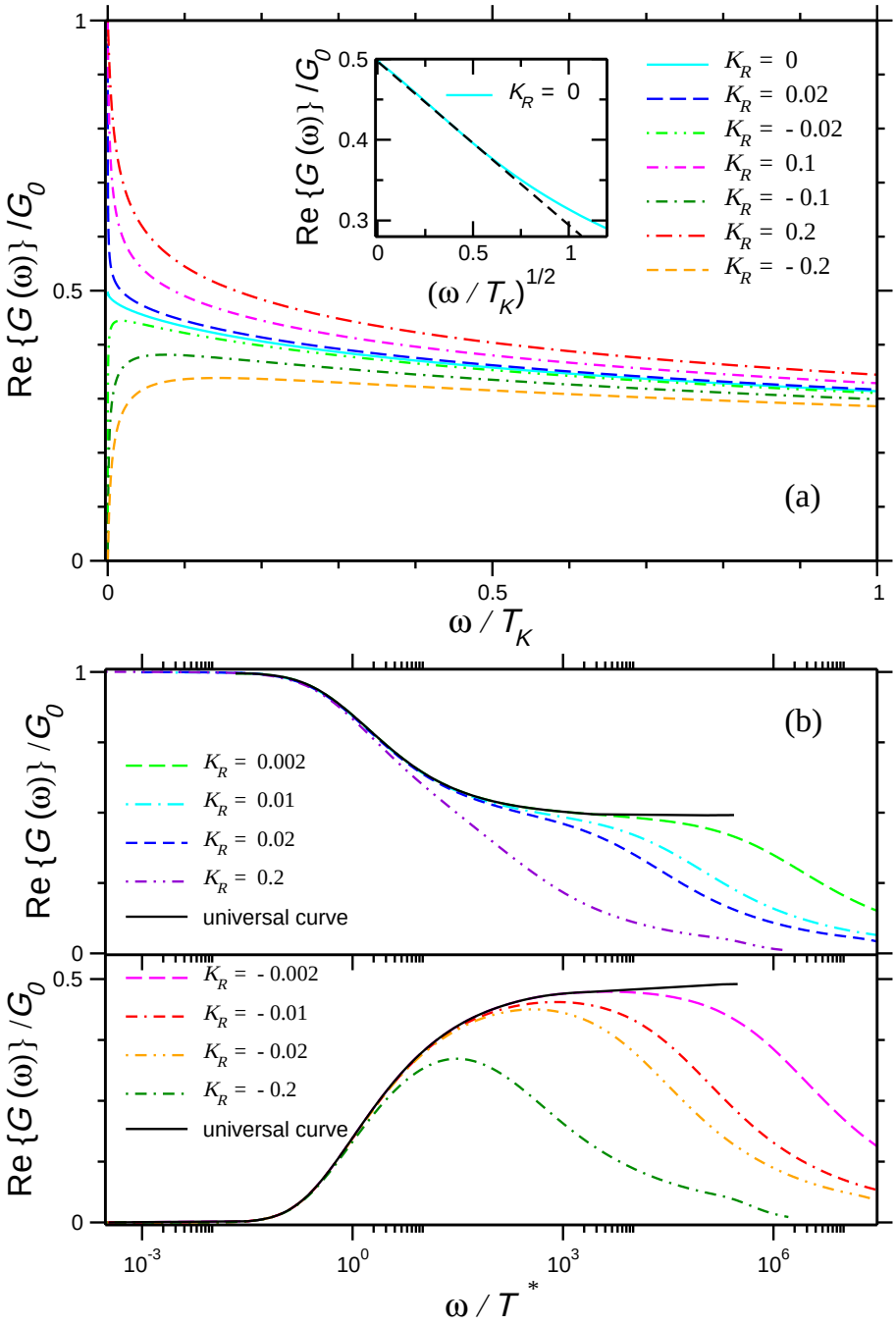


Figure 4.26: Top: (a) AC conductance as the function of $\omega/T_K$. For $\tilde{J}_1 > \tilde{J}_2$ and $\tilde{J}_1 < \tilde{J}_2$ the curves scale $\mathrm{Re}\, G \to G_0$ and $\mathrm{Re}\, G \to 0$, respectively. Inset: AC conductance for $\tilde{J}_1 = \tilde{J}_2$ as the function of $\sqrt{\omega/T_K}$. Bottom: (b) AC conductance for positive (upper part) and negative (lower part) channel anisotropy parameters as the function of $\omega/T^*$. For $\omega, T^* \ll T_K$, the curves follow the universal cross-over curves.

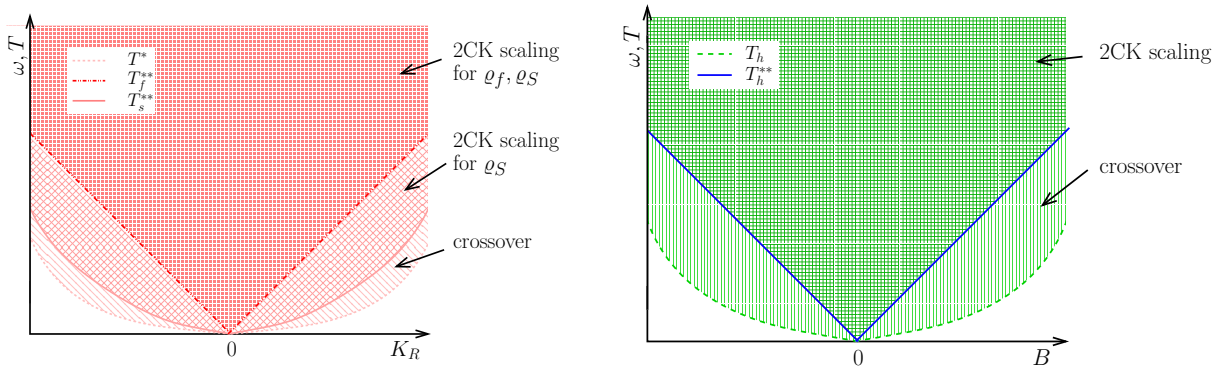


Figure 4.27: (left) Sketch of the various 2CK scaling regimes in the presence of channel anisotropy for the local fermions bounded by $T_f^{**}$ from below and for the spin bounded by $T_s^{**}$, the crossover scale $T^{**}$ is also indicated. (right) Sketch of the 2CK scaling regime for the susceptibilities of the highest-weight fields bounded by $T_h^{**}$, and the crossover scale $T_h$ besides.

are candidates for superconducting ordering in heavy fermion materials. We remark that, in the electron-hole symmetrical case, the other components of the operator multiplet that contains the composite superconducting order parameter $O_{SCC}$ would correspond to a composite channel-mixing charge density ordering. Of course, the susceptibilities of this operator has the same properties as that of $\chi_{SCC}(\omega)$.

In addition to these operators, there are two more operators of possible interest. The so-called composite fermion's Green's function is related to the $t$-matrix, that describes the scattering properties off a two-channel impurity (or the conductance through it in case of a quantum dot), and was already studied to a certain extent in Ref. [140]. A further candidate is the channel anisotropy operator. This also has a logarithmically divergent susceptibility, and would also be associated with a composite orbital ordering in case of a 2CK lattice system. However, the spectral properties of this latter operator are so similar to those of the composite superconductor that we have decided no to show data about them.

To identify the scaling operators we reconstructed the boundary conformal field theory of Affleck and Ludwig for the group $\mathrm{SU}_{C1}(2) \times \mathrm{SU}_{C2}(2) \times \mathrm{SU}_S(2)$. Then we established the scaling properties of the various dynamical correlation functions and identified the corresponding universal cross-over functions and their asymptotic properties, based upon simple scaling arguments. In this way, universal scaling functions describing the cross-over from the two-channel Kondo fixed point to the one-channel Kondo fixed point (for $\hat{J}_1 \neq \hat{J}_2$) and to the magnetically polarized fixed point (for $B \neq 0$) have been introduced, which we then determined numerically. We emphasize again that presently these universal cross-over functions can only be obtained through DM-NRG.

Our numerical calculations confirmed all our analytical expectations, including that in the presence of magnetic field, or channel anisotropy, the 2CK scaling regime is rather restricted, and it may also depend on the physical quantity considered. In Fig. 4.27 we sketched the regimes where the pure two-channel Kondo behavior can be observed. Notice that in the presence of anisotropy the 2CK scaling regime of the spin susceptibility has a boundary that differs from that of the 2CK Kondo scaling regime of the local fermions.

Some of the spectral functions show quite remarkable features. Namely, in a magnetic field the spectral function of the composite fermion, $F^{\dagger}_{\alpha,\downarrow}$ shows a universal peak at a frequency $\omega = T_h$. This peak may appear due to the spin-flip excitations of the impurity spin at the renormalized magnetic field. Remarkably, this peak is accompanied by a dip of the same size at the same frequency for spin down electrons. This dip is actually very surprising and is hard to explain. Similar features appear but with opposite sign in the local fermions' spectral functions. Even more surprisingly, this sharp resonant feature is absent in the spectral function of the spin operators, $S^{\pm}$.

We have also studied, how the 2CK behavior is influenced by electron-hole symmetry breaking. We found that in the presence of a strong potential scattering the singular part of the composite fermion's spectral function remains almost perfectly symmetrical, whereas the singular part of the local fermion's spectral function has a strong asymmetry. We argued that in the presence of electron-hole symmetry breaking the universal cross-over functions should depend on an additional universal phase shift parameter related to the potential scattering strength.

One of the interesting results of our analysis is that only the composite superconductor $\mathcal{O}_{SCC}$ has a logarithmically divergent susceptibility. This is thus the primary candidate for superconducting ordering for a 2CK lattice system.

Interestingly, although the results are still somewhat controversial [211], in the two-channel Kondo lattice these local superconducting correlations do not seem to induce a superconducting transition [213]. This may be, however, an artifact of the standard two-channel Kondo lattice model, which does not account properly for the orbital and band structure of an $f$-electron material [212]. In a more realistic lattice of two-channel Kondo impurities a composite superconducting order may develop, similar to the one suggested in Ref. [212].

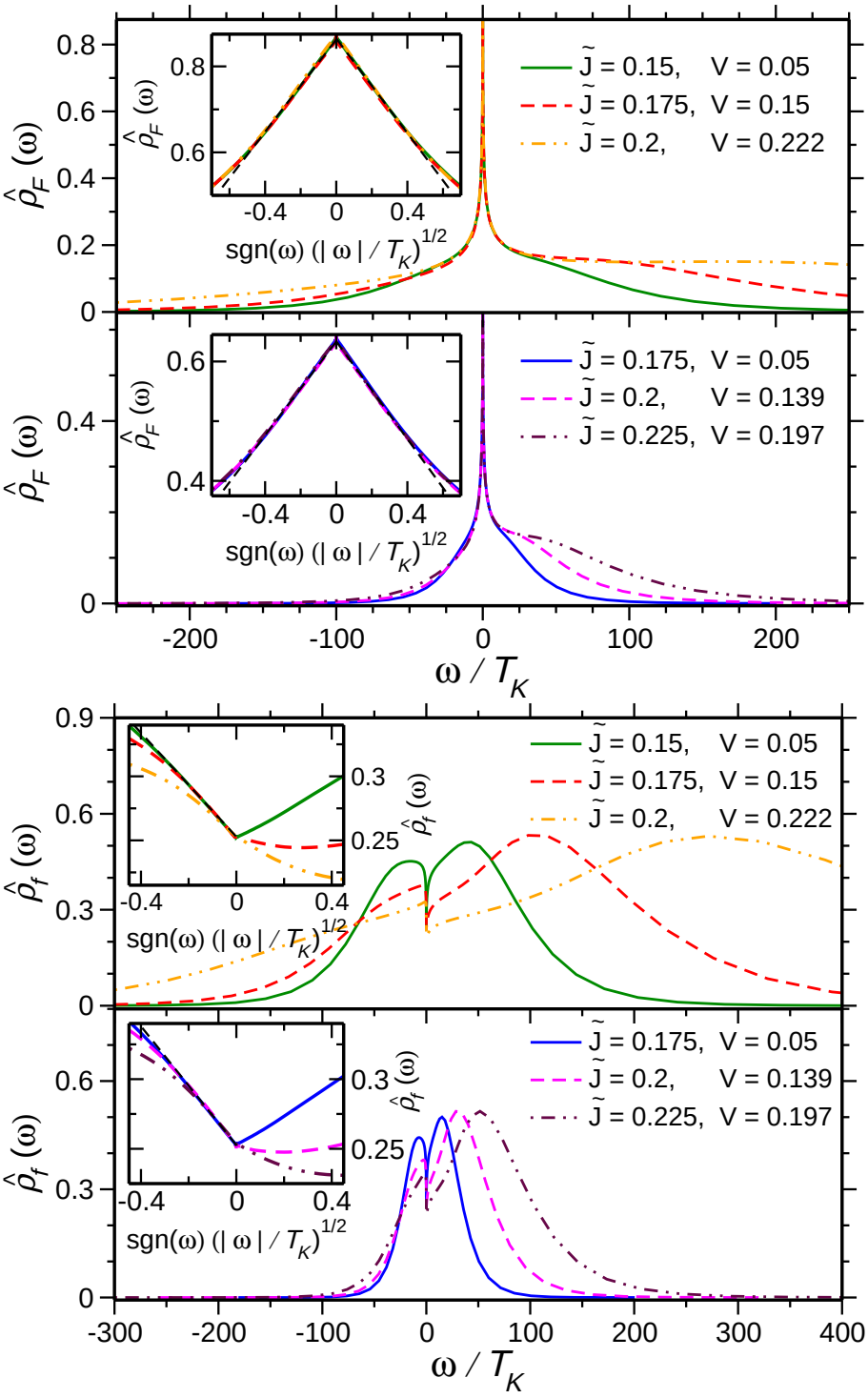


Figure 4.28: Universal scaling of the dimensionless composite fermion's (top) and local fermion's spectral functions (bottom) as a function of $\omega/T_K$ for different values of the exchange coupling, $\tilde{J}$ and potential scattering strength, $V$. The insets show $\sqrt{\omega}$-like behavior for low-frequencies for both operators.

# 5 Summary

The study of strongly correlated electron systems is one of the central themes in condensed matter physics. The investigation of quantum impurity models is a starting point towards the understanding of more complex strongly correlated systems. These models also provide the description of various correlated mesoscopic structures, they appear in molecular electronics and describe phenomena such as dissipation or dephasing. Since their creation, our understanding of these models has evolved considerably due to the powerful theoretical tools available for their study. The Numerical Renormalization Group (NRG) method, devised by Wilson in the seventies, is possibly the most powerful from among them. With this dissertation I have contributed to the efforts improving the accuracy of the spectral function calculations using the recently developed Density Matrix Numerical Renormalization Group (DM-NRG) method. These developments have been timely e.g. because of the possible applications of mesoscopic devices in quantum computing. My DM-NRG studies concentrated on the two-channel Kondo model which is the simplest quantum impurity model exhibiting non-Fermi liquid properties. It has possible relevance in the description of heavy fermion systems. Moreover, the existence of the two-channel Kondo state has recently been justified using a double quantum dot device.

In the following thesis points I summarize the main new results presented in my Ph.D. dissertation.

1. I have worked out a flexible NRG procedure which is capable of handling an arbitrary number of compact Lie group symmetries that a quantum impurity model possesses [26, 90].

2. I have implemented the above procedure for spin- and charge-SU(2) and U(1) symmetries in structure oriented C++ programming language by writing a flexible NRG code [25, 90] which can be downloaded from the site `http://www.phy.bme.hu/~dmnrg/`. I have demonstrated that the use of non-Abelian symmetries is advantageous for reliability and performance reasons.

3. Using NRG, in the presence of channel anisotropy I have calculated the zero temperature, frequency-dependent linear conductance of the double quantum dot device that has recently been built to justify the feasibility of the 2CK states. I have computed the universal conductance scaling curves that connect the one- and two-channel Kondo fixed points of the two-channel Kondo model that describes the system [140]. I remark that presently NRG is the only method to calculate these scaling curves.

4. Based on group theoretical considerations, I have shown that in the recently devised DM-NRG method the reduced density matrix preserves its diagonal form even in such cases when an arbitrary number of compact, non-Abelian Lie group symmetries of the quantum impurity model are considered [90] (see also Appendix D).

5. I have implemented the DM-NRG procedure for an arbitrary number of spin- and charge-SU(2) and U(1) symmetries into the NRG code mentioned above. This way it became possible to calculate very accurate, spectral sum rule preserving spectral functions [25, 90].

6. Based on conformal field theoretical results, I have classified the highest-weight fields of the electron-hole symmetrical two-channel Kondo model at the two-channel Kondo fixed point according to the group $\mathrm{SU}_{C1}(2) \times \mathrm{SU}_{C2}(2) \times \mathrm{SU}_S(2)$, and determined the relevant and leading irrelevant perturbations to the 2CK fixed point Hamiltonian [91]. Using DM-NRG, I have computed the retarded Green's functions of the highest-weight fields at zero temperature at the two-channel Kondo fixed point and in the presence of relevant perturbations such as the channel anisotropy, or the magnetic field using the groups $\mathrm{SU}_{C1}(2) \times \mathrm{SU}_{C2}(2) \times \mathrm{SU}_S(2)$ and $\mathrm{SU}_{C1}(2) \times \mathrm{SU}_{C2}(2) \times \mathrm{U}_S(1)$, respectively. I have also performed spectral function calculations for fermionic operators in the presence of marginal potential scattering with the use of the symmetry $\mathrm{U}_{C1}(1) \times \mathrm{U}_{C2}(1) \times \mathrm{SU}_S(2)$ [91].

7. Based on simple scaling arguments and conformal field theoretical considerations, I have expanded the highest-weight fields at the two-channel Kondo fixed point in terms of the operators of the free theory. I have determined the analytic form of the universal scaling curves in the asymptotic regions and their numerical form for the whole frequency range. In all cases my DM-NRG calculations confirmed the analytic expectations [91].

8. I found that the boundaries of the various 2CK scaling regimes depend not only on the type of the perturbation but also on the operator investigated. In a small magnetic field, I observed a universal resonance in the local fermions' spectral function and that the dominant superconducting instability arises in the composite superconducting channel [91].

# A Relation between the linear response and the spectral function

## A.1 Definition of the linear response function

Let us introduce the following time-dependent perturbation to a static Hamiltonian

$$\delta\hat{H} \;=\; \hat{B}\, f(t)\,, \qquad \text{where} \qquad \hat{B} \;=\; \hat{B}^{\dagger}\,, \tag{A.1}$$

and $f(t)$ is the strength of the perturbation. The time-dependent expectation value of the operator $\hat{A}$ (denoted by the subscript $t$) is expressed to first order in $f(t)$ in terms of the linear response function $\varphi_{A,B}(t,t')$ as

$$\left\langle \hat{A} \right\rangle_t \;=\; \left\langle \hat{A} \right\rangle_0 + \int_{-\infty}^{t} \varphi_{A,B}(t,t') f(t') dt'\,, \tag{A.2}$$

where the subscript 0 indicates the unperturbed expectation value computed using the equilibrium density matrix, $\hat{\rho}$, and the kernel is given by

$$\varphi_{A,B}(t,t') \;=\; -\frac{i}{\hbar} \left\langle \left[ \hat{A}(t), \hat{B}(t') \right]_{\xi} \right\rangle_0\,, \tag{A.3}$$

where $\left[\hat{A},\hat{B}\right]_{\xi} = \hat{A}\hat{B} - \xi\hat{B}\hat{A}$ with $\xi = \pm 1$ for bosonic/fermionic operators. As it is an equilibrium expectation value, $\varphi_{A,B}$ depends only on the time difference: $t - t'$. (From now on the subscript 0 will be omitted and expectation values will be meant implicitly to refer to the equilibrium case.)

The integral in Eq. (A.2) can be extended to $\infty$ by introducing the retarded Green's function as the kernel

$$G^{R}_{A,B}(t) \;=\; -\frac{i}{\hbar}\,\Theta(t)\,\mathrm{Tr}\left\{ \hat{\rho} \left[ \hat{A}(t), \hat{B}(0) \right]_{\xi} \right\}\,, \tag{A.4}$$

with $\Theta(t)$ the Heaviside step function.

## A.2 Spectral/energy representation and the definition of the spectral function

Upon specifying $\hat{\rho}$ as the canonical distribution, the linear response function or the generalized susceptibility reads as[1]

$$\varphi_{A,B}(t) = -i\mathrm{Tr}\left\{\frac{e^{-\beta\hat{H}}}{\mathbb{Z}}\left[\hat{A}(t)\hat{B}(0) - \xi\hat{B}(0)\hat{A}(t)\right]\right\}$$
$$= -i\sum_n \frac{e^{-\beta E_n}}{\mathbb{Z}}\left\langle n\left|\left[\hat{A}(t)\hat{B}(0) - \xi\hat{B}(0)\hat{A}(t)\right]n\right\rangle\right. , \quad \text{(A.5)}$$

where $\hat{H}\, n\rangle = E_n\, n\rangle$, the set $\{n\rangle\}$ forms an orthonormal basis, and $\mathbb{Z} = \sum_n e^{-\beta E_n}$ is the partition function with $\beta \equiv 1/T$ the Boltzmann factor. Making use of the following form of the identity (and omitting the hat from above the operators)

$$\mathbb{1} = \sum_m m\rangle\,\mathrm{Pr}_m\,, \quad \text{(A.6)}$$

with $\mathrm{Pr}_m$ the projection onto the vector $m\rangle$, we get

$$\varphi_{A,B}(t) = -i\sum_{n,m}\frac{e^{-\beta E_n}}{\mathbb{Z}}\left(\langle n\,|(A(t)m)\,\mathrm{Pr}_m Bn\rangle - \xi\,\langle n\,|(Bm)\,\mathrm{Pr}_m A(t)n\rangle\right)$$
$$= -i\sum_{n,m}\frac{e^{-\beta E_n}}{\mathbb{Z}}\left(\langle n\,|A(t)m\rangle\,\langle m\,|Bn\rangle - \xi\,\langle n\,|Bm\rangle\,\langle m\,|A(t)n\rangle\right) . \quad \text{(A.7)}$$

Inserting the definition of the time-dependence of an operator in the Heisenberg picture, the response function reduces further to the form

$$\varphi_{A,B}(t) = -i\sum_{n,m}\frac{e^{-\beta E_n}}{\mathbb{Z}}\left(\left\langle n\left|e^{iHt}Ae^{-iHt}m\right\rangle\right.\langle m\,|Bn\rangle - \xi\,\langle n\,|Bm\rangle\left\langle m\left|e^{iHt}Ae^{-iHt}n\right\rangle\right.\right)$$
$$= -i\sum_{n,m}\frac{e^{-\beta E_n}}{\mathbb{Z}}\left(e^{i(E_n-E_m)t}\,\langle n\,|Am\rangle\,\langle m\,|Bn\rangle - \xi e^{i(E_m-E_n)t}\,\langle n\,|Bm\rangle\,\langle m\,|An\rangle\right)$$
$$= -i\sum_{n,m}\frac{e^{-\beta E_n} - \xi e^{-\beta E_m}}{\mathbb{Z}}e^{-i\omega_{mn}t}\,\langle n\,|Am\rangle\,\langle m\,|Bn\rangle\ , \quad \text{(A.8)}$$

upon introducing $\omega_{mn} \equiv E_m - E_n$. Taking the Laplace transform of $\varphi_{A,B}(t)$ into the half-plane of complex numbers with positive imaginary parts we gain

$$\chi_{AB}(z) \equiv \int_0^\infty \varphi_{A,B}(t)e^{izt}dt = \sum_{n,m}\frac{e^{-\beta E_n} - \xi e^{-\beta E_m}}{\mathbb{Z}}\frac{\langle n\,|Am\rangle\,\langle m\,|Bn\rangle}{z-\omega_{mn}}\ . \quad \text{(A.9)}$$

[1] From now on everything is measured in units of $\hbar$ and $k_B$.

Substituting $\omega + i\,\epsilon$ for $z$, for $\epsilon \to 0^+$ $\chi_{AB}(\omega + i\,\epsilon)$ can be partitioned into two terms as

$$\chi_{AB}(\omega) \;=\; \chi'_{AB}(\omega) + i\,\chi''_{AB}(\omega)\,, \tag{A.10}$$

where

$$\chi'_{AB}(\omega) \;=\; \sum_{n,m} \frac{e^{-\beta E_n} - \xi e^{-\beta E_m}}{\mathbb{Z}}\,\mathcal{P}\,\frac{\langle n\,|Am\rangle\,\langle m\,|Bn\rangle}{\omega - \omega_{mn}}\,, \tag{A.11}$$

$$\chi''_{AB}(\omega) \;=\; -\pi \sum_{n,m} \frac{e^{-\beta E_n} - \xi e^{-\beta E_m}}{\mathbb{Z}}\,\langle n\,|Am\rangle\,\langle m\,|Bn\rangle\,\delta\,(\omega - \omega_{mn})\;, \tag{A.12}$$

with $\mathcal{P}$ the principal part. If $B = A^\dagger$: $\mathrm{Re}\,\chi_{AA^\dagger}(\omega) = \chi'_{AA^\dagger}(\omega)$ and $\mathrm{Im}\,\chi_{AA^\dagger}(\omega) = \chi''_{AA^\dagger}(\omega)$ hold. The definition of the spectral function of the operator $A$ is

$$\varrho_A(\omega) \equiv -\frac{1}{\pi}\chi''_{AA^\dagger}(\omega) \;=\; \sum_{n,m} \frac{e^{-\beta E_n} - \xi e^{-\beta E_m}}{\mathbb{Z}}\,|\langle n\,|Am\rangle|^2\,\delta\,(\omega - \omega_{mn})\;. \tag{A.13}$$

Provided that $A\,A^\dagger + A^\dagger\,A = cst$ , by integrating over $\omega$ in Eq. (A.13) we obtain the relation

$$cst \;=\; \int d\omega\;\varrho_A(\omega)\,, \tag{A.14}$$

called the spectral sum rule.

The Kramers–Kronig relations establish connection between the real and imaginary parts of the response function via a Hilbert transform as

$$\mathrm{Re}\,\chi_{AA^\dagger}(\omega) \;=\; \frac{1}{\pi}\,\mathcal{P}\int_{-\infty}^{\infty} d\omega'\,\frac{\mathrm{Im}\,\chi_{AA^\dagger}(\omega')}{\omega' - \omega} \tag{A.15}$$

$$\mathrm{Im}\,\chi_{AA^\dagger}(\omega) \;=\; -\frac{1}{\pi}\,\mathcal{P}\int_{-\infty}^{\infty} d\omega'\,\frac{\mathrm{Re}\,\chi_{AA^\dagger}(\omega')}{\omega' - \omega}\,. \tag{A.16}$$

Taking the $\beta \to \infty$ limit we get

$$\begin{aligned}\lim_{\beta\to\infty}\varrho_A(\omega) \;&=\; \lim_{\beta\to\infty}\sum_{n,m}\frac{e^{-\beta(E_n-E_0)} - \xi e^{-\beta(E_m-E_0)}}{\sum\limits_i e^{-\beta(E_i-E_0)}}\,|\langle n\,|Am\rangle|^2\,\delta\,(\omega-\omega_{mn}) \\ &=\; \sum_m |\langle 0\,|Am\rangle|^2\,\delta\,(\omega-\omega_{m0}) - \xi\sum_n |\langle n\,|A0\rangle|^2\,\delta\,(\omega-\omega_{0n})\;,\end{aligned} \tag{A.17}$$

with $0\rangle$ referring to the ground state. If $A$ is a self-adjoint operator, the spectral function of it will be an odd/even function of $\omega$ in case $\xi = \pm 1$, respectively.

# B Energy-dependent density of states in NRG

As an alternative to what has been described in Subsecs. 2.4.2 and 2.4.3, NRG has also been extended to deal with energy-dependent $\rho(\epsilon)$ and $t(\epsilon)$ [112, 113, 115]. For its importance e.g. in implementing NRG to dynamical mean-field theory [120, 121, 24, 122, 123, 124, 139, 85], which is supposed to be one of the subsequent applications of our code [25], or treating quantum impurities embedded into pseudo-gap Fermi systems [112], we show how the mapping to the Wilson chain gets modified with energy-dependent DOS and couplings.

In Ref. [112] it is argued that after integrating out the conduction electron degrees of freedom, the following two models result in the same effective action for the impurity degrees of freedom

$$\mathcal{H}'_A \;=\; \int_{-1}^{1} d\mathcal{E}\; g(\mathcal{E})\; a^\dagger_\mu(\mathcal{E})\; a_\mu(\mathcal{E}) \;+\; \mathcal{H}_d \;+\; \int_{-1}^{1} d\mathcal{E}\; h(\mathcal{E})\; \Big[a^\dagger_\mu(\mathcal{E})\; d_\mu \;+\; h.c.\Big]\,, \tag{B.1}$$

and

$$\mathcal{H}_A \;=\; \int_{-1}^{1} d\mathcal{E}\; \mathcal{E}\; a^\dagger_\mu(\mathcal{E})\; a_\mu(\mathcal{E}) \;+\; \mathcal{H}_d \;+\; \int_{-1}^{1} d\mathcal{E}\; \left(\frac{\tilde{\Delta}(\mathcal{E})}{\pi}\right)^{1/2} \Big[a^\dagger_\mu(\mathcal{E})\; d_\mu \;+\; h.c.\Big]\,, \tag{B.2}$$

(with $\tilde{\Delta}(\mathcal{E}) \;=\; \pi\,\tilde{\rho}(\mathcal{E})\,\tilde{t}(\mathcal{E})^2$ the dimensionless hybridization and $\tilde{\rho}(\mathcal{E}) \;\equiv\; \rho(\epsilon)\,D_F$ and $\tilde{t}(\mathcal{E}) \;=\; t(\epsilon)\,/\,D_F$ the dimensionless conduction electron DOS and coupling, respectively) provided that

$$\frac{\partial g^{-1}(x)}{\partial x}\, h\left(g^{-1}(x)\right)^2 \;=\; \tilde{\rho}(x)\,\tilde{t}(x)^2 \tag{B.3}$$

holds with $g^{-1}$ the inverse of $g$. Eq. (B.3) is obviously satisfied with the choice $g(\mathcal{E}) \;=\; \mathcal{E}$ and $h(\mathcal{E}) \;=\; \sqrt{\tilde{\Delta}(\mathcal{E})\,/\,\pi}$. However, to be able to reduce the Hamiltonian to an $s$-channel form, it is better to choose $h(\mathcal{E})$ to be constant in each interval of the logarithmic discretization, and so $g(\mathcal{E})$ has to be modified accordingly to meet Eq. (B.3). Keeping the same notation as in Subsec. 2.4.2, we define $h(\mathcal{E})$ to take the following value in the $n^{th}$ interval

$$h(\mathcal{E}) \;=\; h_n^+ \;\equiv\; \left[\frac{1}{l_n}\int_{\Lambda^{-(n+1)}}^{\Lambda^{-n}} d\mathcal{E}\;\tilde{\rho}(\mathcal{E})\,\tilde{t}(\mathcal{E})^2\right]^{1/2}, \quad \text{if} \quad \Lambda^{-(n+1)} \;<\; \mathcal{E} \;\leq\; \Lambda^{-n}\,, \tag{B.4}$$

$$h(\mathcal{E}) \;=\; h_n^- \;\equiv\; \left[\frac{1}{l_n}\int_{-\Lambda^{-n}}^{-\Lambda^{-(n+1)}} d\mathcal{E}\;\tilde{\rho}(\mathcal{E})\,\tilde{t}(\mathcal{E})^2\right]^{1/2}, \quad \text{if} \quad \Lambda^{-(n+1)} \;<\; -\mathcal{E} \;\leq\; \Lambda^{-n} \tag{B.5}$$

With this choice, the tunneling part is of the form

$$\begin{aligned}\mathcal{H}^t_A \;=\; \sum_\mu d^\dagger_\mu\,(1 \;-\; \Lambda^{-1})^{1/2} \sum_n \Lambda^{-n/2}\; \left(h_n^+\, a_{n0\mu} \;+\; h_n^-\, b_{n0\mu} \;+\; h.c.\right) \\ \;=\; \left(\int_{-1}^{1} d\mathcal{E}\;\tilde{\rho}(\mathcal{E})\,\tilde{t}(\mathcal{E})^2\right)^{1/2} \sum_\mu \left(d^\dagger_\mu\, f_{0,\mu} \;+\; h.c.\right)\,,\end{aligned} \tag{B.6}$$

with

$$f_{0,\mu} \equiv \left( \frac{1 - \Lambda^{-1}}{\int_{-1}^{1} d\mathcal{E}\, \tilde{\rho}(\mathcal{E})\, \tilde{t}(\mathcal{E})^2} \right)^{1/2} \sum_n \Lambda^{-n/2} \left( h_n^+ \, a_{n0\mu} + h_n^- \, b_{n0\mu} \right) , \tag{B.7}$$

so that $\left\{ f_{0,\mu},\, f_{0,\nu}^\dagger \right\}_+ = \delta_{\mu,\nu}$ again.

The next task is to map $\mathcal{H}_A^{kin}$ to the Wilson chain. Here we make the same approximation as in Subsec. 2.4.2 by dropping all terms with $p \neq 0$ contributions, that do not couple directly to the impurity

$$\begin{aligned} \mathcal{H}_A^{kin} \rightarrow \mathcal{H}_A^{kin} &= \sum_\mu \int_{-1}^{1} d\mathcal{E}\, g(\mathcal{E}) \sum_n \frac{1}{l_n} \left( a_{n0\mu}^\dagger \, a_{n0\mu} + b_{n0\mu}^\dagger \, b_{n0\mu} \right) \\ &= \sum_{n\mu} \left( s_n^+ \, a_{n0\mu}^\dagger \, a_{n0\mu} + s_n^- \, b_{n0\mu}^\dagger \, b_{n0\mu} \right) , \end{aligned} \tag{B.8}$$

with

$$s_n^+ \equiv \frac{1}{l_n} \int_{\Lambda^{-(n+1)}}^{\Lambda^{-n}} d\mathcal{E}\, g(\mathcal{E}) , \tag{B.9}$$

$$s_n^- \equiv \frac{1}{l_n} \int_{-\Lambda^{-n}}^{-\Lambda^{-(n+1)}} d\mathcal{E}\, g(\mathcal{E}) . \tag{B.10}$$

As it is argued in e.g. [112], the specific form of $g(\mathcal{E})$ need not be known, as in the formulas only its integrals over the intervals $\pm \left( \Lambda^{-(n+1)}, \Lambda^{-n} \right]$ appear. From Eq. (B.3) $g(\pm \Lambda^{-n}) = \Lambda^{-n}$ can be inferred. Using this relation together with Eq. (B.3) it is straightforward to show that

$$s_n^+ = \frac{\int_{\Lambda^{-(n+1)}}^{-\Lambda^{-n}} d\mathcal{E}\, \mathcal{E}\, \tilde{\rho}(\mathcal{E})\, \tilde{t}(\mathcal{E})^2}{\int_{\Lambda^{-(n+1)}}^{-\Lambda^{-n}} d\mathcal{E}\, \tilde{\rho}(\mathcal{E})\, \tilde{t}(\mathcal{E})^2} , \tag{B.11}$$

$$s_n^- = \frac{\int_{-\Lambda^{-n}}^{-\Lambda^{-(n+1)}} d\mathcal{E}\, \mathcal{E}\, \tilde{\rho}(\mathcal{E})\, \tilde{t}(\mathcal{E})^2}{\int_{-\Lambda^{-n}}^{-\Lambda^{-(n+1)}} d\mathcal{E}\, \tilde{\rho}(\mathcal{E})\, \tilde{t}(\mathcal{E})^2} . \tag{B.12}$$

Now, we demand $\mathcal{H}_A^{kin}$ to be of tridiagonal form, i.e.

$$\sum_{n\mu} \left( s_n^+ \, a_{n\mu}^\dagger \, a_{n\mu} + s_n^- \, b_{n\mu}^\dagger \, b_{n\mu} \right) = \sum_{n\mu} \left[ \epsilon_{n\mu} \, f_{n,\mu}^\dagger \, f_{n,\mu} + t_{n\mu} \left( f_{n+1,\mu}^\dagger \, f_{n,\mu}^\dagger + h.c. \right) \right] , \tag{B.13}$$

here $\epsilon_{n\mu}$ are called the on-site energies, and $t_{n\mu}$ denote the hopping amplitudes. We apply the Lánczos tridiagonalization procedure [119, 113] to achieve this form and find the coefficients in the decomposition Eq. (2.45) and its inverse Eqs. (2.46), (2.47). The coefficients $u_{0m}$ and $v_{0m}$

are already determined by Eq. (B.7). Using their knowledge we set up the recursion relations to determine the further coefficients, $\epsilon_{n\mu}$ and $t_{n\mu}$. Inserting Eqs. (2.46), (2.47) into Eq. (B.13), we get the following relation between the coefficients of $f_n$ on the two sides of Eq. (B.13)

$$\sum_m \left( s_m^+ u_{nm} a_m^\dagger + s_m^- v_{nm} b_m^\dagger \right) = \epsilon_n f_n^\dagger + t_n f_{n+1}^\dagger + t_{(n-1)} f_{n-1}^\dagger , \tag{B.14}$$

which gives for $n = 0$

$$\sum_m \left( s_m^+ u_{0m} a_m^\dagger + s_m^- v_{0m} b_m^\dagger \right) = \epsilon_0 f_0^\dagger + t_0 f_1^\dagger . \tag{B.15}$$

Taking the anticommutator of $f_0$ with both sides of Eq. (B.15) we find $\epsilon_0$ as

$$\epsilon_0 = \sum_m \left( s_m^+ u_{0m}^2 + s_m^- v_{0m}^2 \right) . \tag{B.16}$$

Taking the anticommutator of both sides of Eq. (B.15) with themselves we get

$$\epsilon_0^2 + t_0^2 = \sum_m \left[ \left( s_m^+ u_{0m} \right)^2 + \left( s_m^- v_{0m} \right)^2 \right] , \tag{B.17}$$

and thus

$$t_0^2 = \sum_m \left[ \left( s_m^+ u_{0m} \right)^2 + \left( s_m^- v_{0m} \right)^2 \right] - \left[ \sum_m \left( s_m^+ u_{0m}^2 + s_m^- v_{0m}^2 \right) \right]^2 . \tag{B.18}$$

Now to carry on with the recursion we have to express $u_{1m}$ and $v_{1m}$ in terms of what is known so far. This can be done by using Eq. (B.15). The result is

$$u_{1m} = \frac{u_{0m} \left( s_m^+ - \epsilon_0 \right)}{t_0} , \tag{B.19}$$

$$v_{1m} = \frac{v_{0m} \left( s_m^+ - \epsilon_0 \right)}{t_0} . \tag{B.20}$$

Following the same logic we get for $n > 0$

$$\epsilon_n = \sum_m \left( s_m^+ u_{nm}^2 + s_m^- v_{nm}^2 \right) , \tag{B.21}$$

$$t_n^2 = \sum_m \left[ \left( s_m^+ u_{0m} \right)^2 + \left( s_m^- v_{0m} \right)^2 \right] - \epsilon_n^2 - t_{(n-1)}^2 , \tag{B.22}$$

$$u_{(n+1)m} = \frac{u_{nm} \left( s_m^+ - \epsilon_n \right) - u_{(n-1)} t_{(n-1)}}{t_n} , \tag{B.23}$$

$$v_{(n+1)m} = \frac{v_{nm} \left( s_m^+ - \epsilon_n \right) - v_{(n-1)} t_{(n-1)}}{t_n} . \tag{B.24}$$

Note that in case of electron-hole symmetry, i.e. for an even hybridization function, the on-site energies vanish.

There is one more technical remark concerning the tridiagonalization procedure: Because of the exponentially decaying hopping amplitudes, for large $n$'s one should resort to arbitrary precision routines for the evaluation of the recursion relations above.

# C Initializing the one-channel Kondo model with $\mathrm{SU}_S(2) \times \mathrm{SU}_C(2)$ symmetry

For the above symmetry setup in the first iteration we have three different block multiplets, $u = 1, \ldots, 3$ formed from the impurity spin and the conduction electron at the zeroth site of the Wilson chain, while there are two local/added multiplets in each iteration, $\mu = 1, 2$. These states and their $S, C$ quantum numbers are listed in Tab. C.1 (only highest weight states, i.e. states with the largest $S^z, C^z$ quantum numbers are listed). The reduced matrix elements of the Hamiltonian between the block states then read

$$ {}_0\langle u \parallel H_0 \parallel v \rangle_0 = J \begin{pmatrix} -\frac{3}{4} & 0 & 0 \\ 0 & \frac{1}{4} & 0 \\ 0 & 0 & 0 \end{pmatrix} , \tag{C.1} $$

with $J$ the exchange coupling strength.

For the construction of the hopping Hamiltonian the matrix elements of $f_0^\dagger$ are needed and can be determined using the Wigner–Eckart theorem. In the present case, the four operators ${\gamma^\dagger}_0 \equiv \{f_{0,\uparrow}^\dagger, f_{0,\downarrow}^\dagger, f_{0,\downarrow}, -f_{0,\uparrow}\}$ form an irreducible operator multiplet, thus their invariant matrix elements are the same and are given by

$$ {}_0\langle u \parallel {\gamma^\dagger}_0 \parallel v \rangle_0 = \begin{pmatrix} 0 & 0 & \sqrt{2} \\ 0 & 0 & -\sqrt{2} \\ \frac{1}{\sqrt{2}} & -\sqrt{\frac{3}{2}} & 0 \end{pmatrix} . \tag{C.2} $$

To generate the hopping terms of the Hamiltonian, we also need to know the reduced matrix elements of $\gamma_{n+1}^\dagger$ between the added states. These are as follows

$$ \langle \mu \parallel \gamma_{n+1}^\dagger \parallel \nu \rangle = \begin{pmatrix} 0 & \sqrt{2} \\ -\sqrt{2} & 0 \end{pmatrix} . \tag{C.3} $$

| Block states | $S$ | $C$ |
|---|---|---|
| $\|1\rangle = \frac{1}{\sqrt{2}}(f^\dagger_{0,\downarrow}\|\Uparrow\rangle - f^\dagger_{0,\uparrow}\|\Downarrow\rangle)$ | 0 | 0 |
| $\|2\rangle = f^\dagger_{0,\uparrow}\|\Uparrow\rangle$ | 1 | 0 |
| $\|3\rangle = f^\dagger_{0,\uparrow}f^\dagger_{0,\downarrow}\|\Uparrow\rangle$ | $\frac{1}{2}$ | $\frac{1}{2}$ |

| Local states | $S$ | $C$ |
|---|---|---|
| $\|1\rangle = f^\dagger_{n+1,\uparrow}\|0\rangle$ | $\frac{1}{2}$ | 0 |
| $\|2\rangle = f^\dagger_{n+1,\uparrow}f^\dagger_{n+1,\downarrow}\|0\rangle$ | 0 | $\frac{1}{2}$ |

Table C.1: Block states at the zeroth site of the Wilson chain (left) and local/added states (right) for the single-channel Kondo model using the group $\mathrm{SU}_S(2) \times \mathrm{SU}_C(2)$. Block states are formed from the impurity spin and the conduction electrons at the zeroth site of the Wilson chain. Different states correspond to different irreducible subspaces of the group $\mathrm{SU}_S(2) \times \mathrm{SU}_C(2)$.

# D Proof of the diagonal form of the reduced density matrix for SU(2) symmetries

In a different way from how it was demonstrated in the main part of the thesis we show that the reduced density matrix is diagonal in the representation indices in the case when the local symmetries are direct products of SU(2) groups.

The proof consists of two parts. In the first one we show that a scalar operator with respect to SU(2) over the space $\mathcal{V}_1 \otimes \mathcal{V}_2$, with $\mathcal{V}_1, \mathcal{V}_2$ two, finite dimensional vector spaces, has a special form in terms of tensor products between irreducible tensor operator components acting on $\mathcal{V}_1$ and $\mathcal{V}_2$, respectively. In the second part we show that the trace of this special form over $\mathcal{V}_1$ vanishes unless the trace of a scalar operator was taken. As a consequence the reduced density matrix remains scalar under further reduction.

*Claim:* Let $\mathcal{V}_1$ and $\mathcal{V}_2$ be vector spaces of dimensions $d_1$ and $d_2$, respectively. Let $A$ be a linear mapping of $\mathcal{V}_1 \otimes \mathcal{V}_2$ into itself ( $A \in L(\mathcal{V}_1 \otimes \mathcal{V}_2)$ ) which is a *scalar* with respect to SU(2). Then $A$ can be written of the form

$$A = \sum_{n,m} \sum_{\Omega(n,m) \in \frac{\mathbb{Z}^+}{2}} \sum_{\omega = -\Omega(n,m)}^{\Omega(n,m)} C^{\Omega(n,m),\omega} \, Q^{(\mathcal{V}_1)}_{\Omega(n,m),\omega} \otimes Q^{(\mathcal{V}_2)}_{\Omega(n,m),-\omega} \, , \tag{D.1}$$

where $\Omega(n,m)$ runs over the non-negative integers and half-integers and satisfies the relation $(2\Omega(n,m) + 1) \leq \min(d_1^2, d_2^2)$; for $i = 1,2$, $Q^{(\mathcal{V}_i)}_{\Omega(n,m),\omega}$ is the $\omega^{th}$ component of an irreducible tensor operator of rank $\Omega(n,m)$, acting on $\mathcal{V}_i$. The $C^{\Omega(n,m),\omega}$-s are constants with the restriction that there are at most $\min(d_1^2, d_2^2)$ non-zero among them.

*Proof:* First we show that $A$ can be decomposed as

$$A = \sum_{n,m} \sum_{\Omega_1(n), \Omega_2(m) \in \frac{\mathbb{Z}^+}{2}} \sum_{\omega_1 = -\Omega_1(n)}^{\Omega_1(n)} \sum_{\omega_2 = -\Omega_2(m)}^{\Omega_2(m)} C^{\Omega_1(n),\omega_1}_{\Omega_2(m),\omega_2} \, Q^{(\mathcal{V}_1)}_{\Omega_1(n),\omega_1} \otimes Q^{(\mathcal{V}_2)}_{\Omega_2(m),\omega_2} \, , \tag{D.2}$$

where $(2\Omega_1(n)+1) \leq d_1^2$ and $(2\Omega_2(m)+1) \leq d_2^2$ and among the constants $C^{\Omega_1(n),\omega_1}_{\Omega_2(m),\omega_2}$ at most $d_1^2 d_2^2$ are non-zero. This decomposition is a consequence of $(i)$ that $\forall A \in L(\mathcal{V}_1 \otimes \mathcal{V}_2)$ can be decomposed as

$$A = \sum_{i=1}^{d_1^2} \sum_{j=1}^{d_2^2} c^{i,j} \, \mathcal{B}^{(\mathcal{V}_1)}_i \otimes \mathcal{B}^{(\mathcal{V}_2)}_j \, , \tag{D.3}$$

where for $i = 1,2$, $k = 1, \ldots, d_i^2$, $\mathcal{B}^{(\mathcal{V}_i)}_k$ enumerate the elements of the canonical basis of $L(\mathcal{V}_i)$, the linear mappings of $\mathcal{V}_i$ into itself and the $c^{i,j}$-s are constants; and $(ii)$ that $\forall \mathcal{O} \in L(\mathcal{V}_i)$

can be expressed in terms of the irreducible tensor operator components as these components form a basis of $L(\mathcal{V}_i)$ [103].

Let $D^{(\Omega)}_{\omega,\omega'}(g)$ be the matrix elements of the $(2\Omega+1)$-dimensional, irreducible representation of SU(2), with $g \in \mathrm{SU}(2)$ arbitrary. By using its invariance under the action of SU(2), we can rewrite $A$ as

$$A = \sum_{n,m} \sum_{\Omega_1(n),\Omega_2(m)\in\frac{\mathbb{Z}^+}{2}} \sum_{\omega_1=-\Omega_1(n)}^{\Omega_1(n)} \sum_{\omega_2=-\Omega_2(m)}^{\Omega_2(m)} \sum_{\omega_1'=-\Omega_1(n)}^{\Omega_1(n)} \sum_{\omega_2'=-\Omega_2(m)}^{\Omega_2(m)} C^{\Omega_1(n),\omega_1}_{\Omega_2(m),\omega_2} \times D^{(\Omega_1(n))}_{\omega_1,\omega_1'}(g)\ D^{(\Omega_2(m))}_{\omega_2,\omega_2'}(g)\ Q^{(\mathcal{V}_1)}_{\Omega_1(n),\omega_1'} \otimes Q^{(\mathcal{V}_2)}_{\Omega_2(m),\omega_2'} \ . \quad \text{(D.4)}$$

By decomposing the product of the irreducible representations in Eq. (D.4) into irreducible representations, as usual, we have

$$D^{(\Omega_1)}_{\omega_1,\omega_1'}(g) D^{(\Omega_2)}_{\omega_2,\omega_2'}(g) = \sum_{\Omega=|\Omega_1-\Omega_2|}^{\Omega_1+\Omega_2} \langle \Omega\ \omega_1+\omega_2\,|\Omega_2\ \omega_2\ \Omega_1\ \omega_1\rangle^*\ D^{(\Omega)}_{\omega_1+\omega_2,\omega_1'+\omega_2'}(g) \times \left\langle \Omega\ \omega_1'+\omega_2' \middle| \Omega_2\ \omega_2'\ \Omega_1\ \omega_1' \right\rangle \ . \quad \text{(D.5)}$$

By substituting the form above into Eq. (D.4) and by integrating both sides over SU(2) we obtain Eq. (D.1) with the identification

$$C^{\Omega(n,m),\omega} = \frac{(-1)^{\omega}}{2\Omega(n,m)+1} \sum_{\omega_1=-\Omega(n,m)}^{\Omega(n,m)} C^{\Omega_1(n),\omega_1}_{\Omega_2(m),-\omega_1}(-1)^{\omega_1} \ , \quad \text{(D.6)}$$

with $\Omega(n,m) = \Omega_1(n) = \Omega_2(m)$. Here we have used the fundamental orthogonality theorem [103] in the form

$$\int D^{(\Omega)}_{\omega_1+\omega_2,\omega_1'+\omega_2'}(g)dg = \int D^{(0)}_{0,0}(g)^* D^{(\Omega)}_{\omega_1+\omega_2,\omega_1'+\omega_2'}(g)dg = \delta_{0,\Omega}\delta_{0,\omega_1+\omega_2}\delta_{0,\omega_1'+\omega_2'} \ , \quad \text{(D.7)}$$

and the fact that the $\Omega = 0$ summation index appears in Eq. (D.5) only if $\Omega_1 = \Omega_2$. To get Eq. (D.6) we have also exploited the relation [104]

$$\langle 0\ 0|\Omega-\omega\ \Omega\ \omega\rangle = \frac{(-1)^{\Omega-\omega}}{\sqrt{2\Omega+1}} \ . \quad \text{(D.8)}$$

If we have a direct product of several SU(2) groups instead of only one the above statement remains true with the distinctive feature that instead of one representation index we have an array of indices referring to the different SU(2) groups.

The proof for the diagonal form of the reduced density matrix goes by induction for the iteration steps again. $R^{[N_{\max}]}$ is a scalar and, by making use of the previous claim, it can be written as a sum over tensor products of irreducible tensor operator components acting on the local vector spaces at each site, i.e. of the form

$$R^{[N_{\max}]} = \sum_i \left(T_i^{[loc]}\right)_{\underline{w},\underline{w}^z} \otimes \left(T_i^{[N_{\max}-1]}\right)_{\underline{w},-\underline{w}^z} \ , \quad \text{(D.9)}$$

where $\left(T_i^{[loc]}\right)_{\underline{w},\underline{w}^z}$ and $\left(T_i^{[N_{\max}-1]}\right)_{\underline{w},-\underline{w}^z}$ are irreducible tensor operator components acting on the local vector space at site $N_{\max}$ and on the remaining, local vector spaces, respectively. To obtain $R_{KK}^{[N_{\max}-1]}$ we have to trace over the local basis states, $\left\{\left|\underline{q}_\mu, \underline{q}_\mu^z\right\rangle_{loc}\right\}$, that is we have to recover the following matrix elements

$$\left(R_{KK}^{[N_{\max}-1]}\right)_u^v = \sum_{i,\underline{q}_\mu,\mu} \mathrm{sgn}\left(T_i^{[N_{\max}-1]}, \underline{q}_\mu\right) \left\langle \underline{Q}_u \parallel T_i^{[N_{\max}-1]} \parallel \underline{Q}_v \right\rangle \left\langle \underline{q}_\mu \parallel S_i^{loc} \parallel \underline{q}_\mu \right\rangle$$

$$\times \left\langle \underline{Q}_u\, \underline{Q}_u^z \left| \underline{w}_\mu\, \underline{w}_\mu^z\, \underline{Q}_v\, \underline{Q}_v^z \right\rangle \prod_{\gamma=1}^{\Gamma} \sum_{(q^\gamma)_\mu^z = -(q^\gamma)_\mu}^{(q^\gamma)_\mu} \left\langle (q^\gamma)_\mu (q^\gamma)_\mu^z \left| (w^\gamma)_\mu (w^\gamma)_\mu^z (q^\gamma)_\mu (q^\gamma)_\mu^z \right\rangle \right. , \quad \text{(D.10)}$$

where we have made use of the Wigner–Eckart theorem. The coefficient $\mathrm{sgn}(.,.)$ appears for that the terms above might acquire minus signs according to the number of fermionic operators and excitations present in $T_i^{[N_{\max}-1]}$ and in $\left|\underline{Q}_i, \underline{Q}_i^z\right\rangle$, respectively.

Next we show that

$$\sum_{q^z=-q}^{q} \langle q q^z \,|s s^z\, q q^z\rangle \;=\; (2q+1)\,\delta_{s,0}\,\delta_{s^z,0}\,. \quad \text{(D.11)}$$

$s^z = 0$ must hold otherwise $q^z + s^z = q^z$ would not be satisfied. The sum can be rewritten as [104]

$$\sum_{q^z=-q}^{q} \langle q\; q^z \,|s\; 0\; q\; q^z\rangle \;=\; \sqrt{\frac{2q+1}{2s+1}} \sum_{q^z=-q}^{q} (-)^{-q-q^z}\; \langle s\; 0 \,|\; q\; q^z q - q^z\rangle$$

$$\times\; \langle 0\; 0 \,|\; q\; q^z q - q^z\rangle\; \sqrt{2q+1}\,(-)^{q+q^z} \;=\; (2q\;+\;1)\,\delta_{s,0}\,. \quad \text{(D.12)}$$

It has the implication that the terms from Eq. (D.10) that give non-vanishing contribution to $R^{[N_{\max}-1]}$ are the ones with a scalar $T_i^{[loc]}$ and so $T_i^{[N_{\max}-1]}$ is also an SU(2) invariant, that is $R_{KK}^{[N_{\max}-1]}$ is a scalar. The induction towards smaller iteration steps goes the same way.

# Bibliography


[1] For a recent review see P. A. Lee, *From high temperature superconductivity to quantum spin liquid: progress in strong correlation physics*, Reports on Progress in Physics **71**, 012501 (2008)

[2] E. W. Carlson, V. J. Emery, S. A. Kivelson, D. Orgad, *Concepts in High Temperature Superconductivity* in *The Physics of Conventional and Unconventional Superconductors*, Vol. II. ed. by K. H. Bennemann, J. B. Ketterson, Springer-Verlag (2004)

[3] H. von Löhneysen, A. Rosch, M. Vojta, P. Wölfle, *Fermi-liquid instabilities at magnetic quantum phase transitions*, Rev. Mod. Phys. **79**, 1015 (2007)

[4] P. Coleman, *Heavy Fermions: electrons at the edge of magnetism*, Handbook of Magnetism and Advanced Magnetic Materials, J. Wiley and Sons, (2007)

[5] I. P. Radu, J. B. Miller, C. M. Marcus, M. A. Kastner, L. N. Pfeiffer, K. W. West, *Quasiparticle Tunneling in the Fractional Quantum Hall State at* $\nu = 5/2$, Science **320**, 899 (2008)

[6] J. Cardy, *Scaling and Renormalization in Statistical Physics*, Cambridge University Press (2002)

[7] G. S. Japaridze, *How the relation* $e^2/4\pi = 1/137$ *may be obtained in the framework of Quantum Electrodynamics*, [arXiv:0812.2173]

[8] F. J. Dyson, *The S Matrix in Quantum Electrodynamics*, Phys. Rev. **75**, 1736 (1949)

[9] Curtis G. Callan, *Broken Scale Invariance in Scalar Field Theory*, Phys. Rev. D **2** 1541 (1970)

[10] K. Symanzik, *Small Distance Behaviour in Field Theory and Power Counting*, Comm. Math. Phys. **18**, 227 (1970)

[11] K. G. Wilson, *Anomalouos Dimensions and the Breakdown of Scale Invariance in Perturbation Theory*, Phys. Rev. D **2**, 1478 (1970)

[12] E. C. G. Stueckelberg, A. Petermann, *La normalisation des constantes dans la theorie des quanta*, Helv. Phys. Acta **26**, 499 (1953)

[13] M. Gell-Mann, F. E. Low, *Quantum Electrodynamics at Small Distances*, Phys. Rev. B **95**, 1300 (1954)

[14] L. P. Kadanoff, Physics **3**, 255 (1966)

[15] M. E. Fisher, *The Theory of Condensation and the Critical Point*, Physics **3**, 255 (1967)

[16] F. J. Wegner, *Correction to Scaling Laws*, Phys. Rev. B **5**, 4529 (1972)

[17] K. G. Wilson, J. Kogut, *The renormalization group and the $\varepsilon$ expansion*, Phys. Rep. **12C**, 75 (1974)

[18] M. E. Fisher, *The renormalization group in the theory of critical behavior*, Rev. Mod. Phys. **46**, 597 (1975)

[19] S. Lundqvist, G. Morandi, Y. Lu, *Low-Dimensional Quantum Field Theories for Condensed Matter Physicists*, World Scientific (1995)

[20] G. Morandi, P. Sodano, A. Tagliacozzo (Editor), V. Tognetti eds., *Field Theories for Low-Dimensional Condensed Matter Systems: Spin Systems and Strongly Correlated Electrons*, Springer (2000)

[21] D. L. Cox, *Quadrupolar Kondo effect in uranium heavy-electron materials*, Phys. Rev. Lett. **59**, 12401243 (1987)

[22] C. L. Seaman *et al.*, *Evidence for non-Fermi-liquid behavior in the Kondo alloy $Y_{1-x}U_xPd_3$*, Phys. Rev. Lett. **67**, 2882 (1991)

[23] R. M. Potok, I. G. Rau, H. Shtrikman, Y. Oreg, D. Goldhaber-Gordon, *Observation of the two-channel Kondo effect*, Nature (London) **446**, 167 (2007)

[24] A. Georges, G. Kotliar, W. Krauth, M. J. Rozenberg, *Dynamical mean-field theory of strongly correlated fermion systems and the limit of infinite dimensions*, Rev. Mod. Phys. **68**, 13 (1996)

[25] Ö. Legeza, C. P. Moca, A. I. Tóth, I. Weymann, G. Zaránd, *Flexible Density Matrix Numerical Renormalization Group Code*, public C++ code, distributed under GNU LPGL, `http://www.phy.bme.hu/~dmnrg/`

[26] Ö. Legeza, C. P. Moca, A. I. Tóth, I. Weymann, G. Zaránd, *Manual for the Flexible DM-NRG code*, [arXiv:0809.3143]

[27] I. Affleck, A. W. W. Ludwig, *The Kondo effect, conformal field theory and fusion rules*, Nucl. Phys. B **352**, 849 (1991); *Critical theory of overscreened Kondo fixed points*, *ibid.* **360**, 641 (1991),

[28] V. J. Emery, S. Kivelson, *Mapping of the two-channel Kondo problem to a resonant-level model*, Phys. Rev. B **46**, 10812 (1992)

[29] A. C. Hewson, *The Kondo Problem to Heavy Fermions*, Cambridge University Press (1993)

[30] K. G. Wilson, *The renormalization group: Critical phenomena and the Kondo problem*, Rev. Mod. Phys. **47**, 4 (1975)

[31] W. J. de Haas, J. de Boer, G. J. van den Berg, *The electrical resistance of gold, copper and lead at low temperatures*, Physica **1**, 1115 (1934)

[32] J. Kondo, *Resistance Minimum in Dilute Magnetic Alloys*, Prog. Theor. Phys. **32**, 37 (1964)

[33] J. F. DiTusa, K. Lin, M. Park, M. S. Isaacson, J. M. Parpia, *Finite-size effects in the low-temperature resistivity of CuCr films*, Phys. Rev. Lett. **68**, 678 (1992)

[34] M. A. Blachly, N. Giordano, *Kondo effect in Cu(Fe) films*, Phys. Rev. B **49**, 6788 (1994)

[35] V. Chandrasekhar, P. Santhanam, N. A. Penebre, R. A. Webb, H. Vloeberghs, C. Van Haesendonck, Y. Bruynseraede, *Absence of size dependence of the Kondo resistivity*, Phys. Rev. Lett. **72**, 2053 (1994)

[36] C. Roth, C. Sürgers, H. v. Löhneysen, *Electronic transport and Kondo effect in* $La_{1-x}Ce_x$ *films*, Phys. Rev. B **54**, 3454 (1996)

[37] O. Újsághy, A. Zawadowski, B. L. Gyorffy, *Spin-Orbit-Induced Magnetic Anisotropy for Impurities in Metallic Samples of Reduced Dimensions: Finite Size Dependence in the Kondo Effect*, Phys. Rev. Lett. **76**, 2378 (1996)

[38] I. Martin, Y. Wan, P. Phillips, *Size Dependence in the Disordered Kondo Problem*, Phys. Rev. Lett. **78**, 114 (1997)

[39] O. Újsághy, A. Zawadowski, *Spin-orbit-induced magnetic anisotropy for impurities in metallic samples. I.-II. Surface anisotropy*, Phys. Rev. B **57**, 11598 (1998), *ibid.* 11609 (1998)

[40] O. Újsághy, L. Szunyogh, A. Zawadowski, *Revised theory of the magnetic surface anisotropy of impurities in metallic mesoscopic samples*, Phys. Rev. B **75**, 064425 (2007)

[41] A. Szilva, S. Gallego, M. C. Muñoz, B. L. Györffy, G. Zaránd, L. Szunyogh, *Friedel-oscillations-induced surface magnetic anisotropy*, Phys. Rev. B **78**, 195418 (2008)

[42] J. Li, W. Schneider, R. Berndt, B. Delley, *Kondo Scattering Observed at a Single Magnetic Impurity*, Phys. Rev. Lett. **80**, 2893 (1998)

[43] V. Madhavan, *Tunneling into a single magnetic atom: spectroscopic evidence of the Kondo resonance*, Science **280**, 567 (1998)

[44] H. C. Manoharan, C. P. Lutz, D. M. Eigler, *Quantum mirages formed by coherent projection of electronic structure*, Nature **403**, 512 (2000)

[45] O. Újsághy, J. Kroha, L. Szunyogh, A. Zawadowski, *Theory of the Fano Resonance in the STM Tunneling Density of States due to a Single Kondo Impurity*, Phys. Rev. Lett. **85**, 2557 (2000)

[46] M. Plihal, J. W. Gadzuk, *Nonequilibrium theory of scanning tunneling spectroscopy via adsorbate resonances: Nonmagnetic and Kondo impurities*, Phys. Rev. B **63** 085404 (2001)

[47] I. K. Yanson, V. V. Fisun, R. Hesper, A. V. Khotkevich, J. M. Krans, J. A. Mydosh, J. M. van Ruitenbeek, *Size Dependence of Kondo Scattering in Point Contacts*, Phys. Rev. Lett. **74**, 302 (1995)

[48] N. van der Post, F. L. Mettes, J. A. Mydosh, J. M. van Ruitenbeek, I. K. Yanson, *Size dependence of Kondo scattering in point contacts: Fe impurities in Cu*,Phys. Rev. B **53**, R476 (1996)

[49] G. Zaránd, L. Udvardi, *Enhancement of the Kondo temperature of magnetic impurities in metallic point contacts due to the fluctuations of the local density of states*, Phys. Rev. B **54**, 7606 (1996)

[50] O. Újsághy, A. Zawadowski, *Kondo Effect on Mesoscopic Scale*, J. Phys. Soc. Jpn. **74**, 80 (2005)

[51] P. W. Anderson, *Localized Magnetic States in Metals*, Phys. Rev. **124**, 41 (1961)

[52] U. Fano, *Effects of Configuration Interaction on Intensities and Phase Shifts*, Phys. Rev. **124**, 1866 (1961)

[53] O. Sakai, Y. Shimizu, T. Kasuya, *Single-Particle and Magnetic Excitation Spectra of Degenerate Anderson Model with Finite Coulomb Interaction*, J. Phys. Soc. Jpn. **58**, 3666 (1989)

[54] J. R. Schrieffer, P. A. Wolff, *Relation between the Anderson and Kondo Hamiltonians*, Phys. Rev. **149**, 491 (1966)

[55] S. Kehrein, *The Flow Equation Approach to Many-Body Problems*, Springer (2006)

[56] H. R. Krishna-murthy, J. W. Wilkins, K. G. Wilson, *Renormalization-group approach to the Anderson model of dilute magnetic alloys. I. Static properties for the symmetric case*, Phys. Rev. B **21**, 1003 (1980)

[57] P. W. Anderson, *A poor man's derivation of scaling laws for the Kondo problem*, J. Phys. C **3**, 2436 (1970)

[58] F. D. M. Haldane, *Scaling Theory of the Asymmetric Anderson Model*, Phys. Rev. Lett. **40**, 416 (1978)

[59] A. A. Abrikosov, A. A. Migdal, *On the Theory of the Kondo Effect*, J. Low Temp. Phys. **3**, 519 (1970)

[60] M. Fowler, A. Zawadowski, *Scaling and the Renormalization Group in the Kondo Effect*, Solid State Comm. **9**, 471 (1971)

[61] N. Andrei, K. Furuya, J. H. Lowenstein, *Solution of the Kondo problem*, Rev. Mod. Phys. **55**, 331 (1983)

[62] A. M. Tsvelick, P. B. Wiegmann, *Exact results in the theory of magnetic alloys*, Adv. Phys. **38**, 1143 (1983)

[63] N. Andrei, C. Destri, *Solution of the Multichannel Kondo Problem*, Phys. Rev. Lett. **52**, 364 (1984)

[64] A. M. Tsvelick, P. B. Wiegmann, *Exact Solution of the Multichannel Kondo Problem, Scaling, and Integrability*, J. Stat. Phys. **38**, 125 (1985)

[65] I. Affleck, A. W. Ludwig, H.-B. Pang, D. L. Cox, *Relevance of anisotropy in the multichannel Kondo effect: Comparison of conformal field theory and numerical renormalization-group results*, Phys. Rev. B **45**, 7918 (1992)

[66] Ph. Nozières, C. T. De Dominicis, *Singularities in the X-Ray Absorption and Emission of Metals. III. One-Body Theory Exact Solution*, Phys. Rev. **178**, 1097 (1969)

[67] G. Yuval, P. W. Anderson, *Exact Results for the Kondo Problem: One-Body Theory and Extension to Finite Temperature*, Phys. Rev. B **1**, 1522 (1970)

[68] K. Vladár, G. T. Zimányi, A. Zawadowski, *Theory of a two-level system strongly interacting with a degenerate Fermi gas*, Phys. Rev. Lett. **56**, 286 (1986)

[69] A. A. Abrikosov, *Electron Scattering on Magnetic Impurities in Metals and Anomalous Resistivity Effects*, Physics **2**, 5 (1965)

[70] Ph. Nozières, *A "Fermi-Liquid" Description of the Kondo Problem at Low Temperatures*, J. Low Temp. Phys. **17**, 31 (1974).

[71] N. E. Bickers, *Review of techniques in the large-N expansion for dilute magnetic alloys*, Rev. Mod. Phys. **59**, 845 (1987)

[72] D. L. Cox, A. E. Ruckenstein, *Spin-flavor separation and non-Fermi-liquid behavior in the multichannel Kondo problem: A large-N approach*, Phys. Rev. Lett. **71**, 1613 (1993)

[73] J. Gan, N. Andrei, P. Coleman, *Perturbative approach to the non-Fermi-liquid fixed point of the overscreened Kondo problem*, Phys. Rev. Lett. **70**, 686 (1993)

[74] R. Bulla, N. Tong, M. Vojta, *Numerical Renormalization Group for Bosonic Systems and Application to the Sub-Ohmic Spin-Boson Model*, Phys. Rev. Lett. **91**, 170601 (2003)

[75] R. Bulla, H. Lee, N. Tong, M. Vojta, *Numerical renormalization group for quantum impurities in a bosonic bath*, Phys. Rev. B **71**, 045122 (2005)

[76] L. N. Oliveira, J. W. Wilkins, *New approach to the X-ray-absorption problem* , Phys. Rev. B **24**, 4863 (1981), *ibid.* **32**, 696 (1985)

[77] H. O. Frota, L. N. Oliveira *Photoemission spectroscopy for the spin-degenerate Anderson model*, Phys. Rev. B **33**, 7871 (1986)

[78] T. A. Costi, A. C. Hewson, *Resistivity cross-over for the non-degenerate Anderson model*, Phil. Mag. B **65**, 1165 (1992)

[79] T. A. Costi, A. C. Hewson, V. Zlatić, *Transport coefficients of the Anderson model via the numerical renormalization group*, J. Phys.: Cond. Mat. **6**, 2519 (1994)

[80] S. Suzuki, O. Sakai, Y. Shimizu, *Magnetic Excitation and Transport Coefficients of the Impurity Anderson Model -Comparison between the 2-Fold and 4-Fold Models-*, J. Phys. Soc. Jpn. **65**, 4034 (1996)

[81] M. Yoshida, M. A. Whitaker, L. N. Oliveira, *Renormalization-group calculation of excitation properties for impurity models*, Phys. Rev. B **41**, 9403 (1990)

[82] W. C. Oliveira, L. N. Oliveira, *Generalized numerical renormalization-group method to calculate the thermodynamical properties of impurities in metals*, Phys. Rev. B **49**, 11986 (1994)

[83] R. Bulla, A. C. Hewson, T. Pruschke, *Numerical renormalization group calculations for the self-energy of the impurity Anderson model* J. Phys.: Cond. Mat. **10**, 8365 (1998)

[84] V. L. Campo, L. N. Oliveira, *Alternative discretization in the numerical renormalization-group method*, Phys. Rev. B **72**, 104432 (2005)

[85] R. Žitko, Th. Pruschke, *Energy resolution and discretization artefacts in the numerical renormalization group*, [arXiv:0810.4765]

[86] W. Hofstetter, *Generalized Numerical Renormalization Group for Dynamical Quantities*, Phys. Rev. Lett. **85**, 1508 (2000)

[87] F. B. Anders, A. Schiller, *Real-time dynamics in Quantum Impurity Systems: A Time-dependent Numerical Renormalization Group Approach*, Phys. Rev. Lett. **95**, 196801 (2005)

[88] R. Peters, T. Pruschke, F. B. Anders, *A Numerical Renormalization Group approach to Green's Functions for Quantum Impurity Models*, Phys. Rev. B **74**, 245114 (2006)

[89] A. Weichselbaum, J. von Delft, *Sum-rule Conserving Spectral Functions from the Numerical Renormalization Group*, Phys. Rev. Lett. **99**, 076402 (2007)

[90] A. I. Tóth, C. P. Moca, Ö Legeza, G. Zaránd, *Density matrix numerical renormalization group for non-Abelian symmetries*, Phys. Rev. B **78**, 245109 (2008), Editors' Suggestion

[91] A. I. Tóth, G. Zaránd, *Dynamical correlations in the spin-half two-channel Kondo model*, Phys. Rev. B **78**, 165130 (2008), Editors' Suggestion

[92] D. M. Cragg, P. Lloyd, *Potential Scattering and the Kondo Problem*, J. Phys. C: Solid State Phys. **11**, L597 (1978)

[93] D. M. Cragg, P. Lloyd, *Universality and the renormalisability of rotationally invariant Kondo Hamiltonians* J. Phys. C: Solid State Phys. **12**, 3301 (1979)

[94] D. M. Cragg, P. Lloyd, *Kondo Hamiltonians with a non-zero ground-state spin*, J. Phys. C: Solid State Phys. **12**, L215 (1979)

[95] T. A. Costi *et al.*, *Kondo decoherence: finding the right spin model for iron impurities in gold and silver*, [arXiv:0810.1771]

[96] D. M. Cragg, P. Lloyd, P. Nozières, *On the ground states of some s-d exchange Kondo Hamiltonians*, J. Phys. C: Solid State Phys. **13** 803 (1980)

[97] A. A. Migdal, *A Diagram Technique near the Curie Point and the Second Order Phase Transition in a Bose Liquid*, Sov. Phys. JETP **28**, 1036 (1969)

[98] M. Fowler, *Renormalization-Group Techniques in the Kondo Effect*, Phys. Rev. B **6**, 3422 (1972)

[99] Michael E. Peskin, Daniel V. Schroeder, *An Introduction to Quantum Field Theory*, Addison-Wesley Publishing Company (1995)

[100] F. B. Anders, *On steady-state currents through nano-devices: a scattering-states numerical renormalization group approach to open quantum systems*, Phys. Rev. Lett. **101**, 066804 (2008)

[101] A. Fetter, J. D. Walecka, *Quantum Theory of Many-Particle Systems*, Dover Publications, Inc. (2003), pp. 53-61

[102] F. B. Anders, *A Numerical Renormalization Group approach to Non-Equilibrium Green's Functions for Quantum Impurity Models*, J. Phys.: Cond. Mat. **20**, 195216 (2008)

[103] J. F. Cornwell, *Group Theory in Physics, An Introduction*, Academic Press (1997)

[104] A. Messiah, *Quantum Mechanics*, Dover Publications, Inc. (1999), pp. 358-359 for the expansion of a plane wave in spherical harmonics

[105] D. C. Langreth, *Friedel Sum Rule for Anderson's Model of Localized Impurity States*, Phys. Rev. **150**, 516 (1966)

[106] B. A. Jones, C. M. Varma, *Study of two magnetic impurities in a Fermi gas*, Phys. Rev. Lett. **58**, 843 (1987)

[107] B. A. Jones, C. M. Varma, J. W. Wilkins, *Low-Temperature Properties of the Two-Impurity Kondo Hamiltonian*, Phys. Rev. Lett. **61**, 125 (1988)

[108] B. A. Jones, Ph.D. dissertation, Cornell University (1988).

[109] I. Affleck, *A current algebra approach to the Kondo effect*, Nucl. Phys. B **336**, 517 (1990)

[110] H.-B. Pang, D. L. Cox, *Stability of the fixed point of the two-channel Kondo Hamiltonian*, Phys. Rev. B **44**, 9454 (1991)

[111] K. Vladár, A. Zawadowski, G. T. Zimányi, *Theory of a two-level system interacting with a degenerate electron gas. I. Partition function* Phys. Rev. B, **37**, 2001 (1988); *Theory of a two-level system interacting with a degenerate electron gas. II. Scaling theory of a one-dimensional Coulomb gas*, *ibid.* **37**, 2015 (1988)

[112] R. Bulla, Th. Pruschke, A. C. Hewson, *Anderson impurity in pseudo-gap Fermi systems*, J. Phys.: Cond. Mat. **9**, 10463 (1997)

[113] W. Hofstetter, *Renormalization Group Methods for Quantum Impurity Systems*, Ph.D. dissertation, Augsburg (2000)

[114] L. Borda, *Kondo effektus különféle mezoszkopikus rendszerekben*, Ph.D. dissertation, Budapest (2001)

[115] M. Sindel, *Numerical Renormalization Group studies of Quantum Impurity Systems in the Strong Coupling Limit*, Ph.D. dissertation, Munich (2004)

[116] L. de Leo, *Non-Fermi liquid behavior in multi-orbital Anderson impurity models and possible relevance for strongly correlated lattice models*, Ph.D. dissertation, Trieste (2004)

[117] R. Žitko, *Many-particle effects in resonant tunneling of electrons through nanostructures*, Ph.D. dissertation, Ljubljana (2007)

[118] Th. Hecht, *Numerical Renormalization Group studies of Phase Coherent effects through Quantum Dots*, Ph.D. dissertation, Munich (2008)

[119] C. Lánczos, *An Iteration Method for the Solution of the Eigenvalue Problem of Linear Differential and Integral Operators*, Journal of Research of the National Bureau of Standards **45**, 255 (1950)

[120] W. Metzner, D. Vollhardt, *Correlated Lattice Fermions in $d = \infty$ Dimensions*, Phys. Rev. Lett. **62**, 324 (1989)

[121] O. Sakai, Y. Kuramoto, *Application of the numerical renormalization group method to the Hubbard model in infinite dimensions*, Solid State Comm. **89**, 307 (1994)

[122] R. Bulla, *Zero Temperature Metal-Insulator Transition in the Infinite-Dimensional Hubbard Model*, Phys. Rev. Lett. **83**, 136 (1999)

[123] Th. Pruschke, R. Bulla, M. Jarrell, *Low-energy scale of the periodic Anderson model*, Phys. Rev. B **61**, 12799 (2000)

[124] R. Bulla, T. A. Costi, D. Vollhardt, *Finite-temperature numerical renormalization group study of the Mott transition*, Phys. Rev. B **64**, 045103 (2001)

[125] O. Sakai, Y. Shimizu, T. Kasuya, *Excitation spectra of two impurity Anderson model* , Solid State Comm. **75**, 81 (1990)

[126] J. B. Silva, W. L. C. Lima, W. C. Oliveira, J. L. N. Mello, L. N. Oliveira, J. W. Wilkins, *Particle-Hole Asymmetry in the Two-Impurity Kondo Model*, Phys. Rev. Lett. **76**, 275 (1996)

[127] C. A. Paula, M. F. Silva, L. N. Oliveira, *Low-energy spectral density for the Alexander-Anderson model*, Phys. Rev. B **59**, 85 (1999)

[128] R. Žitko, J. Bonča, A. Ramšak, T. Rejec, *Kondo effect in triple quantum dots*, Phys. Rev. B **73**, 153307 (2006)

[129] R. Žitko, J. Bonča, *Fermi-Liquid versus Non-Fermi-Liquid Behavior in Triple Quantum Dots*, Phys. Rev. Lett. **98**, 047203 (2007)

[130] A. C. Hewson, D. Meyer, *Numerical renormalization group study of the Anderson–Holstein model*, J. Phys.: Cond. Mat. **14**, 427 (2002)

[131] D. Meyer, A. C. Hewson, R. Bulla, *Gap Formation and Soft Phonon Mode in the Holstein Model*, Phys. Rev. Lett. **89**, 196401 (2002)

[132] G. S. Jeon, T. Park, H. Choi, it Numerical renormalization-group study of the symmetric Anderson-Holstein model: Phonon and electron spectral functions, Phys. Rev. B **68**, 045106 (2003)

[133] P. S. Cornaglia, D. R. Grempel, *Magnetoconductance through a vibrating molecule in the Kondo regime*, Phys. Rev. B **71**, 245326 (2005)

[134] M. T. Glossop, K. Ingersent, *Numerical Renormalization-Group Study of the Bose-Fermi Kondo Model*, Phys. Rev. Lett. **95**, 067202 (2005)

[135] M. T. Glossop, K. Ingersent, *Kondo physics and dissipation: A numerical renormalization-group approach to Bose-Fermi Kondo models*, Phys. Rev. B **75** 104410 (2007)

[136] W. Izumida, O. Sakai, Y. Shimizu, *Kondo Effect in Single Quantum Dot Systems – Study with Numerical Renormalization Group Method –*, J. Phys. Soc. Jpn. **67**, 2444 (1998)

[137] U. Gerland, J. von Delft, T. A. Costi, Y. Oreg, *Transmission Phase Shift of a Quantum Dot with Kondo Correlations*, Phys. Rev. Lett. **84**, 3710 (2000)

[138] R. Bulla, T. A. Costi, T. Pruschke, *Numerical renormalization group method for quantum impurity systems*, Rev. Mod. Phys. **80**, 395 (2008)

[139] R. W. Helmes, T. A. Costi, A. Rosch, *Kondo Proximity Effect: How Does a Metal Penetrate into a Mott Insulator?*, Phys. Rev. Lett. **101**, 066802 (2008)

[140] A. I. Tóth, L. Borda, J. von Delft, G. Zaránd, *Dynamical conductance in the two-channel Kondo regime of a double dot system*, Phys. Rev. B **76**, 155318 (2007)

[141] T. Maier, M. Jarrell, T. Pruschke, M. H. Hettler, *Quantum cluster theories*, Rev. Mod. Phys. **77**, 1027 (2005)

[142] L. De Leo, M. Civelli, G. Kotliar, *Cellular dynamical mean-field theory of the periodic Anderson model*, Phys. Rev. B **77**, 075107 (2008)

[143] L. De Leo, M. Civelli, G. Kotliar, *T=0 Heavy-Fermion Quantum Critical Point as an Orbital-Selective Mott Transition*, Phys. Rev. Lett. **101**, 256404 (2008)

[144] B. Su, V. J. Goldman, J. E. Cunningham, *Observation of single-electron charging in double-barrier heterostructures*, Science **255**, 313 (1992)

[145] P. Guéret, N. Blanc, R. Germann, H. Rothuizen, *Confinement and single-electron tunneling in Schottky-gated, laterally squeezed double-barrier quantum-well heterostructures*, Phys. Rev. Lett. **68**, 1896 (1992)

[146] A. T. Johnson, L. P. Kouwenhoven, W. de Jong, N. C. van der Vaart, C. J. P. M. Harmans, C. T. Foxon, *Zero-dimensional states and single electron charging in quantum dots*, Phys. Rev. Lett. **69**, 1592 (1992)

[147] J. Weis, R. J. Haug, K. v. Klitzing, K. Ploog, *Transport spectroscopy of a confined electron system under a gate tip*, Phys. Rev. B **46**, 12837 (1992)

[148] E. B. Foxman, P. L. McEuen, U. Meirav, N. S. Wingreen, Y. Meir, P. A. Belk, N. R. Belk, M. A. Kastner, *Effects of quantum levels on transport through a Coulomb island*, Phys. Rev. B **47**, 10020 (1993)

[149] Y. Oreg, David Goldhaber-Gordon, *Two-Channel Kondo Effect in a Modified Single Electron Transistor*, Phys. Rev. Lett. **90**, 13 (2003)

[150] D. Goldhaber-Gordon, J. Göres, M. A. Kastner, H. Shtrikman, D. Mahalu, U. Meirav, *From the Kondo Regime to the Mixed-Valence Regime in a Single-Electron Transistor*, Phys. Rev. Lett. **81**, 5225 (1998)

[151] D. Goldhaber-Gordon, H. Shtrikman, D. Mahalu, D. Abusch-Magder, U. Meirav, M. A. Kastner, *Kondo effect in a single-electron transistor*, Nature **391**, 156 (1998)

[152] L. P. Kouwenhoven, C. M. Marcus, P. L. McEuen, S. Tarucha, R. M. Westervelt, N. S. Wingreen, , in L. L. Sohn, L. P. Kouwenhoven, G. Schön (Eds.), Mesoscopic Electron Transport, Kluwer, Dordrecht, 1997

[153] T. A. Costi, *Kondo Effect in a Magnetic Field and the Magnetoresistivity of Kondo Alloys*, Phys. Rev. Lett. **85**, 1504 (2000)

[154] T. A. Costi, *Magnetotransport through a strongly interacting quantum dot*, Phys. Rev. B **64**, 241310(R), (2001).

[155] I. L. Aleiner, P. W. Brouwer, L. I. Glazman, , Physics Reports **358**, 309 (2002)

[156] S. M. Reimann, M. Manninen, *Electronic structure of quantum dots*, Rev. Mod. Phys. **74**, 1283 (2002)

[157] L. I. Glazman, M. Pustilnik, *Low-temperature transport through a quantum dot* in *Nanophysics: Coherence and Transport*, pp. 427-478, ed. by H. Bouchiat *et al.*, Elsevier (2005)

[158] G.-L. Ingold, Y. V. Nazarov, *Single Charge Tunneling* in NATO ASI Series B **294**, 21, ed. by H. Grabert, M. Devoret, Plenum (1992)

[159] R. Wilkins, E. Ben-Jacob, R. C. Jaklevic, *Scanning-tunneling-microscope observations of Coulomb blockade and oxide polarization in small metal droplets*, Phys. Rev. Lett. **63**, 801 (1989).

[160] H. van Houten, C. W. J. Beenakker, *Comment on "Conductance oscillations periodic in the density of a one-dimensional electron gas"*, Phys. Rev. Lett. **63**, 1893 (1989)

[161] W. G. van der Wiel, S. De Franceschi, J. M. Elzerman, T. Fujisawa, S. Tarucha, L. P. Kouwenhoven, *Electron transport through double quantum dots*, Rev. Mod. Phys. **75**, 1 (2002)

[162] P. Lafarge, *Macroscopic Charge Quantization in Metallic Nanostructures*, Ph.D. dissertation, Paris (1993)

[163] J. Toppari, *Transport Phenomena and Decoherence in Short Josephson Junction Arrays*, Ph.D. dissertation, Jyväskylä (2003)

[164] M. A. Reed, J. N. Randall, R. J. Aggarwal, R. J. Matyi, T. M. Moore, A. E. Wetsel, *Observation of discrete electronic states in a zero-dimensional semiconductor nanostructure*, Phys. Rev. Lett. **60**, 535 (1988)

[165] S. Tarucha, D. G. Austing, T. Honda, R. J. van der Hage, L. P. Kouwenhoven, *Shell Filling and Spin Effects in a Few Electron Quantum Dot*, Phys. Rev. Lett. **77**, 3613 (1996)

[166] T. Schmidt, R. J. Haug, K. v. Klitzing, A. Förster, H. Lüth, *Spectroscopy of the Single-Particle States of a Quantum-Dot Molecule*, Phys. Rev. Lett. **78**, 1544 (1997)

[167] R. C. Ashoori, *Electrons in artificial atoms*, Nature **379**, 413 (1996)

[168] J. Stangl, V. Holý, G. Bauer, *Structural properties of self-organized semiconductor nanostructures*, Rev. Mod. Phys. **76**, 725 (2004)

[169] L. P. Kouwenhoven, Ch. M. Marcus, P. L. McEuen, S. Tarucha, R. M. Westervelt, N. S. Wingreen, *Electron transport in quantum dots*, in Proc. of the Adv. Study Inst. on Mesoscopic Electron Transport, ed. by L. L. Sohn, L. P. Kouwenhoven, G. Schn (Kluwer 1997)

[170] L. I. Glazman, M. Pustilnik, *Coulomb blockade and Kondo effect in quantum dots*, in *New Directions in Mesoscopic Physics (Towards Nanoscience)*, pp. 93-115, ed. by R. Fazio, V. F. Gantmakher, Y. Imry, (Kluwer, Dordrecht, 2003)

[171] P. Hadley, G. Lientschnig, M. Lai, *Single-Electron Transistors*, http://qt.tn.tudelft.nl/publi/2002/ISCS/ISCS2002.html

[172] S. Tomonaga, *Remarks on Bloch's Method of Sound Waves applied to Many-Fermion Problems*, Prog. Theor. Phys. **5**, 544 (1950)

[173] J. M. Luttinger, *An Exactly Soluble Model of a Many-Fermion System*, J. Math. Phys. **4**, 1154 (1963).

[174] D. L. Cox, M. B. Maple, *Electronic Pairing in Exotic Superconductors*, Physics Today **48**, 32 (1995)

[175] For a review see D. L. Cox, A. Zawadowski, *Exotic Kondo Effects in Metals: Magnetic Ions in a Crystalline Electric Field and Tunneling Centers*, Adv. in Phys. **47**, 599 (1998)

[176] Q. Si, S. Rabello, K. Ingersent, J. L. Smith *et al.*, *Locally critical quantum phase transitions in strongly correlated metals*, Nature **413**, 804-808 (2001)

[177] M. Vojta, *Impurity Quantum Phase Transitions*, Phil. Mag. **86**, 1807 (2006)

[178] M. Vojta, *Quantum phase transitions*, Rep. Prog. Phys. **66**, 2069 (2003)

[179] M. Bockrath *et al.*, *Luttinger-liquid behaviour in carbon nanotubes*, Nature **397**, 598 (1999)

[180] H. Ishii *et al.*, *Direct observation of Tomonaga–Luttinger-liquid state in carbon nanotubes at low temperatures*, Nature **426**, 540 (2003)

[181] P. M. Singer, P. Wzietek, H. Alloul, F. Simon, H. Kuzmany, *NMR Evidence for Gapped Spin Excitations in Metallic Carbon Nanotubes*, Phys. Rev. Lett. **95**, 236403 (2005)

[182] B. Dóra, M. Gulácsi, F. Simon, H. Kuzmany, *Spin Gap and Luttinger Liquid Description of the NMR Relaxation in Carbon Nanotubes*, Phys. Rev. Lett. **99**, 166402 (2007)

[183] E. Miranda, V. Dobrosavljevic, *Disorder-driven non-Fermi liquid behaviour of correlated electrons*, Rep. Prog. Phys. **68**, 2337 (2005).

[184] M. Milovanović, S. Sachdev, R. N. Bhatt, *Effective-field theory of local-moment formation in disordered metals*, Phys. Rev. Lett. **63**, 82 (1989)

[185] V. Dobrosavljević, T. R. Kirkpatrick, G. Kotliar, *Kondo effect in disordered systems*, Phys. Rev. Lett. **69**, 1113 (1992)

[186] Ph. Nozières, A. Blandin, *Kondo effect in real metals*, J. Phys. Paris, **41**, 193 (1980)

[187] S. Katayama, S. Maekawa, H. Fukuyama, *Kondo-like Effect of Atomic Motion on Resistivity in* $Pb_{1-x}Ge_xTe$, J. Phys. Soc. Jpn. **56**, 697 (1987)

[188] J. von Delft *et al.*, *The 2-Channel Kondo Model: I. Review of Experimental Evidence for Its Realization in Metal Nanoconstrictions*, Ann. Phys. **263**, 1 (1998)

[189] T. Cichorek *et al.*, *Two-Channel Kondo Effect in Glasslike ThAsSe*, Phys. Rev. Lett. **94**, 236603 (2005)

[190] S. Yotsuhashi, H. Maebashi, *Crossover Temperature from Non-Fermi Liquid to Fermi Liquid Behavior in Two Types of Impurity Kondo Model*, J. Phys. Soc. Jpn. **71**, 1705 (2002)

[191] G. Zaránd, K. Vladár, *Low Temperature Dynamics of an* $N_f$*-Flavor Two Level System in a Metal: Equivalence with the* $N_f$*-Channel Kondo Model to* $1/N_f^2$ *Order*, Phys. Rev. Lett. **76**, 2133 (1996)

[192] L. Borda, L. Fritz, N. Andrei, G. Zaránd, *Theory of inelastic scattering from quantum impurities*, Phys. Rev. B **75**, 235112 (2007).

[193] I. Affleck, A. W. W. Ludwig, *Exact conformal-field-theory results on the multichannel Kondo effect: Single-fermion Green's function, self-energy, and resistivity*, Phys. Rev. B **48**, 7297 (1993)

[194] J. Kroha, P. Wölfle, T. A. Costi, *Unified Description of Fermi and Non-Fermi Liquid Behavior in a Conserving Slave Boson Approximation for Strongly Correlated Impurity Models*, Phys. Rev. Lett. **79**, 261 (1997)

[195] A. M. Sengupta, A. Georges, *Emery-Kivelson solution of the two-channel Kondo problem*, Phys. Rev. B **49**, 10020 (1994)

[196] S. Suzuki, O. Sakai, Y. Shimizu, *An extended Anderson model that shows decreasing resistivity with decreasing temperature*, Solid State Comm. **104**, 429 (1997)

[197] F. B. Anders, *Renormalization-group approach to spectral properties of the two-channel Anderson impurity model*, Phys. Rev. B **71**, 121101(R) (2005)

[198] P. Mehta, N. Andrei *Nonequilibrium Transport in Quantum Impurity Models: The Bethe Ansatz for Open Systems*, Phys. Rev. Lett. **96**, 216802 (2006)

[199] M. Pustilnik, L. Borda, L. I. Glazman, J. von Delft, *Quantum phase transition in a two-channel-Kondo quantum dot device*, Phys. Rev. B, **69**, 115316 (2004)

[200] P. Di Francesco, P. Mathieu, D. Sénéchal, *Conformal Field Theory*, 1997 Springer-Verlag New-York, Inc.

[201] J. Polchinski, *Renormalization and effective lagrangians*, Nucl. Phys. B **231**, 269 (1984)

[202] G. Zaránd, *Orbital fluctuations and strong correlations in quantum dots*, Phil. Mag. **86**, 2043 (2006)

[203] M. A. Kastner, *The single-electrons transistor*, Rev. Mod. Phys. **64**, 849 (1992)

[204] D. V. Averin, Yu. V. Nazarov *Virtual electron diffusion during quantum tunneling of the electric charge*, Phys. Rev. Lett. **65**, 2446 (1990)

[205] T. K. Ng, P. A. Lee, *On-Site Coulomb Repulsion and Resonant Tunneling*, Phys. Rev. Lett. **61**, 1768 (1988)

[206] J. König, *Quantum Fluctuations in the Single-Electron Transistor*, Shaker Verlag 1999

[207] L. I. Glazman, M. E. Raikh, *Resonant Kondo transparency of a barrier with quasilocal impurity states*, JETP Lett. **47**, 452 (1988)

[208] J. König, H. Schöller, G. Schön, *Zero-Bias Anomalies and Boson-Assisted Tunneling Through Quantum Dots*, Phys. Rev. Lett. **76**, 1715 (1996)

[209] W. G. van der Wiel, S. de Francheschi, T. Fujisawa, J. M. Elzerman, S. Tarucha, L. P. Kouwenhoven, *The Kondo Effect in the Unitary Limit*, Science **289**, 2105 (2000)

[210] J. Fuchs, *Affine Lie Algebras and Quantum Groups*, Cambridge University Press (1992)

[211] M. Jarrell, H. Pang, D. Cox, K. Luk, *Two-Channel Kondo Lattice: An Incoherent Metal*, Phys. Rev. Lett. **77**, 1612 (1996)

[212] P. Coleman, A. M. Tsvelik, N. Andrei, H. Y. Kee, *Co-operative Kondo effect in the two-channel Kondo lattice*, Phys. Rev. B **60**, 3608 (1999)

[213] F. B. Anders, M. Jarrell and D. L. Cox, *Magnetoresistance in the Two-Channel Anderson Lattice*, Phys. Rev. Lett. **78**, 2000 (1997)

[214] M. Garst, P. Wölfle, L. Borda, J. von Delft, L. Glazman, *Energy-resolved inelastic electron scattering off a magnetic impurity*, Phys. Rev. B **72**, 205125 (2005)

[215] Y. Meir, N. S. Wingreen, *Landauer formula for the current through an interacting electron region*, Phys. Rev. Lett. **68**, 2512 (1992)

[216] H. Suhl, *Dispersion Theory of the Kondo Effect*, Phys. Rev. **138**, A515 (1965)

[217] A. A. Abrikosov, , Physics **2**, 61 (1965)

[218] A. O. Barut, R. Raczka, *Theory of Group Representations and Applications*, World Scientific (1986)